2023-04-25

Investigating Groundwater Impacts and Sulfur Cycling in Urban Stormwater Ponds

Ogrins, Lucas

UNIVERSITY OF CALGARY

Investigating Groundwater Impacts and Sulfur Cycling in Urban Stormwater Ponds

by

Lucas Ogrins

A THESIS

SUBMITTED TO THE FACULTY OF GRADUATE STUDIES

IN PARTIAL FULFILMENT OF THE REQUIREMENTS FOR THE

DEGREE OF MASTER OF SCIENCE

GRADUATE PROGRAM IN GEOSCIENCE

CALGARY, ALBERTA

APRIL, 2023

Abstract

Stormwater ponds have been used to manage water quality and quantity during high flow events. Groundwater can potentially impact the operations of stormwater ponds by altering pond water chemistry, although this influence is poorly understood. This study was undertaken to improve understanding of groundwater and surface water interactions and sulfur cycling in a stormwater system. A pair of interconnected stormwater ponds were investigated at an airport in Calgary Alberta where one pond, Pond M, was known to generate noticeable quantities of hydrogen sulfide. A site investigation was carried out to evaluate groundwater flow directions, groundwater and surface water chemical compositions, sulfur sources and fate through stable isotope analysis, and water budgets. At both ponds, groundwater accounted for a minor fraction of the total water budget and surface water flows dominated. While groundwater contributions were low, elevated sulfate was seen in groundwater samples in the study area, which was attributed to evaporative concentration, with concentrations being the highest around Pond M. Sulfate was shown to enter the pond bottom by diffusion at an estimated rate of 8.9 to 17 kg per day and is the main sulfur source for bacterial sulfate reduction. Other possible sulfate inputs into Pond M are groundwater leakages into stormwater pipes above the pond and preferential flow paths in fractured till adjacent to the pond. Groundwater with high dissolved solid content contributes to stratification at Pond M and likely enhances hydrogen sulfide generation by reducing oxygenation of the water column. Hydrogen sulfide generated in Pond M oxidizes into elemental sulfur and contributes to turbidity encountered at the second pond, Pond E. Stormwater at Pond E was found to exit the study area by seeping into the ground, potentially bypassing the outlet control structure. Groundwater interactions with stormwater ponds have the potential to alter pond structure and can contribute to hydrogen sulfide generation by diffusion of sulfate into pond sediments where bacterial sulfur reduction can occur.

Acknowledgements

A research project of this scope is not something that can be done alone, and this project was no exception. I would like to thank and acknowledge all those who have supported me throughout this project. First of all, I would like to acknowledge the help and support my wife, Kristina, and my family have been for me through my post-secondary studies. I would not have been able to get this far without them.

I would also like to thank my research supervisor, Ed Cey, for guiding me throughout the project, giving me a chance at research during my undergraduate years, and giving me this wonderful research opportunity. I would also like to thank Sam Johnson and Sean Elliot for their camaraderie and help out in the field. And of course, I would like to thank Stu Merrett for his help and support with sample and data collection and being an invaluable help to me in the field.

Additionally, I would like to thank Baseline Water Resources for providing me with the telemetry data from their flow monitoring equipment. And thank you Chris Debuhr at the Dynamic Imaging Laboratory for helping with the SEM analysis. I would also like to thank everyone at the University of Calgary Isotope Science Lab for helping with isotope sample preparation as well as helping with running the centrifuge for porewater extraction.

I would also like to thank those at Calgary International Airport for providing this project in the first place. Thank you, Harris Switzman, Sarah Nelson, Megan Roche, Gary Kindrat, and Reid van Drecht, for helping with site access and support with sampling and data collection. It was wonderful to work with all of you throughout this research project.

This work was supported by Mitacs through the Mitacs Accelerate program.

Table of Contents

Abstract I
Acknowledgements II
List of Tables 1
List of Figures 2
Chapter 1 – Introduction 1
1.1 – Introduction 1
1.2 – Site Description 6
1.3 – Objectives 8
1.4 – Thesis Outline 8
Chapter 2 – Manuscript 13
2.1 – Introduction 13
2.2 – Site Description 15
2.3 – Methods 17
2.3.1 – *Existing Monitoring Infrastructure and Operations* 17
2.3.2 – *Groundwater Monitoring* 18
2.3.3 – *Surface Water Monitoring* 21
2.3.4 – *Stable Isotope Samples* 21
2.3.5 – *Sediment Sampling* 22
2.3.6 – *SEM Sample Preparation* 23
2.3.7 – *Water Column Measurements* 23
2.3.8 – *Water Budget Calculations* 24
2.3.9 – *Near-Surface Geophysical Survey* 27
2.3.10 – *Storm Flow Simulation* 27
2.3.11 – *Sulfur Diffusion Mass Flux Estimates* 28
2.4 – Results 30
2.4.1 – *Water Levels* 30
2.4.2 – *Water Quality* 32
2.4.3 – *Sulfur Distribution* 33
2.4.4 – *SEM Analysis* 34
2.4.5 – *Simulated Storm Flow* 35

2.4.6 – *Stable Isotopes* 36
2.5 – Discussion 38
2.5.1 – *Pond M Hydrology and Hydrogeology* 38
2.5.2 – *Pond M Sulfur Sources* 41
2.5.3 – *Pond M Sulfur Transport and Fate* 43
2.5.4 – *Pond E* 47
2.6 – Conclusion 48
Chapter 3 – Implications, Future Research, Recommendations 66
3.1 – Research Implications 66
3.2 – Future Research 68
3.3 – Recommendations 71
3.4 – Personal Reflection 71
Bibliography 73
Appendix A – Borehole Logs and Well Completion Details 84
Appendix B – Correlation Between EC and TDS and Water Density 93
Appendix C – Estimated Evapotranspiration Calculations 95
Appendix D – Diffusion Model Calculations 99
Appendix E – Spring Snowmelt and Precipitation Responses 102
Appendix F – Geochemistry 107
Appendix G – Pond E Geophysical Survey 113
Appendix H – Sediment Core and SEM 114

List of Tables

Table 1 – Water and sulfur mass budgets for Pond M and the Pond E water budget between May 2022 and October 2022. ..... p. 55

List of Figures

Figure 1 - Study area and relevant stormwater infrastructure which are highlighted. Highlighted areas are ponds and water treatment facilities. Black arrows indicate stormwater flow directions. Basemap provided by Open Street Maps. ..... p. 15

Figure 2 - Sulfate concentrations measured at the outlet of Pond E (PE-BERM) from October 2021 to October 2022 collected by YYC. Daily average air temperature and hourly precipitation is included. Data set also includes a snowmelt event that occurred in January 2022 as well as a series of rainstorms in June and July of 2022. ..... p. 16

Figure 3 - Photo of Pond E taken June 22 2021 looking towards the northeast. The pond water has visible discoloration and elevated turbidity. ..... p. 17

Figure 4 - Photo of Pond M taken July 12, 2021 looking west by northwest. The pond has taken on an opaque blue/black coloration and smelled of hydrogen sulfide at the time the photo was taken. ..... p. 18

Figure 5 - Regional groundwater levels for YYC. The green line represents the inferred contact between the Cordilleran and Laurentide till material (Moran 1986). Highlighted are the outlines of the Pond M and Pond E stormwater ponds. Water table elevations show that groundwater flows towards Pond M and through Pond E. Modified from Merrett (2022). ..... p. 56

Figure 6 - Sampling locations around Pond M. Red circles indicate groundwater sampling locations, blue circles indicate surface water sampling locations, and yellow squares indicate where water column measurements were made. Arrows indicate where stormwater enters and leaves Pond M. Basemap provided by Open Street Maps. ..... p. 57

Figure 7 - Sampling locations in the vicinity of Pond E. Red circles indicate groundwater sampling locations and blue circles indicate surface water sampling locations. Blue arrows indicate where stormwater enters and leaves Pond E. Basemap provided by Open Street Maps. ..... p. 58

Figure 8 - Well water elevations in the vicinity of Pond M. Well locations are given in Fig. 6. The dashed line is the estimated average operating level of Pond M. p. 59

Figure 9 - Groundwater elevations and pond elevations for the Pond E study area. PE-STAFF is the measured pond water elevation. ..... p. 60

Figure 10 - Piper plot displaying the composition of groundwater during three sampling events. Grey indicates the sampling done on Feb 17 2022. Green indicates sampling completed between July 7-8 2022. Orange indicates sampling completed between October 13-14 2022. ..... p. 61

Figure 11 - Distribution of sulfate concentrations around Pond M during the July 7-8 2022 sampling period. Blue circles indicate surface water sampling locations and red circles indicate groundwater sampling locations. Basemap provided by Open Street Maps. p. 62

Figure 12 - Distribution of sulfate concentrations around Pond E during the July 7-8 2022 sampling period. Blue circles indicate surface water sampling locations and red circles indicate groundwater sampling locations. Basemap provided by Open Street Maps. ..... p. 63

Figure 13 - Figure 13 - Interpolated results of the EM31 survey conducted around Pond M in March 2022 along with TDS from the July 7-8 2022 sampling set. The south bench has the largest region of high EC in the survey area which coincides with marshy regions and salt pans. Basemap provided by Open Street Maps. ..... p. 64

Figure 14 - Estimated sulfate concentration with respect to depth in Pond M sediments. The modeled diffusion curve provides an approximation of sulfate concentrations with respect to depth using the Ogata-Banks solution (Ogata 1970). ..... p. 65

Figure 15 - SEM analysis results on material that dropped out of suspension from a Pond M water sample. A) SEM image displaying crystalline sulfur. B) Sulfur distribution in A. C) Iron distribution in A. Iron is abundant, but notably absent where suflur is present. D) Carbon distribution in A. Iron and carbon more closely relate to each other than sulfur. ..... p. 66

Figure 16 – SEM analysis results on material suspended in a Pond M water sample. A) SEM image showing filamentous sulfur. B) Sulfur distribution in A. C) Iron distribution in A. Iron is less abundant and does not show up where sulfur or carbon is present. D) Carbon distribution in A. Carbon is abundant. ..... p. 67

Figure 17 -Sulfate and hydrogen sulfide concentrations during the simulated storm event. Labels on the x-axis represent progressively downstream sampling locations in the storm drain network. A) Pre-Event concentrations. B) Event concentrations. C) Post-event concentrations. ..... p. 68

Figure 18 - Water column profiles for the forebay and rearbay of Pond M. Highlighted is the threshold for thermal stratification based on a water surface temperature of 1 C. ..... p. 69

Figure 19 - Sulfate stable isotope results displaying distinct clustering between groundwater, surface water, and porewater from Pond M core sediments. ..... p. 70

Figure 20 - Comparison of oxygen isotopes between sulfate and water. Clustering by water δ18O values is likely an artifact of temporal difference between samples. Black lines on the plot indicate upper and lower boundaries for sulfide oxidation field given in Van Stempvoort & Krouse (1993). ..... p. 71

Figure 21 - Comparison of sulfur isotopes in sulfate and hydrogen sulfide during the simulated storm event. Hydrogen sulfide is heavily depleted in comparison to sulfate. ..... p. 73

Chapter 1 – Introduction

1.1 – Introduction

Urban environments, by their nature, create a host of water quality and water quantity issues when it comes to managing intense precipitation or storm events. Impervious surfaces such as sidewalks and roadways are common in urban settings and these features reduce or eliminate infiltration of stormwater into the soil which can lead to flash flooding during particularly intense rainstorms (Wright et al. 2012, Smith et al. 2013). To help mitigate surface flows of stormwater along with the associated water quality concerns, stormwater infrastructure such as detention ponds have been employed to retain sediments and to make storm flows more manageable by acting as temporary reservoirs that retain incoming stormwater and slowly release it over time (Persson & Wittgren 2003). Stormwater ponds have been commonly used to not only manage urban runoff during intense precipitation events, but also to manage the assortment of dissolved and solid contaminants that frequently accompany urban runoff (van Buren & Marsalek 1997). Stormwater ponds can be built with stilling basins called forebays or sediment traps that collect sediment mobilized by runoff and reduce the quantity of suspended solids that leave the pond (Shammaa et al. 2002). Depending on the design of the system, stormwater is eventually discharged directly into surface waterways or is allowed to percolate into the subsurface and recharge local groundwater resources.

Urban runoff has the potential to negatively impact receiving waters in terms of water quality and quantity. In the absence of impoundment structures such as stormwater ponds, runoff discharged during storm events into urban streams can drastically increase stream flow rates for short periods of time and increase the risk of erosion (Walsh et al. 2012). Untreated stormwater discharged into urban streams negatively impacts water quality through high nutrient loads and other contaminants (Walsh et al. 2005). Stormwater ponds have been utilized to help with these water flow and water quality concerns to mitigate the effects of urban runoff on receiving waters.

While not originally designed to, stormwater ponds have been found to improve water quality beyond removing suspended solids by facilitating biogeochemical reactions to

remove dissolved contaminants from the water column. Dissolved contaminants, such as heavy metals (Camponelli et al. 2010, Karlsson et al. 2010, Egemose et al. 2015) and nutrients (Sønderup et al. 2016, Yazdi et al. 2021, Janke et al. 2022) become bound to pond sediments through adsorption onto sediments (Stutter & Lumsdon 2008, Reddy et al. 2021) and biological processes (Yazdi et al. 2021). Contaminant removal from the water column largely depends on how long the water resides in the pond. A longer residence time tends to sequester more contaminants into pond sediments when compared with a shorter residence time, leading to improved water quality at the pond outflow (Kusin et al. 2010). Residence time in a water body plays an important role in the redox state of the water column. Longer residence times can cause stormwater ponds to be a contaminant source rather than a sink due to a shift to more reducing and anoxic conditions.

Most chemical species can exist in a variety of redox states. When a chemical species loses or donates electrons to another species, it is considered oxidized. When a chemical species receives an electron from another species, it is considered reduced. Many redox sensitive species, such as iron, manganese, sulfur, and phosphorus, change solubility depending on their redox state. As an example, iron is insoluble in its oxidized state of Fe^{3+} at neutral pH. But reduced iron (Fe^{2+}) is soluble in water under the same pH conditions. Under reducing conditions, insoluble species can dissolve and become remobilized during high flow events (Woiciechowska & Waara 2011, Frost et al. 2019, Taguchi et al. 2020). Reducing conditions can be mitigated by oxygenating the water column through regular mixing due to diurnal temperature variations throughout the pond body (He et al. 2015) or artificial means (Hao et al. 2021). However, natural mixing of the water column can be impeded through pond stratification where little to no mixing can occur due to density differences between the water at the surface and the bottom of the pond.

Water bodies, like stormwater ponds, have two main mechanisms that drive density driven stratification that reduces mixing of the water column. Thermal stratification occurs when there is a difference in temperature between the top and bottom of the

water column which in turn introduces a change in density between the surface water and the bottom water (Mazumder & Taylor 1994). A warm water surface and a cold pond bottom will resist mixing because the bottom water is denser than water at the surface. The second stratification mechanism is due to density differences from dissolved solid content where water with a higher dissolved solids content will be denser and will remain closer to the bottom of the pond (Boehrer & Schultze 2008). As with temperature, or thermal, stratification, ponds with high total dissolved solids (TDS) content would resist mixing and lead to what is called chemical stratification. Lack of water column mixing decreases the depth at which atmospheric oxygen can penetrate the water column, leading to oxygen depletion at the pond bottom (Koretsky et al. 2012, Martinsen et al. 2019, Ahmed et al. 2022). Urban contaminants, in the form of nutrients and salts, have the capability to contribute to both forms of stratification. In agricultural regions, nitrate and phosphorus inputs into stormwater ponds through fertilizer runoff can bring about eutrophication (Song et al. 2013, Ivanovsky et al. 2018, Janke et al. 2022). Eutrophication increases the heating of the upper portion of the pond due to poor light penetration and leads to thermal stratification (Fee et al. 1996). In cold regions, chloride from ice control measures makes its way to stormwater ponds where they accumulate in the bottom waters and induce chemical stratification (Marsalek 2003, Semadeni-Davies 2006). Both forms of stratification reduce oxygenation of the water column and increase the potential for reducing conditions in stormwater ponds.

Redox state plays a large role in managing nutrients, such as sulfur, in any aquatic system. While research into sulfur dynamics within stormwater ponds is limited, extensive research has been conducted on sulfur cycling in wetlands. Sulfur commonly exists in its most oxidized state as sulfate. Near the earth's surface, sulfate is typically reduced by bacteria to form sulfide, or some other intermediate form as organic carbon is anaerobically metabolized (Baldwin & Mitchell 2011, Pester et al. 2012, Torgeson et al. 2022):

$$SO_4^{2-} + 2CH_2O \rightarrow S^{2-} + 2CO_2 + 2H_2O$$

where CH_2O represents organic carbon. In this reduced form, sulfide can undergo a variety of transformations. It can react with dissolved metals such as iron and

manganese to form sulfide minerals (Rickard & Luther III 2007, Johnston et al. 2013, Noël et al. 2020):

$$Fe^{2+} + 2S^{2-} \rightarrow FeS_2$$

Where these metals are absent, sulfide can react with hydrogen ions to form hydrogen sulfide:

$$2H^{+} + S^{2-} \rightarrow H_2S$$

Hydrogen sulfide carries a distinct 'rotten egg' odor, is toxic (EPA 2003), flammable, and can corrode stormwater infrastructure (Vollersten et al. 2008). Hydrogen sulfide production typically occurs in the waterbody sediments where anaerobic microbial populations can flourish and be protected from oxygenation of the water column (Wiessner et al. 2005, Pallud & Cappellen 2006). As hydrogen sulfide enters the water column, microorganisms or the presence of oxidizing chemicals can convert the hydrogen sulfide into elemental sulfur (Afonso & Stumm 1992, Lyn & Taylor, 1992, Avetisyan et al. 2019) in the following reaction:

$$2H_2S + O_2 \rightarrow 2S + 2H_2O$$

The above reactions are not one-way reactions and are dependent on pH and redox conditions. Additionally, these reactions where sulfur changes from one form to the next can have a variety of intermediate reaction steps before the final product is achieved. Sulfite and thiosulfate are some examples of these intermediate sulfur species. Most of these reactions are facilitated by microbial processes that use enzymes to provide the activation energy required for these reactions to proceed.

In the context of a stormwater system, sulfur can come from anthropogenic and natural sources. Anthropogenic sulfur sources include atmospheric deposition of sulfur dioxide from burning fossil fuels with high sulfur content such as coal or diesel (Cullis & Hirschler 1980). Natural sulfur sources can come from the weathering of sulfide minerals (e.g. pyrite), the dissolution of sulfate bearing evaporite deposits (e.g. gypsum or anhydrite), or from plant material in the form of organic sulfur. No matter the source, some sulfur compounds, such as sulfate, are readily soluble in water and will be transported wherever the water is flowing. In the case of precipitation events, sulfur can

mobilize as surface runoff, or it can infiltrate into the soil to eventually reach the groundwater table.

Because stormwater infrastructure is typically installed in the subsurface, there is potential for interactions between stormwater and groundwater that could cause noticeable quantities of sulfate to exchange between the two systems. Interactions between a stormwater pond and the surrounding groundwater are dictated by differences in water elevation. When pond water levels are higher than the surrounding groundwater table, stormwater has the potential to seep out of the pond into groundwater. In the reverse scenario, groundwater can seep into the pond. It is possible that these flow scenarios can change throughout the year such as during snowmelt periods and/or rainy seasons where there is a higher chance of groundwater seeping into a stormwater pond. During dry periods, such as summer and fall, groundwater elevations can fall below the pond water level, allowing stormwater to seep out of the pond. Some stormwater ponds are deliberately designed to allow infiltration into the subsurface as a means of groundwater resource replenishment, and extensive work has been conducted investigating those interactions (e.g. Kidmose et al. 2015, Bonneau et al. 2018, Thompson et al. 2021, McQuiggan et al. 2022, Pophillat et al. 2022).

While stormwater seeping into groundwater resources has been the subject of much research, investigations on the impact of groundwater on stormwater quality is limited. Previous work of groundwater seepage into stormwater infrastructure has mostly focused on characterizing groundwater seepage rates into ponds and how that affects stormwater pond outflows. Corely (2015) found that overall groundwater contributions to two stormwater ponds in South Carolina could be substantial due to highly permeable soils in the region. Work performed by Karpf & Krebs (2013) and Shepley at al. (2020) investigated groundwater seeping into the utility trenches surrounding stormwater pipes and found that these trenches can allow groundwater to flow at higher rates than the surrounding native material. Houhou et al. (2010) investigated groundwater leakage into sewer pipes using stable isotope analysis for sulfur, oxygen, and deuterium and found that groundwater seeps at a constant rate into the stormwater system studied. In one

study on stormwater conducted in Florida, Thomas & Lucius (2016) found that during low flow periods, groundwater supplied most of the nutrients found in the pond. While their study investigated how groundwater can influence stormwater pond chemistry, they tentatively associated nutrient loads with eutrophication that was occurring within the pond, indicating a lack of evaluation of direct groundwater impacts on stormwater quality. Because groundwater can have a very different geochemical composition than urban runoff, it can have an outsized influence on pond water composition and redox state relative to the volume of groundwater entering the pond (Kidmose et al. 2013).

Where research has investigated stormwater pond redox states by looking at hydrogen sulfide generation specifically, the potential role of groundwater has been overlooked. A study conducted by Ku et al. (2016) in Edmonton, Alberta investigated a pair of stormwater ponds and found that sulfate reduction to sulfide competed with nitrate reduction to ammonia such that sulfate reduction only occurred after denitrification was completed. Work conducted at a pair of stormwater ponds in Ottawa, Ontario found that hydrogen sulfide production originated in the sediments and ice cover contributed to low oxygen conditions that favored hydrogen sulfide generation (D'Aoust et al. 2017, D'Aoust et al. 2018, Chen et al. 2019). However, neither of these research groups investigated the potential role of groundwater and stormwater exchange in influencing pond water geochemistry. Addressing this data gap will improve understanding on how groundwater influences stormwater pond water chemistry helping guide siting and design of stormwater ponds to ensure proper water treatment processes are unimpeded by groundwater influences.

1.2 – Site Description

The study investigated a pair of stormwater ponds (Pond M and E) and connected stormwater drainage infrastructure on the property of Calgary International Airport (YYC) (Fig. 1). Topography at YYC is dominated by gently undulating, low relief terrain except on the western boundary of the property. The western portion of YYC consists of bluffs that mark the edge of the Nose Creek valley. Prairie grasses are the main forms

of vegetation with the exceptions of shallow depressions where water collects, and wetland vegetation is present.

Pond M is a retention pond and was constructed in 2008 to accommodate increased runoff for future infrastructure projects at YYC. Pond M is located close to the center of YYC where surrounding topography is gently undulating, and vegetation is dominated by prairie grasses. Pond M drains portions of the eastern runway along with portions of the main airport terminal. In addition to receiving runoff from the parallel runway and the main terminal, Pond M also receives discharge from Pond K to the east as well as YYC's glycol treatment facility to the northeast. At the treatment facility, glycol contaminated water is oxygenated to facilitate the aerobic breakdown of glycol compounds commonly found in aircraft deicing formulations (Revitt & Worrall 2003, Lissner et al. 2013), and reduce their environmental impacts. To accommodate water inputs, Pond M was built to hold 48,196 m^3 under normal operating conditions with additional capacity for high flow events, giving a total storage capacity of 168,692 m^3. The pond was not constructed with an engineered geotextile liner, but instead used compacted native till material in the vicinity. Pond M has three inlets located on the east end of the pond where storm water enters a forebay. There is a single outlet draining Pond M located on the southern edge of the rearbay. From there, stormwater flows westward and is discharged at Pond E, which is hydraulically down gradient of Pond M.

Pond E is located on the western edge of YYC property and was completed in 2016. In this area of the YYC site, gently undulating terrain gives way to bluffs that mark the boundary of the Nose Creek valley. Prairie grasses dominate the bluffs, but the pond itself is host to wetland vegetation such as cattails. Pond E has a single inlet that receives outflow from Pond M as well as stormwater discharge from other areas of YYC (e.g. portions of the eastern runway, some maintenance buildings on the west end of YYC). While Pond M was built as a detention pond, Pond E was built as a dry pond to help manage storm flows going off site. There is an emergency spillway that serves to discharge pond water to a secondary dry pond when water levels in Pond E exceed

safe operating levels. Stormwater leaving Pond E passes through the City of Calgary's stormwater network before discharging into Nose Creek to the west.

Water quality at the outflow of Pond E varies seasonally, resulting in considerable variability in sulfur concentrations that make stormwater management and release from the site more challenging. Sulfate measured at the outflow rapidly decreases in response to spring snow melt events and significant precipitation events (Fig. 2). Between these events, sulfate concentrations can fluctuate significantly, with concentrations varying between 499 mg/L and 1,050 mg/L from April to June 2022. In addition, water clarity in both Pond M and Pond E also varies seasonally in response to changing water chemistry. Pond E can take on a grey/white coloration and becomes opaque (Fig. 3). Upgradient to Pond E, Pond M can become black and opaque and carries the characteristic smell of hydrogen sulfide (Fig. 4). This study was motivated by the significant variations in surface water composition and the desire to understand the mechanisms driving these changes, notably the potential role of groundwater in influencing pond water quality.

1.3 – Objectives

The main objectives of this research project were to understand why hydrogen sulfide was being generated in Pond M, evaluate potential downstream impacts of hydrogen sulfide export, and determine whether groundwater played a role. To that end, three tasks were identified to accomplish these objectives. The first task was determining how groundwater and surface water behaved in the study area and identifying how they interact which was completed by monitoring seasonal groundwater elevations relative to pond water levels as well as water budget estimation. The second was examining conditions that encourage the generation of hydrogen sulfide through geochemical and stable isotope analysis. The third task was determining the fate of hydrogen sulfide after it is formed and its potential impacts downstream from the generating location through water quality measurements, stable isotope analysis, and scanning electron microscopy (SEM).

1.4 – Thesis Organization

This thesis consists of three chapters. The first introductory chapter provides relevant background information about the stormwater infrastructure, existing literature knowledge, and the study area. The second chapter is intended as a standalone manuscript for future publication, where the bulk of the research methodology, results, and discussion are described, along with noting major conclusions. As a standalone unit, some aspects of the introduction, site description, and conclusions from Chapter 2 may be repeated in Chapters 1 and 3. The third and final chapter of this thesis discusses the broader implications of the findings of this research project. Additionally, it provides some insight as to the lessons learned during this research project as well as potential avenues for future work. Figures and tables are at the end of each chapter where they are first referenced.

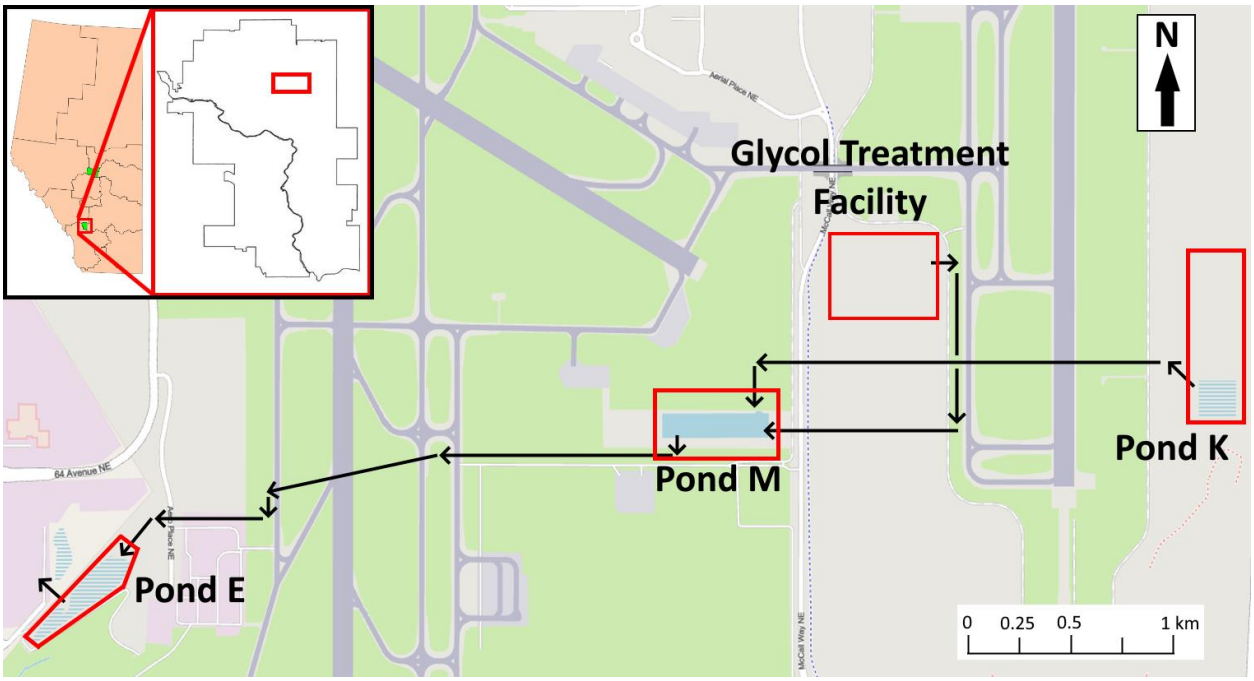

Figure 1 - Study area and relevant stormwater infrastructure which are highlighted. Highlighted areas are ponds and water treatment facilities. Black arrows indicate stormwater flow directions. Basemap provided by Open Street Maps.

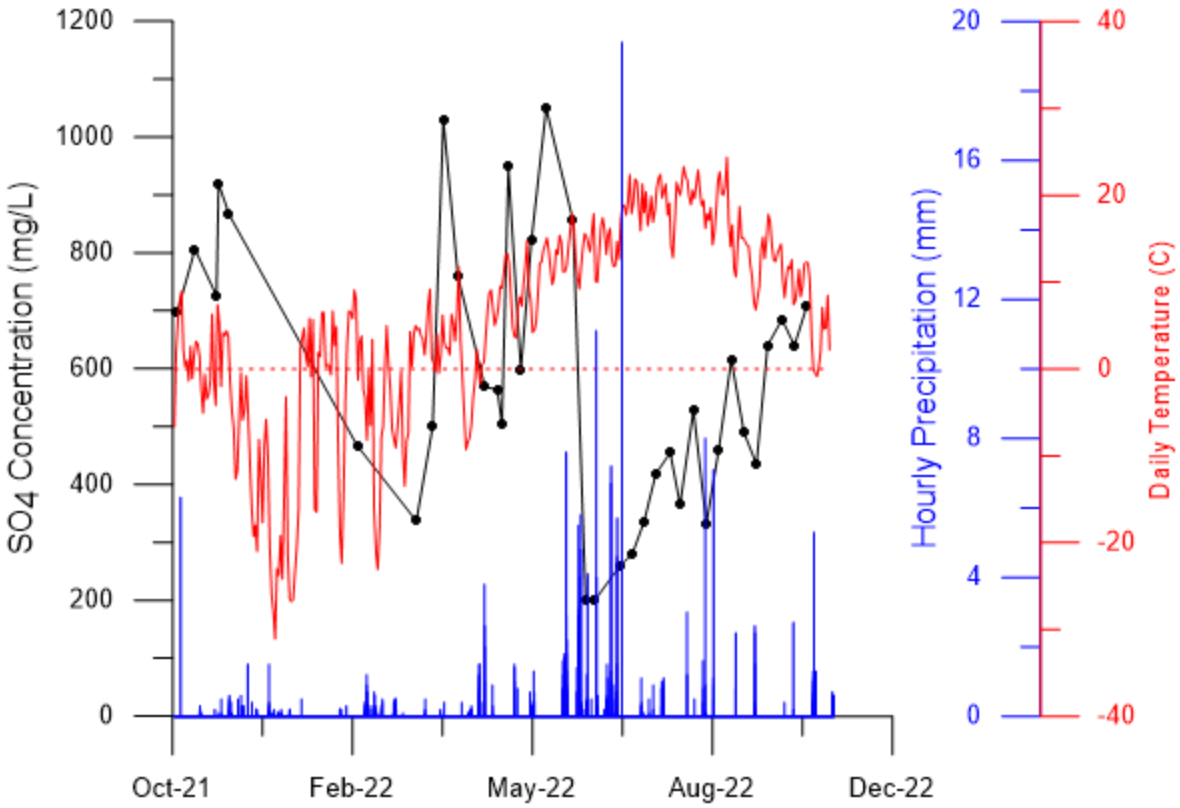

Figure 2 - Sulfate concentrations measured at the outlet of Pond E (PE-BERM) from October 2021 to October 2022 collected by YYC. Daily average air temperature and hourly precipitation is included. Data set also includes a snowmelt event that occurred in January 2022 as well as a series of rainstorms in June and July of 2022.

Figure 3 - Photo of Pond E taken June 22 2021 looking towards the northeast. The pond water has visible discoloration and elevated turbidity.

Figure 4 - Photo of Pond M taken July 12, 2021 looking west by northwest. The pond has taken on an opaque blue/black coloration and smelled of hydrogen sulfide at the time the photo was taken.

Chapter 2 – Manuscript

2.1 – Introduction

Stormwater ponds are a ubiquitous element in stormwater infrastructure. These ponds are designed to handle intense precipitation events by impounding stormwater and slowly releasing it over time. By reducing storm flows, pond outflows can be brought down to levels that are within the safe operating parameters of downstream infrastructure (Persson & Wittgren 2003). However, these storm flows also bring with them a mix of contaminants that are associated with urban runoff into these ponds. In addition to managing stormflows, these stormwater ponds are also being used as a pre-treatment to reduce contaminant loads to watercourses where these stormwater systems eventually discharge to (Stutter & Lumsdon 2008, Reddy et al. 2021, Yazdi et al. 2021). Urban stormwater contaminants can include nutrients, such as nitrate and phosphorus (Sønderup et al. 2016, Yazdi et al. 2020, Janke et al. 2022), heavy metals (Camponelli et al. 2010, Karlsson et al. 2010, Egemose et al. 2015), and chloride from road salt applications (Marsalek 2003, Semadeni-Davies 2006). These urban contaminants can influence the structure of the pond water column and alter the redox state of the pond water.

Elevated concentrations of dissolved species can introduce density gradients in the pond water column. These density gradients chemically stratify the pond and reduce the efficacy of water column oxygenation through turnover (Koretsky et al. 2011, Martinsen et al. 2019, Ahmed et al. 2022), as well as contribute to short circuiting of storm flows across the stormwater pond, both of which impact hydraulic retention time (Marsalek et al. 2000). Additionally, nutrient loads can contribute to pond eutrophication (Song et al. 2013, Ivanovsky et al. 2018, Janke et al. 2022). Eutrophication reduces water column oxygen by the decomposition of organic matter and decreases light penetration which restricts thermal heating to the upper portion of the water column (Fee et al. 1996). Much like chemical stratification, thermal stratification reduces water column mixing which in turn reduces the oxygen content of the water column, especially the lower portion. Low oxygen conditions impact chemical species stability and solubility by

making conditions more reducing. Heavy metals in the sediment may become mobilized in their reduced form (Camponelli et al. 2010, Karlsson et al. 2010). Phosphorus is more mobile under reducing conditions which can lead to eutrophication in receiving waters (Taguchi et al. 2020, Janke et al. 2022). Previously non-toxic species, such as sulfate, can be reduced to hydrogen sulfide (Ku et al. 2016, D'Aoust et al. 2017, D'Aoust et al. 2018, Chen et al. 2019), which is toxic, flammable, and can damage stormwater infrastructure (Vollersten et al. 2008). Reducing conditions can also arise in cold climates when stormwater ponds freeze over during the winter. Ice cover prevents oxygenation of the water column and has been documented to contribute to the generation of hydrogen sulfide (D'Aoust et al. 2017).

While storm flows can deliver large volumes of chemical species to stormwater ponds, groundwater can also play a role in importing aqueous species into stormwater infrastructure. Stormwater infrastructure is commonly installed below grade where it can readily interact with groundwater that can have a very different chemical composition than stormwater. If the groundwater table is higher than the hydraulic head of a pond or stormwater pipe, groundwater will seep or leak into the pond or pipe. If hydraulic head in the stormwater infrastructure is higher than the groundwater table, stormwater will seep into the ground and interact with the groundwater. This latter scenario has been examined extensively to determine the influence of stormwater on groundwater quantity and quality (e.g. Kidmose et al. 2015, Bonneau et al. 2018, Thompson et al. 2021, McQuiggan et al. 2022, Pophillat et al. 2022). However, studies examining groundwater discharge to stormwater infrastructure through subsurface drainpipes or seepage into stormwater ponds in the context of sulfur cycling have been lacking. Some work has been performed focusing on quantifying groundwater leakage fluxes into storm pipes (Houhou et al. 2009, Shepley et al. 2020) while others focused on identifying groundwater fluxes into stormwater ponds specifically (Corely 2015, Thomas & Lucius 2016, Kim et al. 2019). The above-mentioned studies focused on quantifying groundwater seepage rates into stormwater infrastructure without investigating how groundwater influences stormwater quality.

Similarly, research into the generation of hydrogen sulfide in stormwater ponds is limited. Previous investigations conducted in Ottawa, Ontario showed that hydrogen sulfide generation was correlated with ice cover episodes as well as stratification of the pond water column during the summer (Chen et al. 2019). Other work focused on the microbial kinetics in sulfide generation (D'Aoust et al. 2017, D'Aoust et al 2018) or on possible management techniques to reduce the generation of hydrogen sulfide (Ku et al. 2016). In all of these studies, the role of groundwater potentially influencing the sulfur geochemistry of stormwater has been neglected.

This study investigated the role groundwater can play in influencing stormwater chemistry and geochemical conditions within stormwater ponds by focusing on sulfur cycling. A pair of stormwater ponds at Calgary International Airport (YYC) were selected for investigation where one stormwater pond is known to generate hydrogen sulfide. The objectives were to determine the source of sulfur, the role groundwater could play in contributing sulfur to stormwater, and the transport and fate of sulfur through the stormwater system. The role of groundwater influencing the geochemistry of the second pond and potential effects of receiving sulfur was also investigated to further constrain how sulfur was being cycled in the study area at YYC.

2.2 - Site Description

This study focused on two stormwater ponds (Pond M and E) and connecting infrastructure at YYC (Fig. 1). The first of these ponds is Pond M which has been previously identified as the main source of the hydrogen sulfide generation at YYC. Pond M was built close to the center of YYC property in 2008. It has a wet storage capacity of 48,196 m^3 with a combined wet and dry storage capacity of 168,692 m^3. Pond M was built with a submerged berm separating the pond into a forebay and a rearbay. The forebay allows the settling of suspended solids mobilized during storm events. During the construction of Pond M, native clay rich soil was compacted in lieu of a formal liner system. Pond M receives inflow from three major sources. The first water major source is runoff from portions of the eastern runway along with portions of the

main airport terminal. The second major source is outflow from Pond K. Between Pond M and Pond K, the entire eastern runway is drained during storm events. The third major input is the glycol treatment facility that was built to treat glycol and deicer contaminated water and snow through extensive oxygenation. Treated water is discharged to Pond M annually in preparation for the next deicing season. Pond M has a single outlet with a flow control gate nearby that discharges water towards Pond E to the west.

In addition to generating hydrogen sulfide, Pond M experiences water quality changes throughout the year. During ice cover periods and during the summer, Pond M becomes opaque and takes on a dark grey coloration with noticeable hydrogen sulfide odors (Fig. 4). During low flow periods, this opaque dark water would take on a lighter grey/blue coloration while the smell of hydrogen sulfide would disappear as the water entered Pond E (Fig. 3). These anoxic conditions temporarily disappear during high flow events such as the spring snow melt or from intense summer precipitation. To help combat these anoxic conditions, the Pond M forebay was dredged in September of 2022 and is annually dewatered in late October or early November.

Pond E is located on the western edge of the YYC property. Pond E was completed in 2016 and in contrast to Pond M, was built as a temporary dry pond but it functions more as a wetland with phreatophytes present within the pond. Pond E has a single inlet as well as a single outlet. In addition to outflow from Pond M, stormwater from other parts of YYC enters into the stormwater line between Pond M and Pond E and mix before entering Pond E.

YYC consists of relatively flat, gently undulating terrain with low relief except on the western edge. Here, the low relief of the uplands transition into bluffs that mark the edge of the Nose Creek Valley. Pond E is located at the base of these bluffs, whereas Pond M is in the low relief terrain. Vegetation is dominantly prairie grasses, although phreatophytes such as cattails can be seen in depressions and ditches. The region receives an average annual precipitation of 419 mm between 1981 and 2010, with 129

mm of that falling as snow (ECCC 2010). Most of the rainfall occurs between May and August with snowfall being common in the winter months from November to March (ECCC 2010). Evaporative demand exceeds annual precipitation with annual shallow lake evaporation estimated to be 761 mm (ESRD 2013).

The study area straddles the apparent contact between two glacial till sheets, resulting in a distinct change in surficial geology from east to west across the site. The contact runs approximately north to south along the western main runway (Fig. 5). On the eastern side of the contact is the Crossfield Formation that was deposited by the Laurentide Ice Sheet originating in Hudson's Bay to the east during the last glaciation (Moran 1986). Being derived in part from craton material, the Crossfield Formation contains granitic and gneissic sediments along with silt lenses (Moran 1986). Till material deposited by the Laurentide ice sheet also contains disseminated pyrite (Grasby et al. 2010). On the western side of the contact is the Balzac Formation which was deposited by the Cordilleran Ice sheet and has noticeable amounts of limestone in the till (Moran 1986). The Cordilleran Ice Sheet was sourced from the Rocky Mountains to the west out of the Bow Valley (Utting & Atkinson, 2019). Underneath both till sheets is the Paskapoo Formation which is an interbedded sandstone and mudstone/siltstone formation (Hamblin 2004). Groundwater within and underneath the Laurentide till sheet tends to be dominated by sodium and sulfate due to pyrite weathering whereas groundwater within and underneath Cordilleran till tends to have elevated calcium and bicarbonate (Grasby et al. 2010).

2.3 - Study Methods

2.3.1 – Existing Monitoring Infrastructure and Operations

YYC has an extensive network of groundwater monitoring wells in place as part of previous site investigations and monitoring programs. A number of these existing wells were used to measure site wide groundwater geochemistry as well as better characterize groundwater flow directions over the course of the study period from December 2021 to October 2022. Where possible, well pairs, which consisted of a

shallow (<6 m depth) and deep (>9 m depth) well within approximately two meters of each other, were selected to be sampled and instrumented to help constrain vertical groundwater flow directions. Wells used to examine groundwater influences on stormwater infrastructure in the vicinity of Pond M consisted of a shallow and deep well pair installed near a firefighting mockup area (3D-MW14 and 3D-MW15). Around Pond E such shallow and deep well pairs were unavailable, but wells 3B-MW2 in the bluffs in the east and 3B-MW9 by the pond outlet provided opportunity to examine the horizontal flow directions of groundwater. Other wells across the YYC site were used together with the wells mentioned here to study site wide hydrogeology (Merrett 2022).

YYC as part of their operations carry out surface water and groundwater monitoring across their property. As part of an agreement with the City of Calgary, surface water quality samples are taken weekly at Pond E to monitor potential impacts of discharged stormwater on Nose Creek. Constituents of interest included major ions, dissolved and total metals, and hydrogen sulfide. The outlet of Pond E is sampled and the stormwater outfall into Nose Creek is sampled as well along with portions of Nose Creek itself.

2.3.2 – Groundwater Monitoring

Investigation of groundwater and surface water interactions around Pond M and Pond E required the installation of multiple wells to supplement existing wells present at YYC. Six shallow wells were installed on the north and south benches of Pond M with an additional shallow and deep well pair being installed above Pond M. Another well pair was installed at the north end of Pond E. Deeper wells were drilled using a hollow stem auger to allow the collection of sediment samples and the visual logging of sediment lithology. The balance of the wells were drilled using solid stem augers. All monitoring wells were constructed using 50 mm diameter (2”) schedule 40 PVC and well screens with 0.5 mm wide slots (20 slot) of 1.5 m in length located at the base of each well. Each well also was constructed with a filter pack of medium-coarse sand (10/20 sand) that reached 30 cm above the top of the well screen. Bentonite clay was placed in the borehole annulus above the filter sand up to ground surface to complete and seal off the

well bore. Details about the well lithology, construction details, and well depth are given in Appendix A.

Installed groundwater wells were developed by purging them repeatedly over several weeks owing to poor water level recovery rates. Top of well casing elevations were later surveyed relative to mean sea level (MSL). After development, the shallow and deep well pairs at Pond M, the deeper well at Pond E, as well as a selection of previously installed wells at YYC, were subjected to single well slug/bail tests. Of the well pair installed at Pond E, only the deeper well could be tested since the shallower well was consistently dry during the study period. A 1L stainless steel slug was used for all tests and water levels were monitored using a combination of manual measurements and the use of pressure transducers. Details of the well test analysis and interpretation is given in Merrett (2022).

Seasonal well water levels and Pond E water levels were measured using pressure transducers (Solinst Levelogger 5) set to measure absolute pressure at hourly intervals. In the case of Pond E, the pressure transducer was deployed in a stilling well to reduce noise. Periodically data was downloaded from the pressure transducers and a manual water level measurement, using an electronic water level tape, was recorded to assist in data correction. Absolute pressure from the non-vented pressure transducers was first corrected for barometric influences on well water levels (Rasmussen & Crawford 1997), and then converted into water elevation using the conversion factor provided by Solinst (Solinst 2022). Water elevations were then adjusted for sensor drift in spreadsheet software by using the manual water level measurements as reference points. The result was well water elevations relative to MSL.

Groundwater samples for water quality were collected in accordance with procedures outlined by ALS Laboratories which performed the analysis. Species of interest in this study were major ions (Ca, Na, K, Mg, Cl, HCO_3, SO_4), dissolved and total iron and manganese, dissolved and total organic carbon, and hydrogen sulfide. Samples that required filtering, such as dissolved metals and dissolved organic carbon, were field

filtered using 0.45 µm membranes on 60 mL syringes. Water samples for metals and major cations analysis were preserved using nitric acid and analyzed using ICP-MS. Major anions were analyzed using ion chromatography. Water samples for total and dissolved organic carbon analysis were preserved using sulfuric acid and were analyzed by combusting the sample and detecting the infrared emission of carbon dioxide. Samples for hydrogen sulfide analysis were field flocculated using zinc acetate and then preserved using sodium hydroxide. Hydrogen sulfide content was analyzed using the gas dialysis automated methylene blue colorimetric method. All samples and duplicates were kept chilled using coolers and ice packs until samples were submitted to the ALS laboratory the same day that they were collected. Temperature, electrical conductivity (EC), oxidation reduction potential (ORP), and pH were measured using a field meter (YSI ProDSS) that was calibrated monthly.

Most groundwater samples were collected using a purge and bail approach where wells were pumped dry using a 12V submersible well pump and then allowed to recover for 48 hours, after which samples were then taken using a disposable bailer according to Yeskis & Zavala (2002). For wells that took less than six hours to recover from purging, low-flow sampling was performed using a peristaltic pump in conjunction with a flow-through cell in accordance to Puls & Barcelona (1996). Pumped water volume and field parameters were recorded in 5 min intervals along with manual water level measurements until field parameter values stabilized and samples could be collected. A different location during each sampling round was selected for duplicates.

Water level monitoring and sampling began in December 2021 after newly installed wells were sufficiently developed. Pressure transducers were deployed as they became available with deployments taking place in December 2021, March 2022, and May 2022. Groundwater was sampled on February 17, 2022, between July 7-8, 2022, and between October 13-14, 2022. Shallow wells installed on the bench of Pond M were only sampled between July 7-7, 2022, due to either insufficient water volumes for sampling or the wells being frozen.

2.3.3 – Surface Water Monitoring

Pond water samples were collected in a stainless-steel bucket. Sampling manhole locations required the use of a sampling boom with a 1L plastic bottle mounted on the end. Sample collection containers were first rinsed with sample water which was discarded. After rinsing, samples were collected, and field parameters were measured. Field parameters were recorded in the same fashion as groundwater samples discussed previously. Water samples were processed and submitted in the same manner as per groundwater samples discussed previously. Surface water samples were collected between July 7-8, 2022, and between October 13-14, 2022. Extra surface water samples were taken during a simulated stormflow event that will be discussed in section 2.3.10. All monitoring locations, both groundwater and surface water, are displayed in Fig. 6 and Fig. 7.

2.3.4 – Stable Isotope Samples

Water samples for stable isotope analysis were collected and processed in accordance with the procedures outlined by the University of Calgary Isotope Science Lab (ISL). Sulfate stable isotope samples were collected in polyethylene bottles that were rinsed prior to sample collection. All samples were kept refrigerated after collection at 4°C until processing. Samples were first vacuum filtered using 0.45 µm nitrocellulose filter membranes. Subsamples for water stable isotope analysis were collected using disposable pipets after filtering and approximately 1.5 mL was transferred into small glass vials for submission to ISL. The rest of the filtered sample was acidified to a pH of 2 using 5M hydrochloric acid (ISL - Sulfate). Next, saturated barium chloride solution was added to precipitate barium sulfate. Where sulfate concentrations were to be estimated, barium chloride was added in excess to ensure all sulfate had reacted. The precipitate was vacuum filtered and collected on the filter membranes and was rinsed multiple times using warm deionized water. The filter paper was then placed in a glass vial and allowed to air dry. Due to elevated turbidity in surface water sampling locations, sulfide stable isotope samples were filtered in the field using 0.45 µm nitrocellulose filter membranes, placed in rinsed 125 mL amber bottles with zero head space, and stabilized using cadmium acetate (ISL – Sulfide). Bottles were then stored refrigerated

and kept dark until processing. Sulfide stable isotope samples were then vacuum filtered and silver nitrate solution was added to the collected cadmium sulfide to form silver sulfide. Filter papers were placed in glass vials and allowed to air dry. For sulfate concentration estimates, vials and filter papers were weighed together (Ohaus Ranger) and compared against an unused filter paper in an unused vial. Barium sulfate mass was converted into sulfate mass, which in turn was divided by sample volume to get an estimated sulfate concentration.

Barium sulfate precipitate was then weighed into metal cups for analysis. Samples for sulfur stable isotopes were weighed into tin cups and samples for oxygen isotopes of sulfate were weighed into silver cups. Barium sulfate was thermally decomposed and analyzed by ISL. All stable isotope results are reported in delta notation relative to their respective standards. Sulfur stable isotopes ($\delta^{34}S$) were measured relative to the Canyon Diablo Troilite (CDT) standard. Oxygen stable isotopes for both sulfate and water ($\delta^{18}O$) were measured relative to the Standard Mean Ocean Water (SMOW) standard.

2.3.5 – Sediment Sampling

Sediment core samples were taken from both Pond M and from Pond E. Two 25 mm diameter (1”) cores were taken from Pond M using a gravity corer during a low water period in November 2021. Three 50 mm diameter (2”) sediment cores were taken from Pond E by directly pushing the core tubes into the pond bottom in March 2022. Core tube ends were promptly sealed with plastic wrap and electrical tape after collection. Core samples were refrigerated at 4°C until they were processed. One Pond M sediment core was processed for scanning electron microscope (SEM) analysis and was divided based on observed sediment coloration and texture. The other Pond M sediment core was divided into approximately 15 cm segments used for porewater extraction and subsequent stable isotope analysis. Pond E sediment cores were processed similarly but were instead divided into 2 cm segments for sulfate isotope analysis. Samples from undisturbed portions of the Pond E sediment cores were

collected for SEM analysis. SEM analysis was performed by Dynamic Imaging Laboratory – SEM.

Sediment samples from each core segment were placed into 60 mL centrifuge tubes that were then loaded into a refrigerated centrifuge (Kendro Biofuge D-37520) and spun at 4500 revolutions per minute (RPM) for 30 minutes at 4°C. Extracted porewater was then poured off into clean polyethylene bottles and refrigerated until processed. Porewater extracts were prepared in accordance with the sulfate stable isotope procedures previously documented and analyzed by ISL.

2.3.6 – SEM Sample Preparation

SEM samples were collected from the Pond M sediment core and from Pond M surface water. Sediment samples had small portions removed and placed on clean tins to dry. Dried samples were ground up using a mortar and pestle and placed in glass vials for analysis. Pond M water samples were left chilled in a refrigerator for approximately 60 days to allow settling of precipitate. Some particulate matter remained in suspension after the 60-day period. Suspended particulates were vacuum filtered and collected on a 0.45 µm filter membrane. The Pond M water sample was then partially discarded to allow filtering of the settled material. Settled sample was collected in the same fashion as the suspended material on a separate filter membrane. Filter papers for both suspended and settled material were placed in glass vials and allowed to air dry. SEM analysis was performed by Dynamic Imaging Laboratory - SEM on both the sediment samples and the filtered material.

2.3.7 – Water Column Measurements

Water quality measurements were collected using a field meter (YSI ProDSS) that was lowered from a dinghy to various depths to determine water column structure in the forebay and rearbay of Pond M. The forebay water column was measured in two locations, one on the east end closer to the inlets and one on the west end towards the submerged berm (Fig. 6). The rearbay water column was profiled at a single location approximately in the middle. Measurement depths of 0.5 m, 1.5 m, and 2.5 m were pre-

measured and marked on the probe cable prior to going out on the water. Once the approximate measurement location was reached, the probe was lowered into the water to the premarked depths and allowed to equilibrate over the course of approximately five minutes at each depth and at the pond bottom. Bottom water quality measurements were made by letting out the probe cable until the probe reached the bottom.

Collected water column profile measurements were then used to determine whether Pond M was stratified. For thermal stratification, a common metric of 1°C difference between surface water temperature and bottom water temperature was used (McEnroe et al. 2012, Song et al. 2013, Martinsen et al. 2019). To determine chemical stratification, a threshold of a change in density between the top and bottom waters exceeding 0.25 kg/m^3 was used which is equivalent to a density change in water between 24°C and 25°C (McEnroe et al. 2012, Ahmed et al. 2022). TDS content of pond water was determined by correlating field measured EC values with laboratory measured TDS values. Using TDS and temperature for both top and bottom waters, a density difference was calculated using standard methods for TDS and temperature (APHA 2012). Details for density calculations are given in Appendix B.

2.3.8 – Water Budget Calculations

Water budgets were calculated for both Pond M and Pond E from May 2022 to October 2022. This time interval was selected because Pond E water elevations started being measured in May 2022 and were stopped in October 2022 due to the pond starting to freeze over. The water budgets were calculated assuming that the change in storage for both ponds over the time period was negligible. While this assumption may not hold true during high flow periods where surface water inflows may exceed surface water outflows, Pond E water levels at the beginning and the end of the monitoring period were similar, indicating relatively little change in storage. This logic was extended to Pond M. When the change in pond storage is negligible, a water budget can be calculated using the following with water inputs equaling water outputs:

$$GW_{in} + SW_{in} = GW_{out} + SW_{out} + ET \quad (1)$$

where GW_{in} and SW_{in} are groundwater and surface water inputs respectively, GW_{out} and SW_{out} are groundwater and surface water outputs respectively, and ET is evapotranspiration. Both the outlets of both Pond M and Pond E were instrumented for flow monitoring prior to the start of the water budget time period, but the Pond E inflow and only one of the Pond M inflows was similarly instrumented during the water budget period, necessitating calculation of the surface water inputs as residual water volumes to balance the water budget.

Pond inflow and outflow measurements were collected using sondes (Starflow QSD SDI-12) capable of measuring both depth and index velocity. Flow rate measurements and calculations were performed by Baseline Water Resources Inc who also provided flow monitoring telemetry. Water depth measurements were calibrated in the laboratory, but index velocity measurements were not calibrated. Volumetric flow rates were calculated by multiplying the measured index velocity by the cross-sectional area of the stormwater pipe occupied by water based on depth. Cross sectional area (A) occupied by water was calculated using two formulae, depending on depth. When depth was less than or equal to the stormwater pipe radius (R), the following equation applied:

$$A = \frac{R^2(\theta - \sin\theta)}{2} \quad (2)$$

where θ is the angle formed between two lines that radiate from the center of the pipe to where the water surface touches the pipe walls. Θ is calculated using the following equation:

$$\theta = 2\cos^{-1}\left(\frac{d-R}{R}\right) \quad (3)$$

where d is the measured water depth (m). In situations where water depth was greater than the radius of the stormwater pipe, the equation to calculate cross sectional area was modified to the following:

$$A = \pi R^2 - \frac{R^2(\theta - \sin\theta)}{2} \quad (4)$$

Actual ET estimates were calculated using the Penman-Monteith equation (Monteith 1965) with some modifications (UN FAO 1998). ET was estimated coming off the pond

water body only and not the surrounding land surface, so the ground heat flux was assumed to be zero. Also, since Pond M is not vegetated, stomatal resistance was set to zero. The same assumption was applied to Pond E even though it is partially vegetated. While this will lead to an underestimate of ET for Pond E, the underestimate is likely minor since ET would be more influenced by radiation forcings than transpiration of vegetation. Meteorological data such as temperature, windspeed, and solar radiation were obtained from a meteorological station installed within two kilometers of both ponds (ECCC 2022). Details about input parameters used and parameter estimates where meteorological data was lacking can be found in Appendix C.

Estimates of groundwater contributions were performed using Darcy's Law:

$$Q = -K_{sat} A \frac{\Delta h}{\Delta l} \quad (5)$$

where Q is the volumetric flow rate (m^3/s), K_{sat} is hydraulic conductivity (m/s), A is the cross-sectional area that groundwater is flowing through (m^2), $\Delta h/\Delta l$ is the hydraulic gradient along the groundwater flowpath. All K_{sat} estimates were obtained by using the Hvorslev analysis method on single well tests as part of a separate study (Merrett 2022).

The change in hydraulic head at the bottom of Pond M was calculated using the water elevation difference between PM-NE3D and PM-NE3S since PM-NE3S was completed at approximately the same elevation as the bottom of Pond M. The underlying assumption with this approach is that the hydraulic conditions at the well pair are similar to the hydraulic conditions found at the bottom of the Pond M forebay. The bulk K_{sat} used was taken as the harmonic mean of the K_{sat} estimates for the two wells from a separate study (Merrett 2022). The hydraulic gradient was taken to be the change in hydraulic head between PM-NE3S and PM-NE3D divided by the vertical distance between the top of the well screen at PM-NE3D and the bottom of the well screen at PM-NE3S. The cross-sectional area that groundwater is assumed to be seeping through was taken to be the bottom area of the Pond M forebay.

Since vertical hydraulic gradient data were not available round Pond E, flow estimates were based on horizontal flow only. Groundwater inputs were assumed to be exclusively along the eastern bank since groundwater elevations to the east of Pond E (PE-NE1D and 3B-MW2) were higher than measured pond water elevations. Groundwater outputs were assumed to be exclusively along the western bank since the groundwater elevation on the western side of Pond E (3B-MW9) was lower than the measured pond water elevations. Hydraulic gradients for each side of Pond E were calculated by comparing the pond water level with the well water levels for each respective side. Estimated K_{sat} for each respective well were used for the portion of pond bank they were closest to. 3B-MW9 represented the western bank in its entirety. 3B-MW2 represented the southern portion of the eastern bank while PE-NE1D represented the northeastern portion. Cross sectional area for groundwater fluxes were estimated by calculating the area along the banks that was below the Pond E water elevation at the time of measurement and assumed a flat bottom to the pond.

2.3.9 – Near-Surface Geophysical Survey

A Geonics EM31 was employed to evaluate near-surface soil EC. Both Pond M and Pond E were surveyed around the pond perimeter with measurements being taken every second at approximately one meter above ground surface. The instrument was operated in normal vertical dipole mode and used a coil separation of two meters. Pond M was first surveyed in December 2021 with a second survey completed in March 2022 to evaluate potential seasonal changes in soil EC. Pond E was surveyed in March 2022 for data completeness. Survey EC data were then imported into mapping software (ArcGIS) and were interpolated using empirical Bayesian kriging under ordinary kriging with a spherical semi-variogram model.

2.3.10 – Storm Flow Simulation

As part of operational procedure at YYC, effluent from the glycol treatment facility is released toward the end of summer in preparation for storing and treating water contaminated with glycol generated during the upcoming fall and winter seasons. This release period provided the opportunity to examine the impacts of a simulated storm

event on surface water chemistry in the stormwater drainage network. To maintain water quality during the simulation, releases were spread out over a three-week period. Releases commenced on August 23, 2022, and were completed on September 13, 2022. Sampling was conducted prior to the releases to establish baseline conditions, during the releases to examine water quality impacts of displaced water from Pond M, and after the releases to determine the new state of stormwater quality. Sampling started at Pond M, PM-E specifically, and moved progressively downstream to the outlet of Pond E or PE-BERM. Released water was directly discharged into the forebay of Pond M (PM-E). Displaced pond water and simulated stormwater flowed through the forebay and over the submerged berm (PM-BERM) where it entered the rearbay. Water in the rearbay flowed out of Pond M at the outlet toward Pond E (PM-O). The released water entered Pond E (PE-I) and flowed over a riprap apron to the pond body (PE-RIPRAP). After flowing across Pond E (PE-T), released water encountered a riprap berm (PE-BERM-E) where it either flowed through or around the berm to the outlet (PE-BERM).

Water quality samples collected during the storm flow simulation included sulfate, hydrogen sulfide, and water isotopes. Of the samples that were collected during the storm flow simulation, hydrogen sulfide stable isotopes could only be taken at Pond M surface water locations (PM-E, PM-BERM, PM-O) as well as the inlet of Pond E (PE-I) due to insufficient hydrogen sulfide for stable isotope analysis at the rest of the Pond E locations. While the sampling location for the Pond M outflow is presented as PM-O in this work, it was originally labeled as PM-MH1 during sample collection.

2.3.11 – Sulfur Diffusion Mass Flux Estimates

Pond M sediment data suggested a significant gradient in sulfate concentrations in forebay sediment porewater. Therefore, estimates of the sulfate mass flux into the base of the Pond M forebay were calculated using a modified version of Fick's first law of diffusion:

$$F = -D^* \frac{\Delta C}{\Delta x} \quad (6)$$

where F is the mass flux of the species of interest (kg/m^2*day), D* is the effective diffusion coefficient (m^2/day), and $\Delta C/\Delta x$ is the concentration gradient (kg/m^3*m). The effective diffusion coefficient (D*) is determined by multiplying the free water diffusion coefficient (D) by a unitless tortuosity factor to account for solute movement around sediment grains instead of freely diffusing through water (Fetter 2001). Diffusion coefficients ranged from 1×10^{-9} to 2×10^{-9} m^2/s with a tortuosity factor of 0.5. The sulfate mass flux was then multiplied by the estimated bottom area of the Pond M forebay to obtain an estimated mass flux of sulfate into Pond M per day. Additionally, estimated sulfate concentrations with respect to depth in the Pond M sediment core were also used to calibrate a 1D diffusion model based on the Ogata-Banks solution (Ogata 1970). Details for modeling sulfate concentrations with depth are given in Appendix D.

The estimated sulfate diffusion flux into Pond M was also compared against estimated sulfate exports out of the pond in surface water. For surface water contributions, an assumed constant sulfate concentration of 500 mg/L was multiplied by the volumetric flow rate for a given measurement interval to estimate total sulfate mass being exported. These individual sulfate masses were summed to estimate the total sulfate flux leaving Pond M in surface water from May 2022 to October 2022. Diffusion fluxes of sulfate into Pond M were calculated similarly with daily sulfate mass fluxes being multiplied by the number of days in the same time period and added together. Assuming an average sulfate concentration in Pond M surface water will lead to an overestimate of the total mass of sulfate leaving the pond since sulfate concentrations in Pond M vary temporally due to dilution effects from precipitation events. Additionally, the mass flux estimate is only applicable to diffusion alone and neglects advection. While advection could increase the sulfate mass flux into Pond M, it is presumed to be negligible owing to the low hydraulic conductivity of the clay till in the vicinity. Despite this limitation, such analysis is still useful for relative fluxes of sulfate into Pond M.

2.4 – Results

2.4.1 – Water Levels

Throughout the monitoring period, groundwater flowed from the firefighting area (Wells 3D-MW14 and 3D-MW15) towards Pond M (Wells PM-NE3S and PM-NE3D) (Fig. 8). This implies that the region around the firefighting area serves as a recharge location as evidenced by the difference in hydraulic head between the firefighting area and Pond M. Additionally, water elevations are consistently higher in 3D-MW15, the shallower well, when compared to the deeper well 3D-MW14, indicating a downward flow direction during the monitoring period. The downward hydraulic gradient at these two wells is the strongest during the spring snowmelt period and during intense precipitation events reaching a maximum of 0.19 in the downward direction. While the firefighting area serves as a recharge area for Pond M, it is not likely the only recharge area with areas further to the east also serving as recharge regions for the pond (Fig. 5).

In contrast to the firefighting area, groundwater levels around Pond M in wells PM-NE3S and PM-NE3D show a more muted response to precipitation and snow melt events with vertical gradients reaching a maximum of 0.076 in the upwards direction and 0.070 in the downward direction. Vertical hydraulic gradients at the east end of Pond M show a general trend of groundwater discharge although those gradients vary seasonally. Groundwater flowed upward during snowmelt and precipitation events between March and July before transitioning to flowing downward during the balance of the monitoring period. Regardless of the groundwater flow direction near Pond M, groundwater levels throughout most of the year are higher than the typical operating pond level and indicate a general region of groundwater discharge throughout the monitoring period. K_{sat} around Pond M is low with values ranging from 4.3×10^{-8} to 3.5×10^{-7} m/s (Merrett 2022). K_{sat} values near the firefighting area are similar and range from 6.3×10^{-8} to 2.4×10^{-7} m/s (Merrett 2022). More detailed results for water level responses to snow melt and precipitation events are available in Appendix B.

Groundwater elevations in the uplands to the east of Pond E and to the northeast have consistently higher water levels than the pond surface elevation throughout the monitoring period, implying groundwater flow from the uplands around Pond E towards the pond itself (Fig. 9). In the uplands, groundwater levels increase during the spring snow melt period in late April and during precipitation events in mid-June and early July. After these recharge events, groundwater levels show a general decreasing trend from late July to the end of the study period. This recharge-discharge cycling of groundwater causes groundwater elevations to vary as much as 2.1 m over the monitoring period in the uplands, but these variances are much more muted closer to Pond E. Groundwater levels varied by 0.57 m at the north end of Pond E and 0.61 m at the west side of the pond near the outlet. The well near the outlet of Pond E (3B-MW9) mimics the response of pond water levels during intense precipitation events with an approximate 5 hour lag time in the response, indicating a hydraulic connection between Pond E and the well (Fig. B3). This hydraulic connection, along with consistently higher pond water levels than groundwater levels along the western bank, indicates that some water from Pond E seeps out of the pond into the groundwater along that bank. More detailed results for water level responses to snow melt and precipitation events are available in Appendix E.

While groundwater elevations, and by extension groundwater seepage rates, vary seasonally, the overall contribution of groundwater to pond water budgets were minimal between May 2022 to October 2022 (Table 1). At Pond M, groundwater contributed 0.07% of inflows into the pond with surface water contributing the remaining 99.93%. The groundwater contribution is likely an underestimate since groundwater flux calculations did not account for preferential flow in the weathered till closer to surface, which would allow higher near surface groundwater flow rates when compared to more intact till at depth. In the context of the total water budget, preferential flow pathways would marginally increase groundwater contributions to Pond M since it is unlikely that groundwater inputs would meet or exceed the surface inflow volume. However, there exists the possibility that during low flow periods that groundwater inputs through these preferential flow pathways could be comparable to surface inflows. ET at Pond M

represented 5.6% of water export with the balance of the outgoing water (94.4%) being surface water. Groundwater outflow at Pond M was assumed to be non-existent since Pond M appears to be a region of groundwater discharge. Groundwater also represented a smaller contribution to the water budget than surface water at Pond E (Table 1). Groundwater inflow into Pond E represented 0.8% of the total inflow, with surface water being the remaining 99.2%. ET at Pond E contributed to 4.0% of the water outflow and was higher than the estimated groundwater outflow which contributed to 0.8% of the total outflow. Surface water contributed the rest of the outflow at 95.2%. Overall, both stormwater ponds appear to be dominated by surface water flows during precipitation events with groundwater contributing to the water budget in a minor fashion.

2.4.2 – Water Quality

While groundwater may contribute minimally in terms of water volumes to the overall water budget of both ponds, there is a potential for outsized impacts on surface water quality due to the composition of groundwater near the ponds. Groundwater major ion concentrations were greatest in the vicinity of Pond M with sulfate and sodium being the dominant ions (Fig. 10). The largest sulfate concentrations were observed on the benches around the wet storage area of Pond M (Fig. 11), ranging from 5,260 mg/L on the north bench to 24,900 mg/L on the south bench. Sulfate concentrations decreased with depth in the vicinity of Pond M where concentrations decrease as much as 2,100 mg/L on average over 3.5 m from the bottom of PM-NE3S to the top of the screen at PM-NE3D. As groundwater flows towards Pond E from the uplands, sulfate concentrations also showed a decreasing trend (Fig. 12). Sulfate concentrations of 2,970 mg/L to 3,140 mg/L in the uplands decreased to a range of 1,890 mg/L to 2,010 mg/L closer to the eastern bank. Sulfate concentrations decreased significantly on the western side of Pond E where they fell within the range of 454 mg/L to 655 mg/L, likely due to surface water seeping into the subsurface and diluting sulfate. Concentrations of sulfate and other major ions, as well as analytical uncertainty, are given in Appendix F.

2.4.3 – Sulfur Distribution

The EM31 survey that was conducted around Pond M showed regions where there was elevated soil EC. Soil EC is the highest on the south bench with highly conductive regions approaching the pond bank (Fig. 13). High soil EC is also present along the west bench of Pond M and in the northeast corner. Low conductivity areas are those regions that contain infrastructure, such as buried stormwater pipes that can be seen in the southwest corner, or soil with low TDS content which can be seen in the center of the north bench and in areas on the east bench. Because groundwater around Pond M is dominated by sulfate, high EC regions indicate areas where sulfate concentrations are high as well. Results for the Pond E EM31 survey are given in Appendix G.

High sulfate concentrations were also encountered in the sediment beneath Pond M. Estimated sulfate concentrations below Pond M rapidly increased with depth, increasing from an estimated 580 mg/L at the sediment water interface to 11,000 mg/L at 45 cm depth (Fig. 14). This trend loosely follows a modeled diffusion curve and implies that groundwater flow into Pond M through the bottom is diffusion controlled (Hendry & Wassenaar 2000). By applying Fick's first law of diffusion, the estimated sulfate mass flux was 8.9 kg/d to 17 kg/d diffusing into the Pond M forebay. This is likely an underestimate since the model assumed a constant vertically upward hydraulic gradient and as such, represents an ideal case because hydraulic gradients varied in magnitude and direction over the study period. Under diffusion alone, groundwater does not appear to contribute a significant quantity of sulfate to the Pond M forebay (Table 1). Overall, diffusion accounts for 1,410 kg to 2,700 kg of sulfate entering Pond M. In contrast to diffusion inputs, an estimated 165,000 kg of sulfate left Pond M in surface water flows during the study period. This implies that diffusion alone cannot account for the mass of sulfate leaving Pond M and that another source of sulfate is required to address the discrepancy.

No diffusion curve was present in the Pond E sediment core samples (Fig. F5). Estimated sulfate in the upper portion of the sediment core varied from 940 mg/L at the sediment-water interface to 1,700 mg/L at 8 cm depth. At 10 cm depth, sulfate

concentrations increased to 3,900 mg/L and then decreased to 3,200 mg/L at the bottom of the core.

2.4.4 – SEM Analysis

Sediment core from Pond M displayed three distinct horizontal layers (Fig. H2). The top layer, about 15 cm thick, consisted of organic rich, loosely consolidated stormwater sediments with a strong sulfur smell. Below the organic rich layer was a thin layer of grey sand about 5 cm thick. Below the sand was water saturated clay till about 25 cm thick. SEM analysis showed that small quantities of pyrite were present in the stormwater sediment deposit (Fig. H1). The sediment core from Pond E also displayed structure with three distinct horizontal layers (Fig. H4). The upper layer was black and organic rich with gravels present and was 6 cm thick. The middle layer was a grey clay and was also 6 cm thick. The bottom portion of the core was a brown clay. Pyrite at Pond E came from within a grey clay portion of the Pond E sediment core about 8-12 cm below pond bottom.

SEM analysis showed that small quantities of pyrite were present at the base of stormwater deposits in the Pond M core (Fig. H1). The pyrite grain located in the sample was framboidal, indicating a biogenic origin (Popa et al. 2004). Pyrite was also found in the core taken from Pond E, but the grain identified was not well formed which could potentially indicate unstable pyrite conditions (Fig. H3). The pyrite grain from Pond E was present in reduced clay. Images of the sediment core samples can be seen in Appendix H.

SEM analysis was also performed on the black particulate matter found suspended within pond M during an anoxic period. Sulfur was abundant in both the settled and suspended particulates. In the settled portion of the material, crystalline sulfur was present with disseminated iron and carbon (Fig. 15). In the suspended portion of the material, sulfur was present in filaments (Fig. 16). Carbon and iron were also present. For both samples iron species could not be resolved by SEM.

2.4.5 – Simulated Storm Flow

The simulated storm flow event allowed the opportunity to investigate how surface water composition in Pond M and Pond E changed in response to the event. Prior to the release of water from the glycol treatment facility, Pond M surface water had a sulfate concentration of approximately 320 mg/L with notable sulfate concentration increases as water entered Pond E where sulfate concentrations increased to 505 mg/L at the Pond E outlet (Fig. 17A). Pond M was elevated in hydrogen sulfide with a peak concentration of 11.3 mg/L measured at the submerged outlet prior to the simulated event. Hydrogen sulfide showed a decreasing trend as water enters in and moves through Pond E to the point where hydrogen sulfide approaches detection limits at 0.0281 mg/L at the outlet. During the release of water from the glycol treatment facility (Fig. 17B), hydrogen sulfide concentrations at Pond M increased and more closely resembled water found at the Pond M outlet, peaking at 14.5 mg/L near the Pond M berm. As water moved from PM-O to the Pond E inlet, hydrogen sulfide concentrations showed a decreasing trend towards a concentration of 2.74 mg/L at the outlet. While surface water hydrogen sulfide concentrations decreased after leaving Pond M, sulfate showed a general increasing trend from the Pond M forebay, where it had a concentration of 338 mg/L, to the outlet of Pond E where sulfate concentrations reached 418 mg/L. After the release was completed (Fig. 17C), sulfate concentrations at all locations stabilized at 460 mg/L on average while hydrogen sulfide concentrations decreased from concentrations during the release to a range between 1.78 mg/L to 0.466 mg/L at all locations except for PM-O, which showed a hydrogen sulfide concentration of 5.85 mg/L. Figures highlighting the evolution of water composition during the simulated storm event are given in Appendix F.

The water column in the Pond M forebay displayed layering after the simulated storm event (Fig. 18). In the forebay water temperature went from an average of 15.1°C at the water surface to an average of 12.7°C at the bottom of the water column, giving a temperature difference of 2.4°C. Similarly, EC went from an average of 1,358 µS/cm at the surface to a bottom water EC that ranged from 1,854 µS/cm near the inlets to 1,530 µS/cm at the forebay side of the submerged berm. The change in EC between the water

surface and the forebay bottom ranged from 172 µS/cm to 496 µS/cm. Changes in EC correlated with a density change of 0.65 kg/m^3 at the east end of the forebay and 0.45 kg/m^3 at the west end of the forebay. Based on the temperature and density differences in the Pond M forebay, both thermal and chemical stratification is present. However, the strength of chemical stratification varies within the forebay with stronger stratification in the eastern portion.

The stratification seen in the forebay was notably absent in the rearbay when the water column survey was conducted. Temperature near the surface of the rearbay was 15.2°C whereas the temperature at the bottom of the rearbay was 14.3°C, giving a temperature difference of 0.9°C. Similarly, EC went from 1,357 µS/cm to 1,347 µS/cm which is effectively no significant change in EC with depth. The density difference between the top and bottom waters of the rearbay is estimated to be 0.13 kg/m^3 which indicates no chemical stratification present. The rearbay did not pass the threshold of 1°C temperature difference between top and bottom water for thermal stratification, but because the temperature difference is close to that threshold, thermal stratification could be present during hot days.

2.4.6 – Stable Isotopes

Sulfate stable isotope results show distinct clustering of different water 'types' (Fig. 19). Groundwater samples surrounding both Pond M and Pond E appear to be distinct from surface water samples with $\delta^{34}S$ values in groundwater samples averaging -11.9‰ and $\delta^{34}S$ values in surface water samples, including samples collected during the simulated storm event, averaging -7.5‰. The exception to the groundwater and surface water sample clusters is the sample from 3B-MW9 which plots in the region occupied by surface water samples with a $\delta^{34}S$ value of -7.7‰, placing it closer to the average surface water sample rather than groundwater samples.

The sulfate isotope samples from the Pond E core display clustering with some shallower intervals and some deeper intervals being more closely related to surface water with the balance of the porewater being more related to groundwater with no clear

correlation with sulfate concentrations (Fig. E5). Near the surface to 0.02 m depth, $\delta^{34}S$ values range from -5.5‰ to -7.9‰ which is similar to the average surface water $\delta^{34}S$ values at the site. From 0.04 m to 0.12 m depth, $\delta^{34}S$ values range between -10.5‰ to -12.8‰, making these intervals more closely related to the average groundwater $\delta^{34}S$ value. From 0.14 to 0.16 m depth, $\delta^{34}S$ values vary from -7.3‰ to -8.6‰, making these intervals more closely related to surface water. At the bottom of the core, at 0.18 cm depth, $\delta^{34}S$ is -11.1‰, making it more closely related to groundwater. While sulfate concentrations display a distinct change 10 cm below the sediment-water interface, there is no such trend with the sulfate stable isotopes. The variance in $\delta^{34}S$ with depth is likely an artifact of requiring the combination of multiple cores to obtain enough porewater sample for analysis.

The Pond M core results differ significantly from groundwater and surface water populations. Sulfate was the most enriched in the heavier isotope in the upper 15 cm interval with a $\delta^{34}S$ value of 17.5‰ with enrichment decreasing with depth to -5.5‰ at 45 cm depth. The difference in $\delta^{34}S$ between the sediment/water interface and the bottom of the Pond M core is 23‰. That number rises to 29.4‰ when comparing the sediment/water interface of the Pond M core to the average $\delta^{34}S$ value in the surrounding groundwater. Both differences in $\delta^{34}S$ indicate a degree of isotope fractionation with processes at play that enrich porewater sulfate in the heavier isotope. Analytical uncertainty for $\delta^{34}S$ values is ± 0.3‰.

By comparing oxygen isotope values in sulfate and water, possible sources of sulfur can be determined (Van Stempvoort & Krouse 1993). $\delta^{18}O_{SO4}$ values showed a larger spread when compared with $\delta^{18}O_{H2O}$ values with distinct sample clusters being visible in the $\delta^{18}O_{H2O}$ values (Fig. 20). $\delta^{18}O_{SO4}$ values ranged from 0.6‰ to -13.9‰ in groundwater samples and from -2.8‰ to -5.3‰ in surface water samples taken at the same time. The Pond M core had $\delta^{18}O_{SO4}$ values ranging from 8.2‰ to 2.7‰ from the top of the core to the bottom. In the Pond E core, $\delta^{18}O_{SO4}$ values ranged from -3.4‰ to -7.6‰ with no clear trend with respect to depth. $\delta^{18}O_{SO4}$ values for the simulated storm event ranged from -4.2‰ to -6.5‰. In contrast, $\delta^{18}O_{H2O}$ values for each sample cluster

had a much tighter spread than the $\delta^{18}O_{SO4}$ values. Groundwater samples had a $\delta^{18}O_{H2O}$ range of -16.7‰ to -19.0‰ whereas surface water samples collected at the same time ranged from -20.8‰ to -21.6‰. The Pond M core had a $\delta^{18}O_{H2O}$ range of -15.3‰ to -15.5‰ and the Pond E core had a slightly larger range of -17.3‰ to -17.9‰. The simulated storm event had a $\delta^{18}O_{H2O}$ range of -14.5‰ to -14.9‰. Clustering of $\delta^{18}O_{H2O}$ is likely due to isotopic fractionation effects that come through the hydrologic processes of evaporation and precipitation which can vary seasonally (Clark & Fritz 1997). Analytical uncertainty for $\delta^{18}O_{SO4}$ values is ± 0.5‰ and analytical uncertainty for $\delta^{18}O_{H2O}$ values is ± 0.25‰.

Stable sulfur isotopes measured during the simulated storm flow event show significant sulfur isotope fractionation (Fig. 21). Within Pond M, $\delta^{34}S$ values were consistently -26.2‰ for sulfide, indicating depletion of the heavier sulfur isotope whereas sulfate was more enriched with the heavier isotope relative to hydrogen sulfide with a $\delta^{34}S$ value of -7.0‰ on average. This difference in $\delta^{34}S$ values effectively disappear when water reaches the inlet of Pond E where $\delta^{34}S$ values in hydrogen sulfide (-7.2‰) more closely resemble $\delta^{34}S$ values found in sulfate (-6.3‰).

2.5 – Discussion

2.5.1 – Pond M Hydrology and Hydrogeology

A confluence of factors contribute to the water quality concerns that exist in Pond M and its associated storm drain system. Water table elevations, both across YYC and local to the ponds, indicate some groundwater discharge into Pond M. Groundwater appears to converge on Pond M from the east and west of the pond (Fig. 8) with flow from the east varying seasonally. This general pattern of groundwater discharge holds true when examining water levels across YYC (Fig. 5), implying that Pond M captures a portion of groundwater flow that was originally thought to generally flow from east to west without such capture (AECOM 2010). Convergent groundwater flow increases the likelihood of groundwater discharging to the surface. Groundwater discharge can be expressed as a surface seep, it can exfiltrate and then evaporate in the shallow subsurface, or it can

seep directly into a water body. Seepage directly into Pond M is minimal because estimated groundwater inputs contribute only to 0.07% of the total inputs into the pond, but because ET is much higher than estimated groundwater flux into Pond M, additional water inputs are required to maintain the apparent constant water level in Pond M during low flow periods since Pond M did not dry out during the study period. There are two possible factors that likely work in concert that explain the water source that is sustaining pond water levels during low flow periods. One such factor is the interaction between groundwater and stormwater infrastructure upgradient of Pond M and the other is secondary porosity influences on groundwater movement around Pond M.

To ensure safe operation of aircraft, runways and taxiways are constructed with storm drainage systems to convey snow melt and stormwater off impervious surfaces. Runoff then gets conveyed though the stormwater system through a series of pipes that are buried in the subsurface which are frequently surrounded with material that is usually more permeable than native soil. This is especially true for the study area where a utility trench with a gravel fill will have a much higher K_{sat} value than that of the surrounding till, creating additional preferential flow paths and creating what some call “Urban Karst” (Bonneau et al. 2017). Buried pipes and their associated utility trenches can interact with groundwater by intercepting groundwater flow (Karpf & Krebs 2013) and the pipes themselves can leak along cracks and pipe joints, allowing exchange between groundwater and stormwater (Bonneau et al. 2018, Shepley et al. 2019, Thompson et al. 2020). There is the potential that groundwater is contributing more to the pond water budget than direct seepage alone, as groundwater could potentially seep into the stormwater network upgradient from either pond, entering Pond M as ‘surface water’ via the stormwater system rather than direct seepage into the pond. Groundwater with elevated sulfate content could potentially seep into the stormwater system above Pond M and that significance will be discussed in Section 2.5.3.

Additionally, water budget calculations were based on K_{sat} estimates from single well tests in intact till. K_{sat} in glacial till can vary with depth over orders of magnitude with higher variance in conductivity values being found close to the surface due to

preferential flow paths (van der Kamp & Hayashi. 2009, Ferris et al. 2020). Higher flow rates near the surface could potentially allow a higher import of groundwater into Pond M through its banks than estimated seepage through the bottom. This would allow the import of sulfate rich groundwater into Pond M, but flow rates would likely be significantly smaller than surface flows from stormwater pipes upgradient of the pond. Due to pond construction methods, preferential flow paths are not likely to be present at the bottom of a storm pond.

Unless a storm pond is designed to allow infiltration into the subsurface, these ponds are constructed with a liner system to limit the seepage of potentially contaminated stormwater into the environment (City of Calgary 2011). Commonly, some form of clay is used to create this liner which is compacted during construction to reduce potential preferential flow paths and reduce hydraulic conductivity (Hendry & Wassenaar 2000). This limits advective transport of dissolved solids and instead, dissolved species move through the liner due to diffusion along concentration gradients. This diffusion mechanism is seen with estimated sulfate concentrations at Pond M roughly following a diffusion curve where concentration increases exponentially with depth (Fig. 14). Even though K_{sat} may be on the order of 7×10^{-8} m/s near the bottom of Pond M, limiting advective transport, concentration gradients are sufficiently high to allow an estimated sulfate flux of 8.9 to 17 kg/d under diffusion alone. This is a small amount of sulfate relative to the volume of Pond M and is likely an underestimate since additional sulfate import mechanisms such as leaky stormwater pipes and preferential flow were not considered during mass flux estimates. However, there is sufficient sulfate being imported into Pond M through a combination of diffusion through the pond bottom and groundwater seepage from the pond banks and stormwater pipes to influence water column structure and encourage bacterial sulfate reduction. Sulfate, and by extension TDS, influences on the structure of the water column in Pond M and the fate of sulfate in the study area will be discussed in a section 2.5.3.

2.5.2 – Pond M Sulfur Sources

Groundwater at most locations in the study area are dominated by sodium and sulfate concentrations in comparison to other major ions (Fig. 10). The elevated sulfate encountered in the vicinity of Pond M is likely the product of processes occurring over a geologic time frame rather than from construction of the pond. Elevated concentrations of TDS seen at Pond M have been documented in similar semi-arid environments where evaporative concentration of dissolved species has occurred since the last glaciation (e.g. Stein & Schwartz 1990, Berthold et al. 2004, Heagle et al. 2013). Evaporative concentration occurs when groundwater evaporates as it approaches or discharges on the land surface (Nachson et al. 2013). As groundwater continues to discharge in these regions, dissolved species concentrations can become quite high. For example, Fennell & Bentley (1998) reported sulfate concentrations reaching as high as 13,500 mg/L in glacial sediments in southern Alberta, while other studies have shown that sulfate concentrations in the prairies can be in the range of 70 mg/L to almost 30,000 mg/L (Grasby et al. 2010, Heagle et al. 2013). Literature values in the upper end of the range are very similar to sulfate concentrations encountered at Pond M where concentrations range from 7,340 mg/L to 24,900 mg/L on the north and south benches. This phenomenon of evaporative concentration since the last glaciation period is likely the main explanation behind the elevated dissolved solids encountered in the vicinity of Pond M.

Sulfate in groundwater around Pond M has two potential sources. One potential source is reduced sulfur and the oxidation of disseminated pyrite grains embedded in the Laurentide till material (Hendry et al. 1986, Van Stempvoort et al. 1994, Grasby et al. 2010). The other potential source is sulfate evaporite deposits formed through evaporative processes at groundwater discharge zones (Fennell & Bentley 1998, Nachson et al. 2013). Sulfate in evaporite deposits was originally sourced from reduced sulfur in the till material but was transported some distance from its origin and underwent multiple precipitation and dissolution cycles with evaporation forming sulfate evaporite deposits containing gypsum or anhydrite. Sulfate formed from evaporative processes, along with the presence of atmospheric oxygen, tend to have enriched

oxygen and causes samples to plot outside the sulfide oxidation field in Fig. 20 (Van Stempvoort & Krouse 1993, Clark & Fritz 1997). Sulfur from both sources can be seen at Pond M in the groundwater and surface water samples. Sulfur from the groundwater around Pond M and underneath its forebay, as well as surface water in the forebay itself seem to be derived from an evaporite source since they plot outside the sulfide oxidation field. Sulfate minerals such as gypsum, which has been encountered where evaporative concentration of sulfate has been going on for long periods of time (Heagle et al. 2013), could provide such a source of sulfate. Because the Pond M forebay and the surrounding groundwater share a similar sulfur source, it is likely that sulfate in the forebay is largely derived from a groundwater source. This is further supported by diffusion processes noted to be active in the bottom of Pond M along with possible leakage of groundwater into the stormwater pipes above the pond.

Not all sulfur near Pond M is sourced from evaporites. While most locations plot outside the sulfide oxidation field and indicate a previously oxidized sulfur source, a small number of locations plot within the sulfide oxidation field, indicating a reduced sulfur source. Two of the locations are wells 3D-MW14 and 3D-MW15, located upgradient of Pond M to the southwest. Precipitation that falls in this area flows vertically downwards toward the water table year-round since water elevations in the shallower of the two wells is consistently higher than the deeper well (Fig. 8). This infiltrating water encourages the direct oxidation of disseminated sulfide minerals in the till which then flow towards Pond M. This direct oxidation of reduced sulfur in the till material is likely the explanation of $\delta^{18}O$ values plotting in the sulfide oxidation field. The other location is PM-N2 which is not sited in such a recharge area, but rather is much closer to Pond M on the north bench. While it is not immediately clear why PM-N2 would plot within the sulfide oxidation field while other nearby wells do not, it is possible that groundwater at that location is more depleted in atmospheric oxygen than other wells in the vicinity.

Sulfate in the rearbay of Pond M shows a different sulfur source than sulfate in the forebay in that it appears to be sourced from the direct oxidation of pyrite (Fig. 20). While it is possible that sulfate in the rearbay could be sourced from oxidized pyrite from

groundwater seeps on the west end of the pond, an internal source of reduced sulfur being exported from the forebay is far more likely. The source of reduced sulfur for the Pond M rearbay likely comes from the oxidation of hydrogen sulfide being exported from the forebay rather than groundwater derived pyrite oxidation products.

There are some limitations in using $\delta^{18}O$ isotope values for water and sulfate to determine sulfur sources. One limitation is that this method cannot distinguish between different forms of reduced sulfur (Van Stempvoort & Krouse 1993), meaning that the oxidation of hydrogen sulfide can produce a similar signal to that of the oxidation of pyrite. Additionally, the boundaries for the sulfide oxidation field described in Fig. 20 are likely to be transition zones rather than sharp boundaries. Samples that are close to the upper boundary may be sourced from a mix of reduced and oxidized suflur. Furthermore, the oxidation field given in Fig. 20 was based on pure pyrite samples in a laboratory setting (Van Stempvoort & Krouse 1993). Because of natural variability in field samples, laboratory results may not fully capture conditions found in the field. Despite these limitations, most of the samples indicate sulfate produced from the oxidation of reduced sulfur rather than potential atmospheric sources.

2.5.3 – Pond M Sulfur Transport and Fate

As discussed previously, groundwater sourced sulfate is likely entering Pond M through a combination of diffusion, potential leakages in the stormwater pipelines upgradient from Pond M, and lateral flow through preferential flow pathways. Diffusion alone cannot account for the stratification seen in the Pond M forebay because diffusion inputs, an estimated 2,700 kg during the study period on the high end, is significantly less than the estimated sulfate surface water export of 165,000 kg during the study period (Table 1). However, diffusion of sulfate and other solutes into the Pond M forebay would slightly enhance stratification because the import of dissolved solids will alter density differences within the pond water column. To account for stratification of the forebay, high TDS groundwater would have to come from either lateral flow through preferential flow pathways, or from leaks in the stormwater pipes above Pond M. Because the distribution of stratification varies spatially within the forebay, with a density difference of

0.65 kg/m^3 at the east end closer to the inlets versus 0.45 kg/m^3 at the west end closer to the submerged berm, the scenario of high TDS groundwater leaking into the stormwater pipes is more likely to contribute the most to stratification. Incoming high TDS water at the Pond M inlets would be denser than the stored freshwater within the pond body and sink down to the pond bottom as it flows in (Marsalek et al. 2000). During low flow periods, denser water would accumulate within the forebay and reduce oxygenation of the water column due to increased resistance to mixing. While pond sediments are typically anoxic (Baldwin & Mitchell 2012, Johnson et al. 2019), lack of mixing and low oxygen conditions in the pond water column would limit the oxidation of hydrogen sulfide and allow for it to persist near the bottom of the pond.

While the diffusion of sulfate into the Pond M forebay may not account for stratification seen within the forebay, it can still account for the generation of hydrogen sulfide. As sulfate diffuses into the forebay sediments, it interacts with microbial populations. Likely anoxic conditions within the sediments encourage the bacterial reduction of sulfate into sulfide (Wiessner et al. 2005, Pester et al. 2012). This bacterial reduction of sulfate preferentially selects lighter sulfur isotopes due to more favorable thermodynamics, with other factors such as temperature or carbon source contributing to how much sulfur fractionation takes place (Canfield 2001a, Canfield 2001b, Canfield et al. 2006). The residual sulfate becomes enriched with respect to the heavier sulfur isotope, which equates to higher $\delta^{34}S$ values for the Pond M core as shown in sulfate isotope data (Fig. 19). Sulfate in the groundwater around Pond M has $\delta^{34}S$ values that range from -11.5 to -13.8‰ which is typical for sulfate generated by pyrite oxidation in this region (Hendry et al. 1986, Grasby et al. 2010). The Pond M sediment core $\delta^{34}S$ values, which range from 17.5‰ near the sediment-water interface to -5.5‰ at the bottom of the core, indicate enrichment of sulfate in ^{34}S due to microbial reduction preferentially reducing sulfate that contains the lighter isotope, ^{32}S. Sulfate within the Pond M water body is slightly enriched in the heavier sulfur isotope with $\delta^{34}S$ values around -8.3 and -8.5‰, likely due to mixing between sulfate enriched in ^{34}S through microbial processes and ^{32}S depleted sulfate in the groundwater entering the stormwater system.

Further evidence of microbial sulfate reduction is seen in the $\delta^{34}S_{H2S}$ values being exported from Pond M. Measured $\delta^{34}S_{H2S}$ values were consistently -26.2‰ within Pond M and at the outlet whereafter it increased to -7.2‰ at the Pond E inlet (Fig. 21). This stands in contrast with the surface water $\delta^{34}S_{SO4}$ values measured in the sulfate which were consistently between -7.3‰ to -6.5‰ at the same locations. This indicates that microbial reduction of sulfate does not occur in the water column, otherwise the $\delta^{34}S_{SO4}$ values measured alongside the $\delta^{34}S_{H2S}$ values would be more enriched in the heavier isotope. This further indicates that bacterial reduction of sulfate is occurring within the sediments of the Pond M forebay. Taking the difference between the $\delta^{34}S_{SO4}$ values found in the upper portion of the Pond M core and the $\delta^{34}S_{H2S}$ values from the pond water results in a sulfur isotope fractionation of 43.7‰ which is close to the reported upper limit of bacterial sulfur isotope fractionation (Canfield 2001a). Additionally, because the $\delta^{34}S_{SO4}$ values did not change from Pond M to Pond E while $\delta^{34}S_{H2S}$ values increased, the oxidation of hydrogen sulfide did not necessarily directly produce sulfate.

While anoxic conditions can exist in Pond M, the entire water column is unlikely to be anoxic. Atmospheric mixing by wind interactions at the pond surface can oxygenate the upper portion of the water column. Organisms in this upper portion can then oxidize the hydrogen sulfide, or it simply reacts with and consumes dissolved oxygen as sulfate is formed (Chen & Morris 1972, Avetisyan et al. 2019). This in turn can depress oxygen concentrations closer to the water surface and favour the formation of elemental sulfur rather than sulfate during the oxidation of hydrogen sulfide (Avetisyan et al. 2019). Crystalline sulfur settles out of suspension after some period with filamentous sulfur remaining in suspension for longer periods (Fig. 15, Fig. 16). It is possible that some sulfide reacts with dissolved iron present in the water column to form iron sulfide nanoparticles that can contribute to the black colouration of Pond M during anoxic periods (Noël et al. 2020), but higher image magnification than what SEM provides would be required to resolve them if they were present. This suspended sulfur increases water turbidity and can remain in suspension for prolonged periods of time (Lyn & Taylor 1992). Due to the increase in turbidity, light penetration into Pond M decreases and enhances thermal stratification (Mazumder & Taylor 1994). Suspended sulfur and

dissolved hydrogen sulfide, along with the rest of the sulfate present in Pond M, subsequently gets transported along the stormwater line and encounters multiple mixing locations that encourage further oxidation of sulfur species. As hydrogen sulfide transits the storm water line, it can oxidize by reacting with the concrete pipe and corroding it, forming sulfate in the process (Vollertsen et al. 2008). Corrosive oxidation of the concrete pipe, along with oxygenation at mixing zones along the storm line, could produce sulfate and elemental sulfur.

Anoxic episodes at Pond M are periodically interrupted by high flow periods that come from significant snow melt events, heavy rainstorms, and stormwater management operations. Such operations could include the controlled release of water from stormwater ponds upgradient from Pond M due to pond maintenance operations or it could include the release of effluent from the glycol treatment facility. High flow periods decrease sulfate concentrations through dilution and mobilize sulfide rich water downstream towards Pond E (Fig. 17B). Between flushing events, hydrogen sulfide builds up in Pond M forebay due to thermal and chemical stratifying conditions. Due to continual seepage of sulfate into Pond M through diffusion or upstream sources, sulfate also accumulates. This leads to elevated sulfate being measured at the outlet of Pond E (Fig. 2).

High flow periods appear to require a certain threshold to break stratification at Pond M. While sulfate concentrations after the simulated event did become stable across all sampling locations (Fig. 17C), the release was not sufficient to disrupt stratification in the Pond M forebay. Both thermal and chemical stratification conditions were present in the forebay two days after the release was completed (Fig. 18), indicating potential short circuiting of Pond M due to density differences (Marsalek et al. 2000). This implies that during low flow conditions, or even moderate flow events, anoxic and reducing conditions can persist within the Pond M forebay and contribute to hydrogen sulfide generation.

2.5.4 – Pond E

Groundwater flow and geochemistry near Pond E was markedly different than what was encountered at Pond M. Water elevations in the wells to the north (PE-NE1D) and to the east (3B-MW2) of Pond E were consistently higher than pond water elevation during the monitoring period indicating groundwater inflow from the east (Fig. 9). In turn, the well to the west (3B-MW9) had a slightly lower groundwater elevation in relation to Pond E which indicates pond water seeping into the subsurface along the western bank. In contrast to Pond M being a groundwater discharge region, Pond E would be considered a 'flow-through' pond with groundwater entering one side and pond water leaving as groundwater on the other. This is further highlighted by the hydraulic connection between Pond E and well 3B-MW9 (Fig. B3). During an intense precipitation event in June 2022, the water level in Pond E rose to accommodate the incoming flow from its drainage basin. After a lag period, water levels in 3B-MW9 also rose in response to the same precipitation event, closely mimicking the water level response in Pond E. Because Pond E is a flow-through pond in the context of groundwater, contaminants that may be flushed through the stormwater system could still be transported off site as the stormwater infiltrates into the west bank of the pond.

Sulfur in the vicinity of Pond E seems to come from a single source. All the sulfate appears to be derived from the oxidation of reduced sulfur (Fig. 20). While the analytical method does not distinguish between the different forms of reduced sulfur, inferences can be made based on water sources for Pond E. One source of water is the Pond M outflow. As discussed earlier, Pond M exports hydrogen sulfide that oxidizes into elemental sulfur and sulfate as pond water travels to Pond E, providing one source of reduced sulfur to be oxidized and allowing some elemental sulfur to fall out of suspension. The other source of water is groundwater transiting the pond as well as any groundwater that may seep into the storm water network above Pond E. While Pond E is indeed located in the Cordilleran till sheet, the surrounding groundwater does not have the expected calcium and bicarbonate dominated water chemistry (Fig. 10). Instead, it is dominated by sodium and sulfate much like groundwater near Pond M, likely resulting from transport of sulfate rich groundwater to Pond E. While Pond M does

indeed capture some of the groundwater flowing from east to west, it does not capture all the groundwater that flows to Pond E through the Laurentide till sheet, allowing sulfate rich water to reach Pond E through the subsurface and masking the influence of Cordilleran till material on groundwater geochemistry. While till material at YYC is heavily disturbed due to construction activities, weathering of displaced till may not have been occurring long enough to cause a significant shift in groundwater geochemistry when compared to the weathering and evaporative concentration effects that have been operating since the retreat of ice sheets during the Holocene.

2.6 – Conclusions

Groundwater elevations around Pond M indicate that it is a point of regional groundwater discharge and has likely been so for millennia, concentrating sulfate through evaporation. Direct groundwater seepage into the pond contributes 0.07% to the total water budget of Pond M, highlighting its limited contribution when compared to surface water flows. While seepage rates are low into Pond M, elevated sulfate content in the groundwater allows for the diffusion of sulfate into Pond M across the forebay bottom and through leaks of sulfate rich water in the stormwater network above Pond M. Stable isotope results of hydrogen sulfide and sulfate indicate bacterial sulfate reduction in the forebay sediments of Pond M with sulfate being enriched whereas the hydrogen sulfide was depleted in the heavier sulfur isotope. Due to inputs of high TDS groundwater into the Pond M forebay, stratification can occur and reduce oxygenation of the water column, exacerbating hydrogen sulfide generation. Hydrogen sulfide oxidizes into elemental sulfur as it transits Pond M and Pond E, contributing to water turbidity. Evaporative concentration of sulfate is absent at Pond E due to groundwater inflows along the east bank and outflows along the west bank. However, this implies that even when surface outflow at Pond E is restricted, pond water can seep into the ground and migrate off site in the subsurface.

The results show that groundwater can have an outsized influence in stormwater quality even when seepage rates are low, especially when large concentration gradients are present. Groundwater influences can include pond stratification and hydrogen sulfide

generation by bacterial sulfate reduction within pond sediments where sulfate is present. These influences negatively impact stormwater infrastructure performance and highlight the need to characterize groundwater conditions during the design and siting of stormwater infrastructure.

Table 1 – Water and sulfur mass budgets for Pond M and the Pond E water budget between May 2022 and October 2022.

		Pond M		Pond E	
Water		Volume (m^3)	Fraction (%)	Volume (m^3)	Fraction (%)
Inputs	Groundwater	200	0.07	3000	0.8
	Surface water	283200	99.93	375700	99.2
Outputs	Groundwater	N/A	N/A	3000	0.8
	ET	16000	5.6	15100	4.0
	Surface water	270000	94.4	363000	95.2
Sulfur		Mass (kg)	Fraction (%)		
Inputs	Groundwater	1410-2700	0.85-1.6	-	-
	Surface water	162300-163590	98.4-99.15	-	-
Outputs	Groundwater	N/A	N/A	-	-
	Surface water	165000	100	-	-

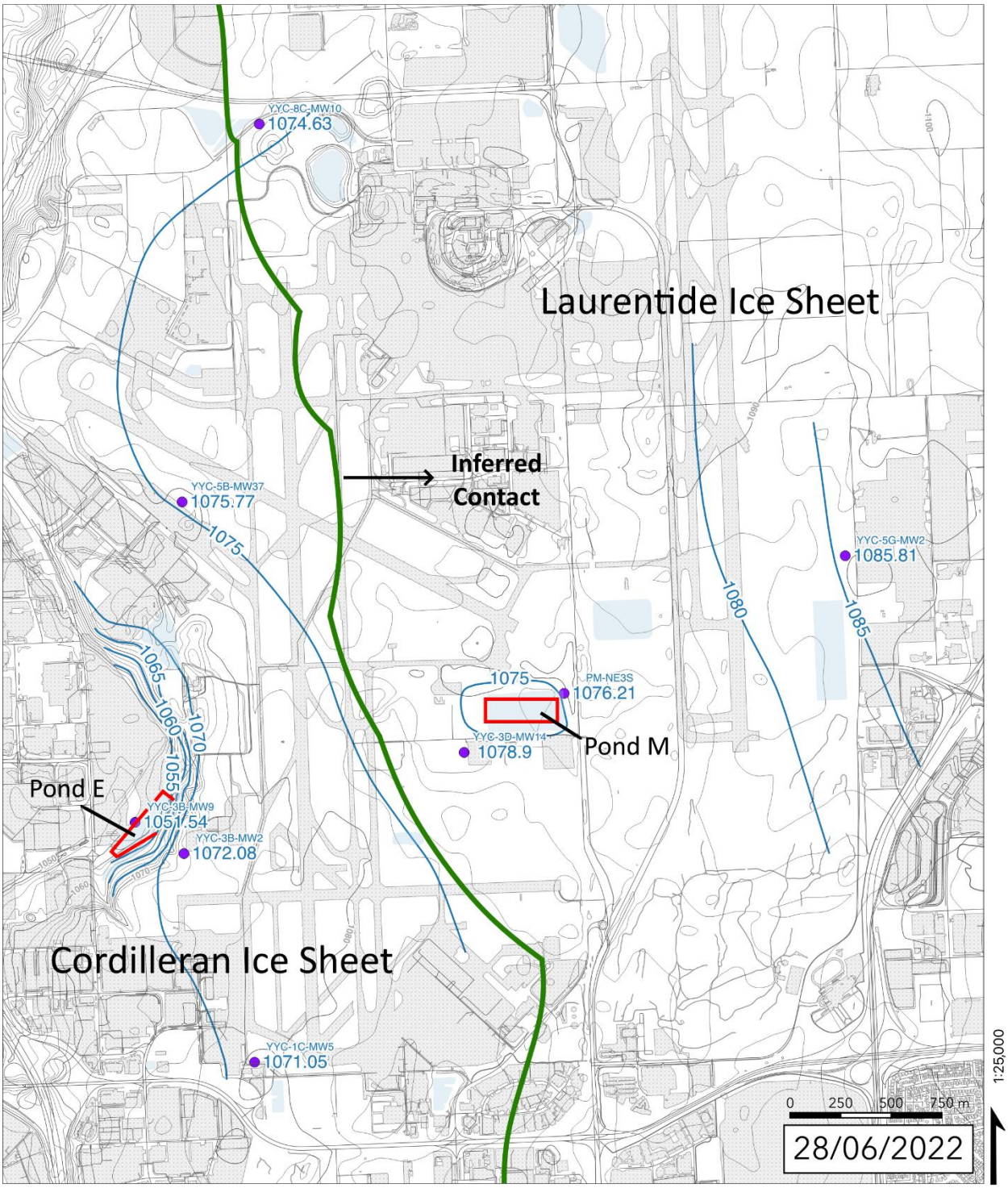

Figure 5 - Regional groundwater levels for YYC. The green line represents the inferred contact between the Cordilleran and Laurentide till material (Moran 1986). Highlighted are the outlines of the Pond M and Pond E stormwater ponds. Water table elevations show that groundwater flows towards Pond M and through Pond E. Modified from Merrett (2022).

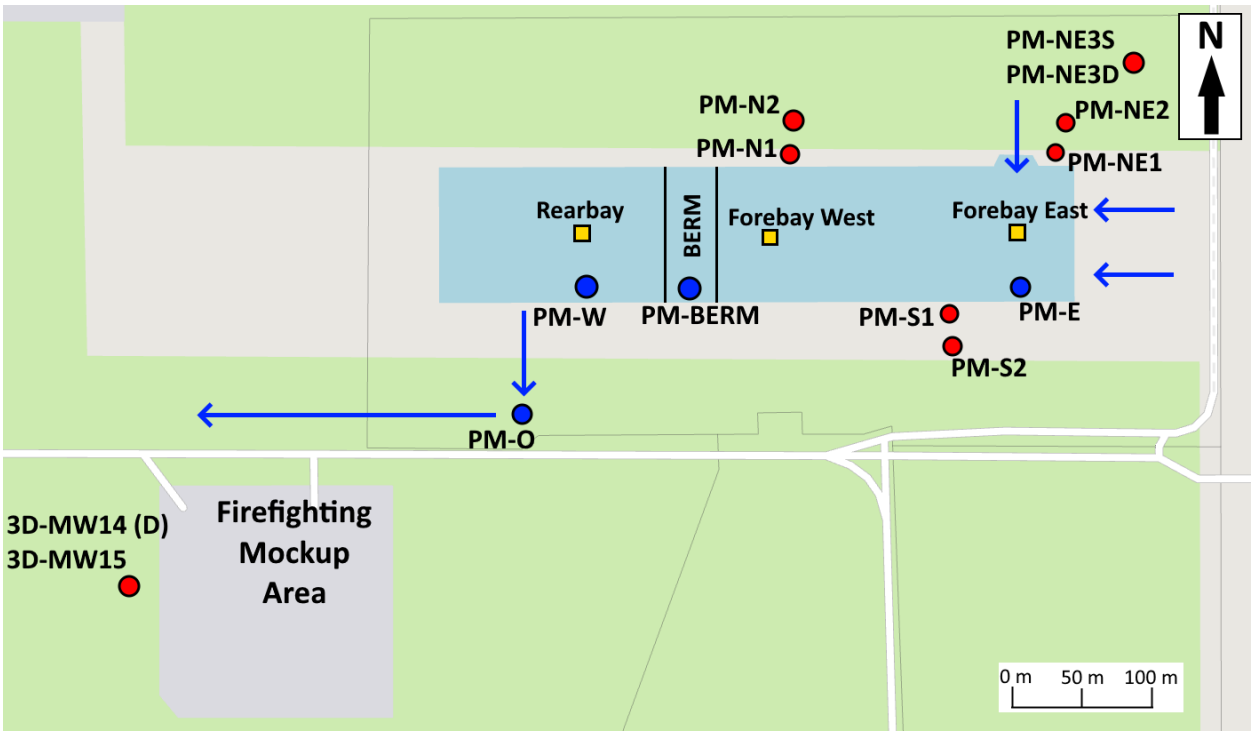

Figure 6 - Sampling locations around Pond M. Red circles indicate groundwater sampling locations, blue circles indicate surface water sampling locations, and yellow squares indicate where water column measurements were made. Arrows indicate where stormwater enters and leaves Pond M. Basemap provided by Open Street Maps.

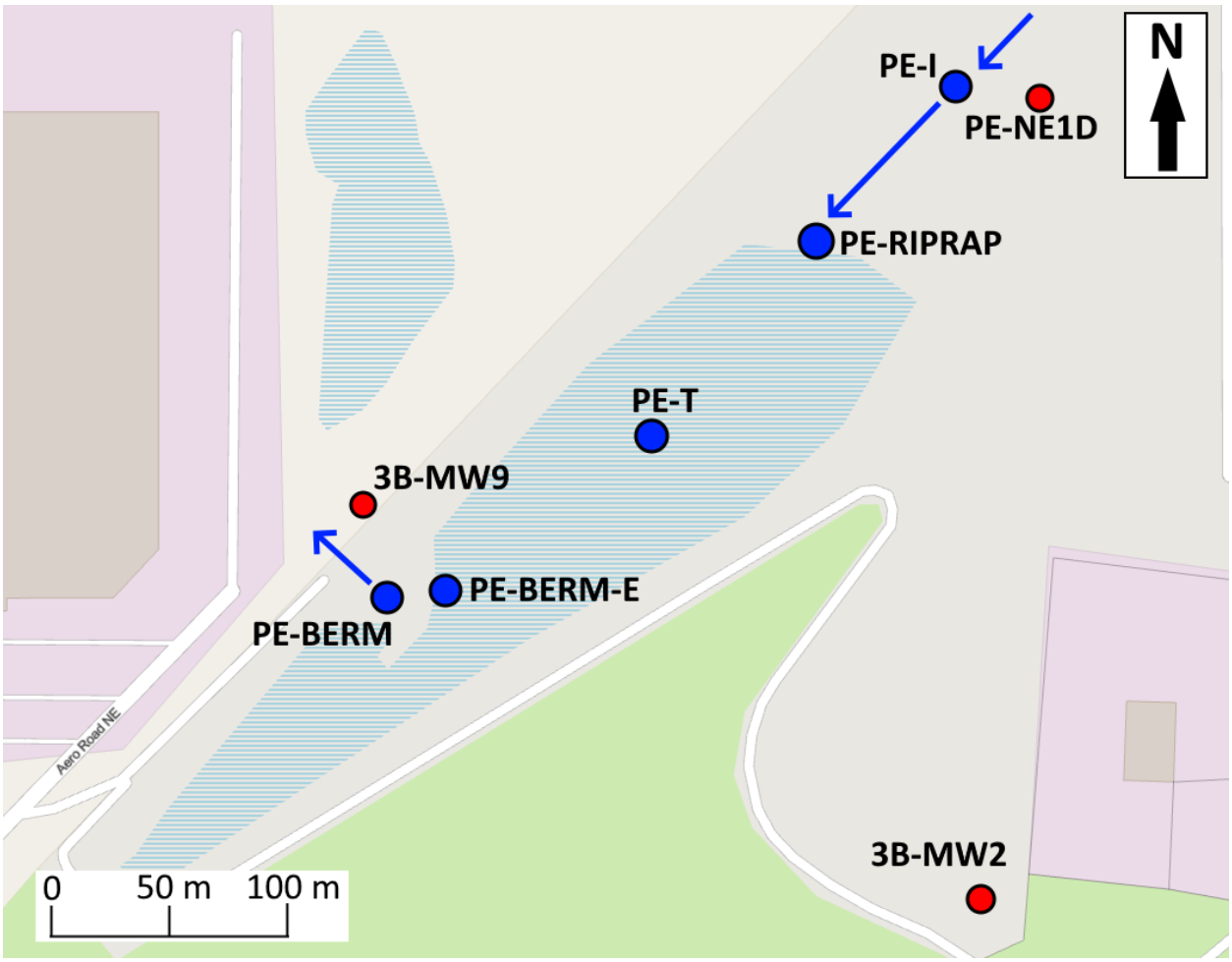

Figure 7 - Sampling locations in the vicinity of Pond E. Red circles indicate groundwater sampling locations and blue circles indicate surface water sampling locations. Blue arrows indicate where stormwater enters and leaves Pond E. Basemap provided by Open Street Maps.

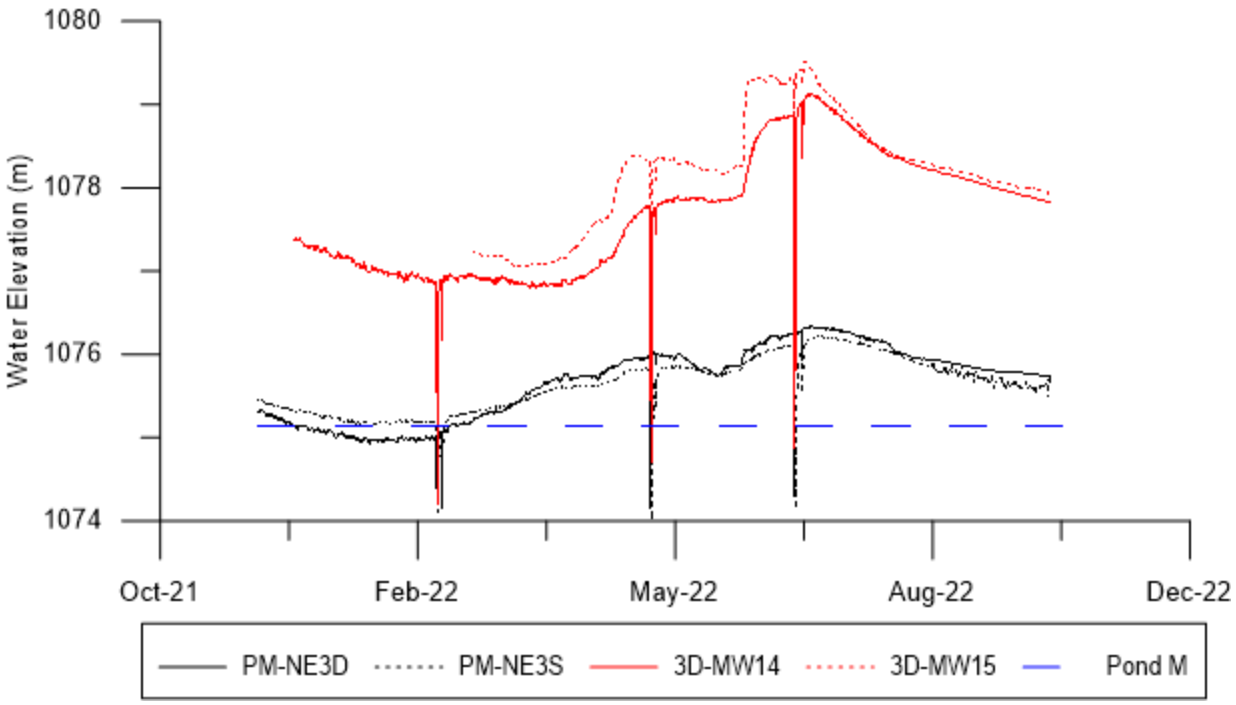

Figure 8 - Well water elevations in the vicinity of Pond M. Well locations are given in Fig. 6. The dashed line is the estimated average operating level of Pond M.

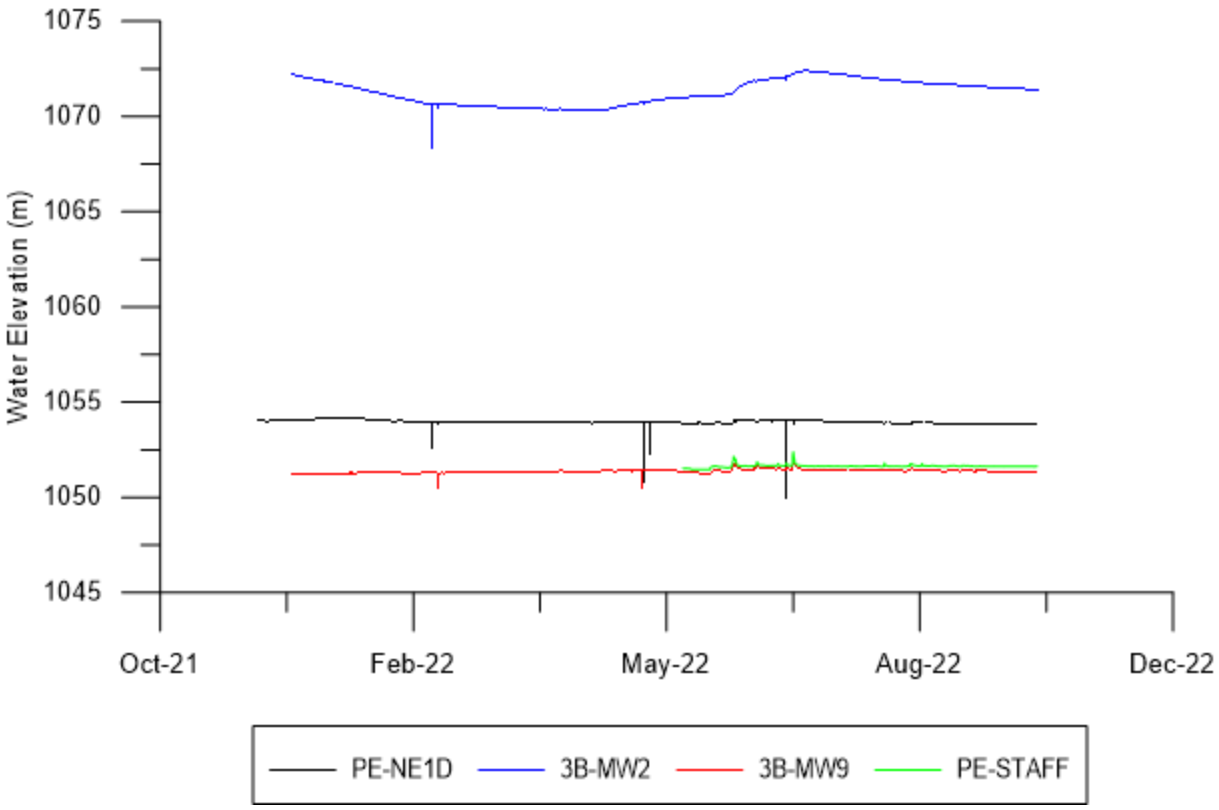

Figure 9 - Groundwater elevations and pond elevations for the Pond E study area. PE-STAFF is the measured pond water elevation.

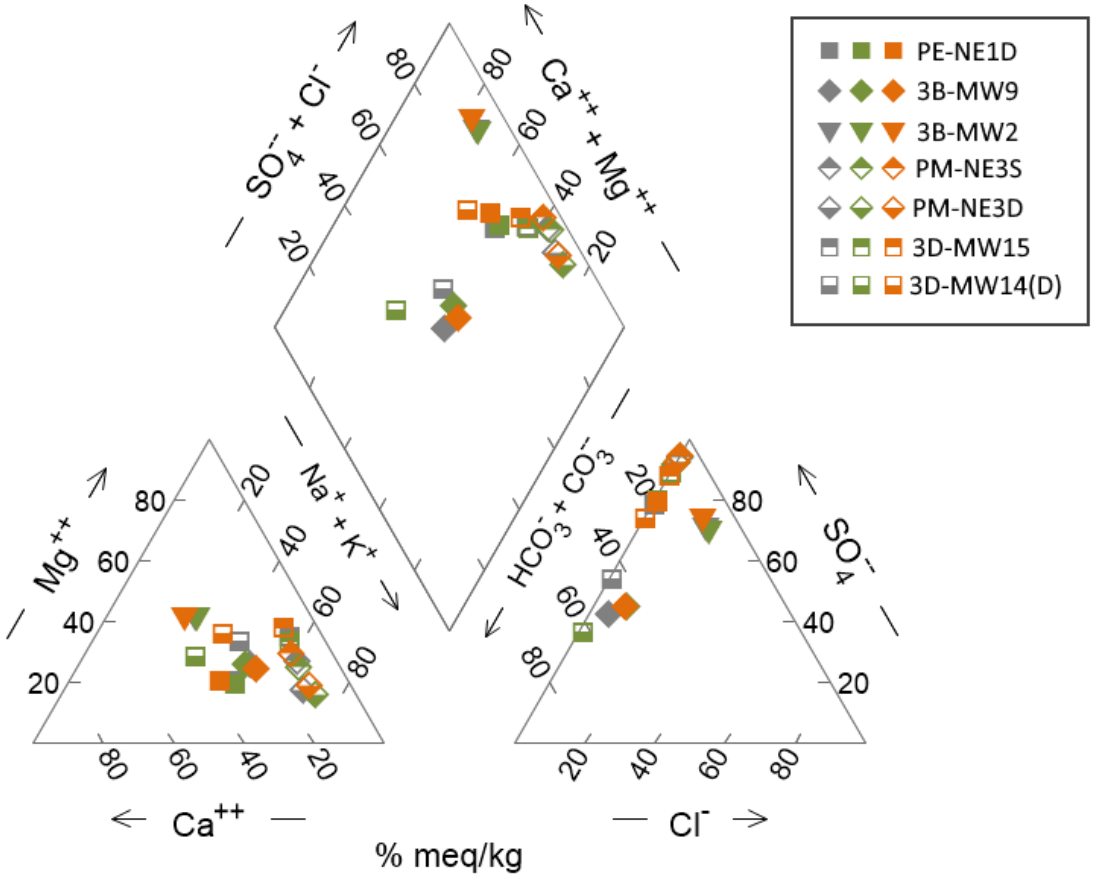

Figure 10 - Piper plot displaying the composition of groundwater during three sampling events. Grey indicates the sampling done on Feb 17 2022. Green indicates sampling completed between July 7-8 2022. Orange indicates sampling completed between October 13-14 2022.

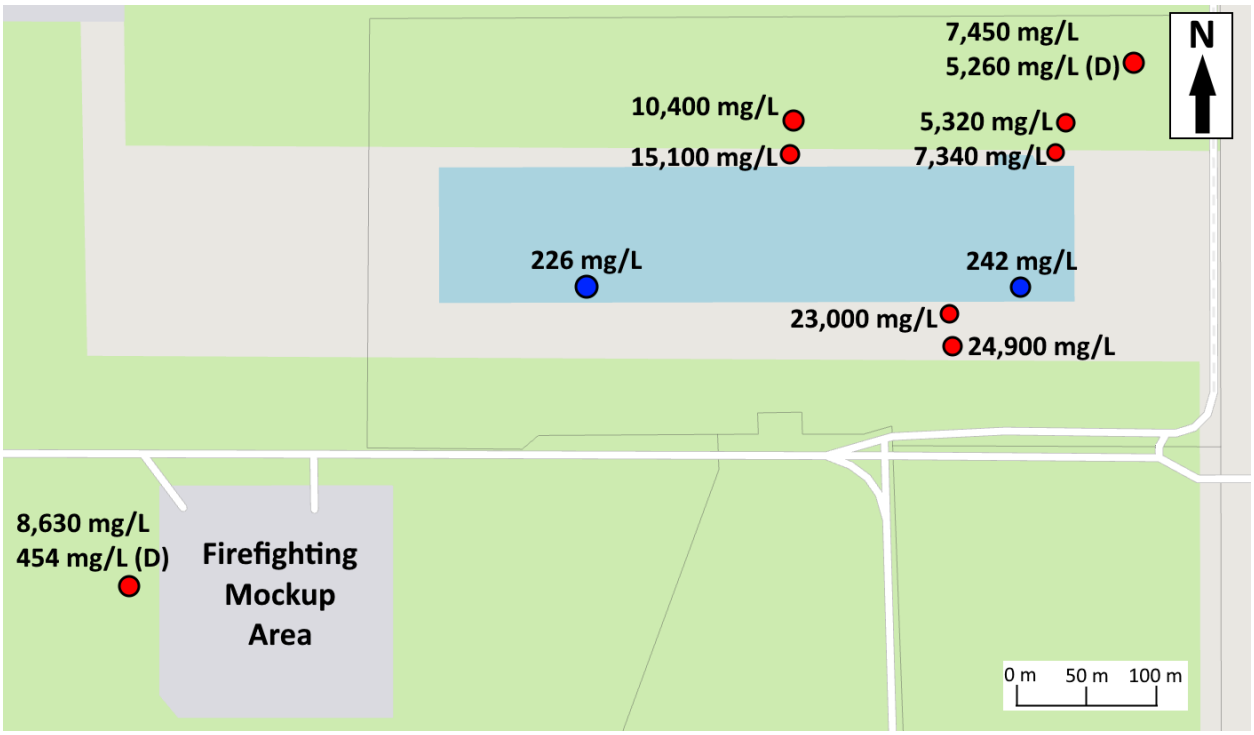

Figure 11 - Distribution of sulfate concentrations around Pond M during the July 7-8 2022 sampling period. Blue circles indicate surface water sampling locations and red circles indicate groundwater sampling locations. Basemap provided by Open Street Maps.

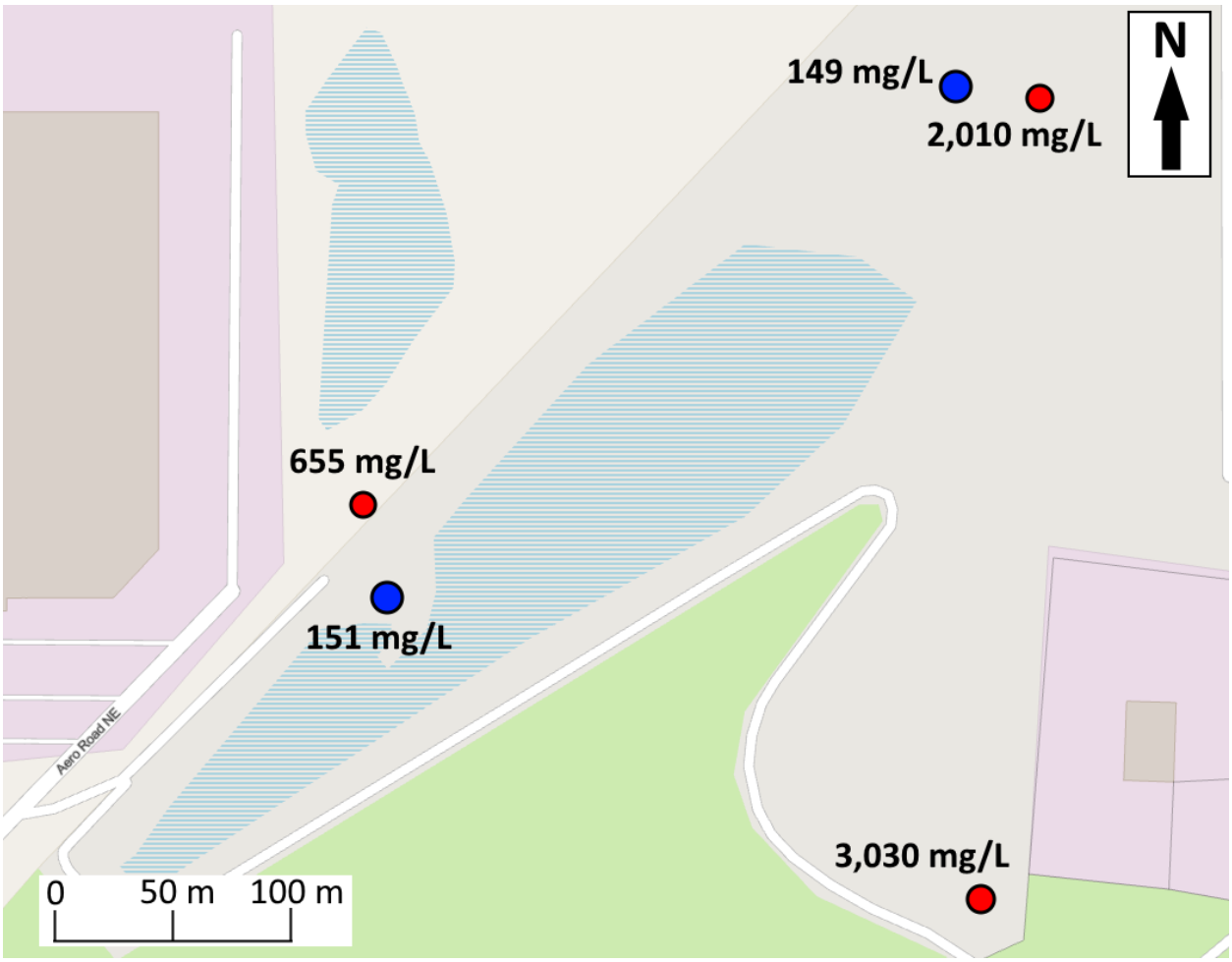

Figure 12 - Distribution of sulfate concentrations around Pond E during the July 7-8 2022 sampling period. Blue circles indicate surface water sampling locations and red circles indicate groundwater sampling locations. Basemap provided by Open Street Maps.

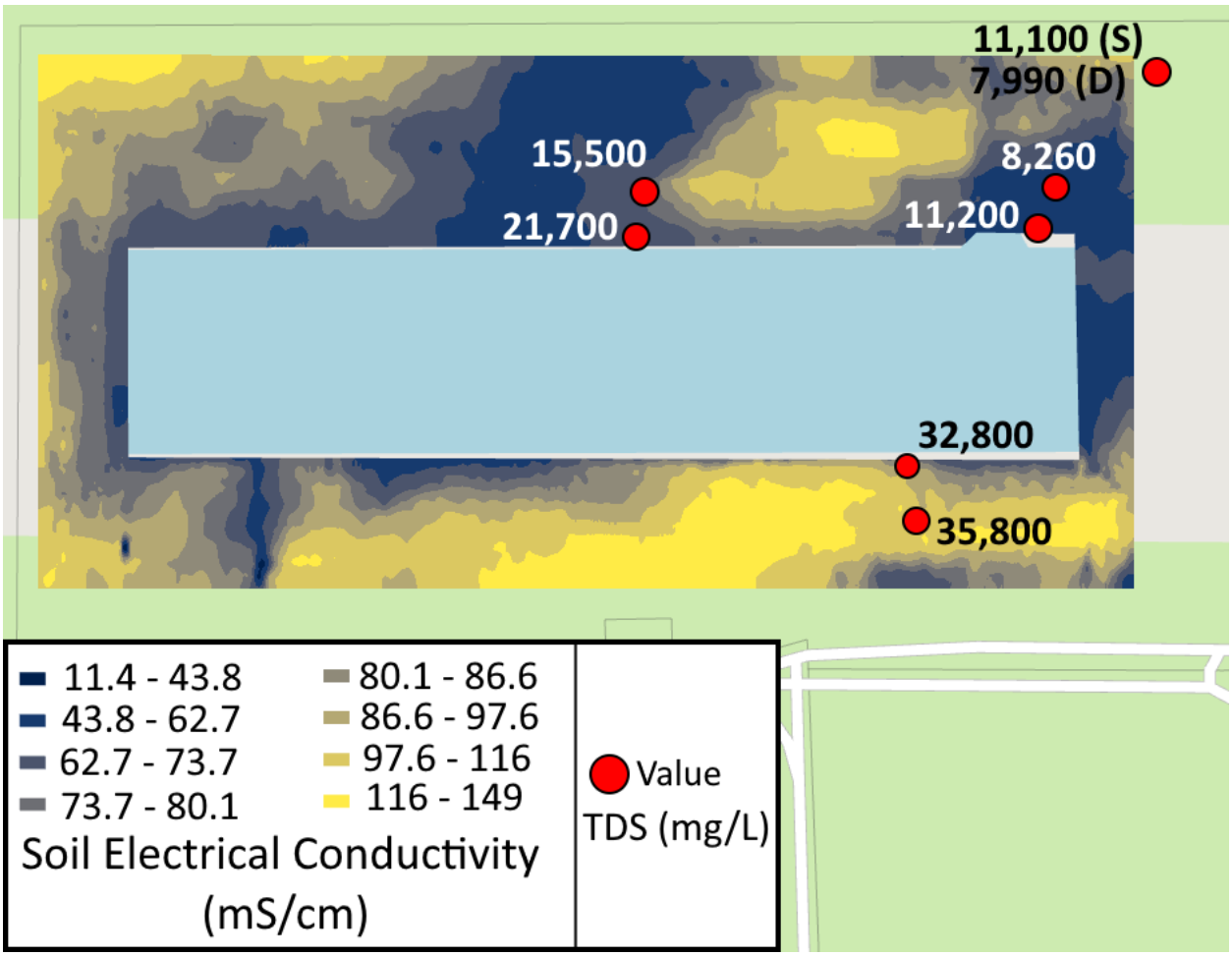

Figure 13 - Interpolated results of the EM31 survey conducted around Pond M in March 2022 along with TDS from the July 7-8 2022 sampling set. The south bench has the largest region of high EC in the survey area which coincides with marshy regions and salt pans. Basemap provided by Open Street Maps.

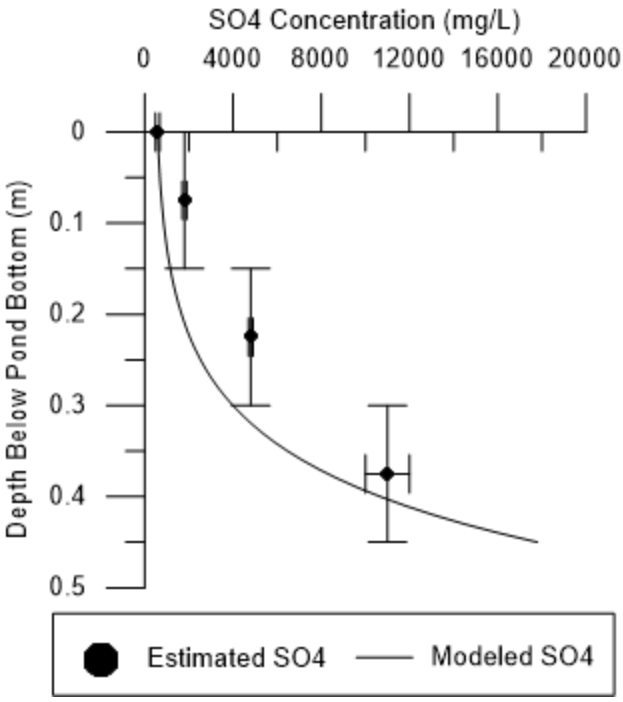

Figure 14 - Estimated sulfate concentration with respect to depth in Pond M sediments. The modeled diffusion curve provides an approximation of sulfate concentrations with respect to depth using the Ogata-Banks solution (Ogata 1970).

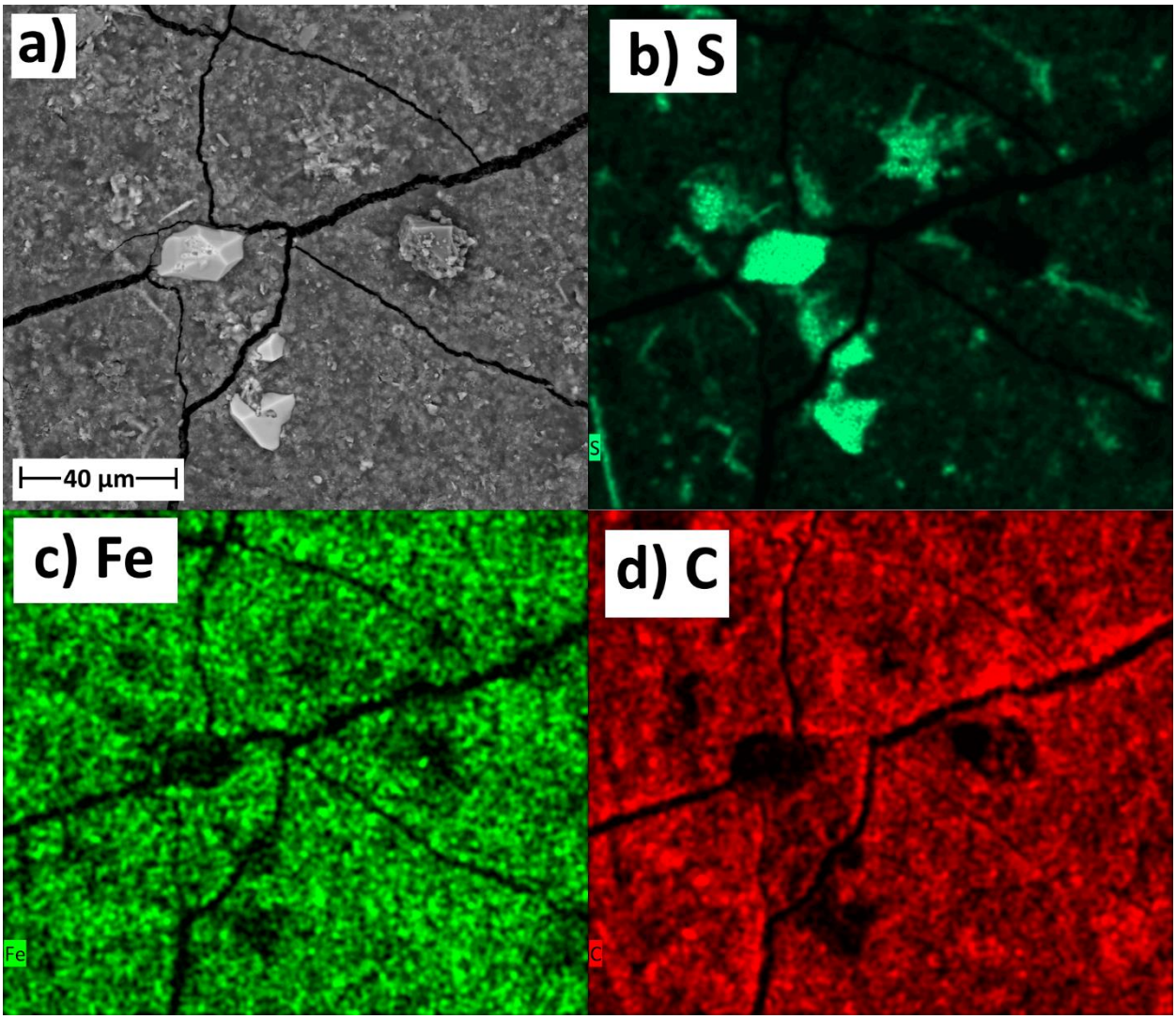

Figure 15 - SEM analysis results on material that dropped out of suspension from a Pond M water sample. A) SEM image displaying crystalline sulfur. B) Sulfur distribution in A. C) Iron distribution in A. Iron is abundant, but notably absent where suflur is present. D) Carbon distribution in A. Iron and carbon more closely relate to each other than sulfur.

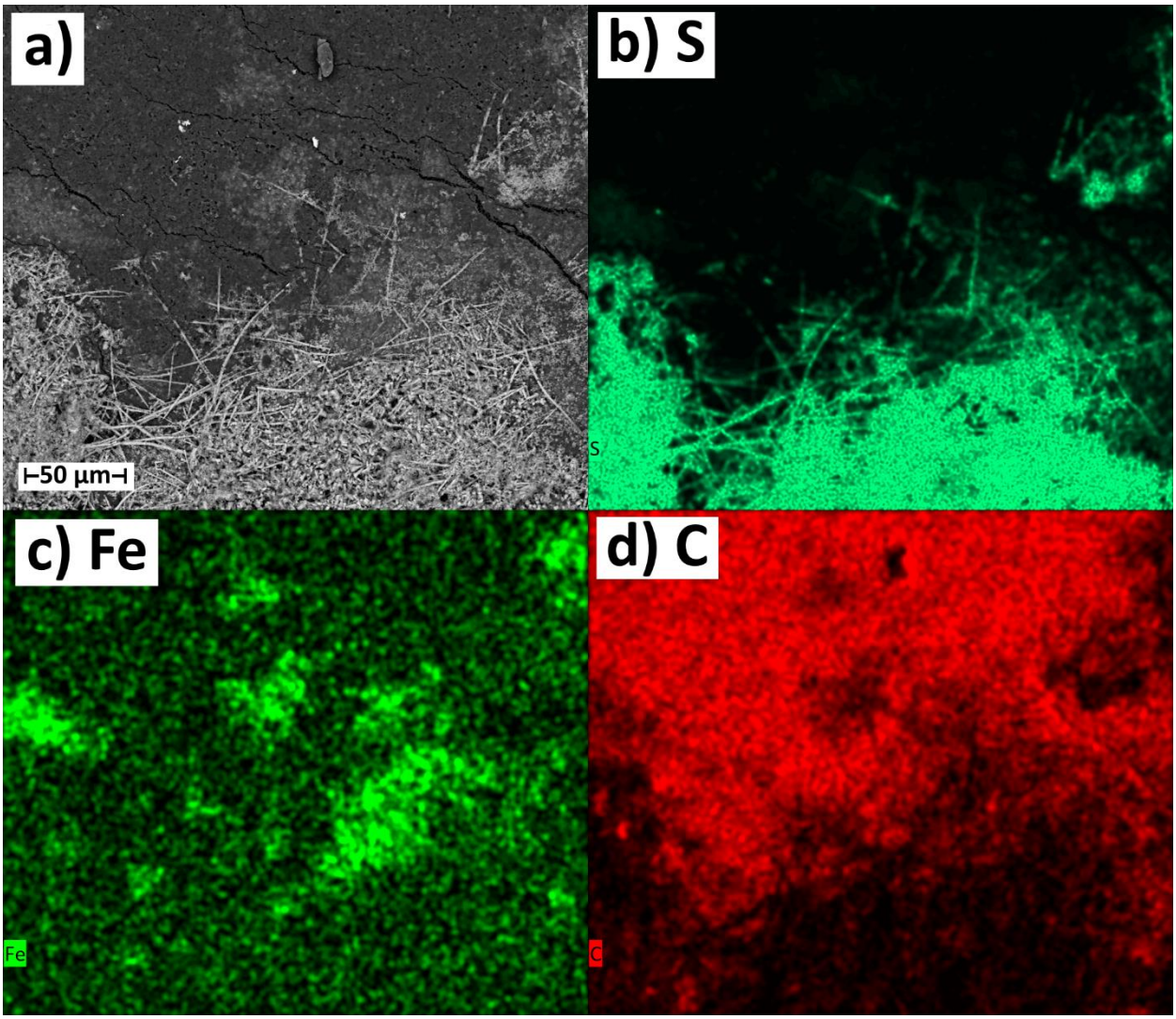

Figure 16 – SEM analysis results on material suspended in a Pond M water sample. A) SEM image showing filamentous sulfur. B) Sulfur distribution in A. C) Iron distribution in A. Iron is less abundant and does not show up where sulfur or carbon is present. D) Carbon distribution in A. Carbon is abundant.

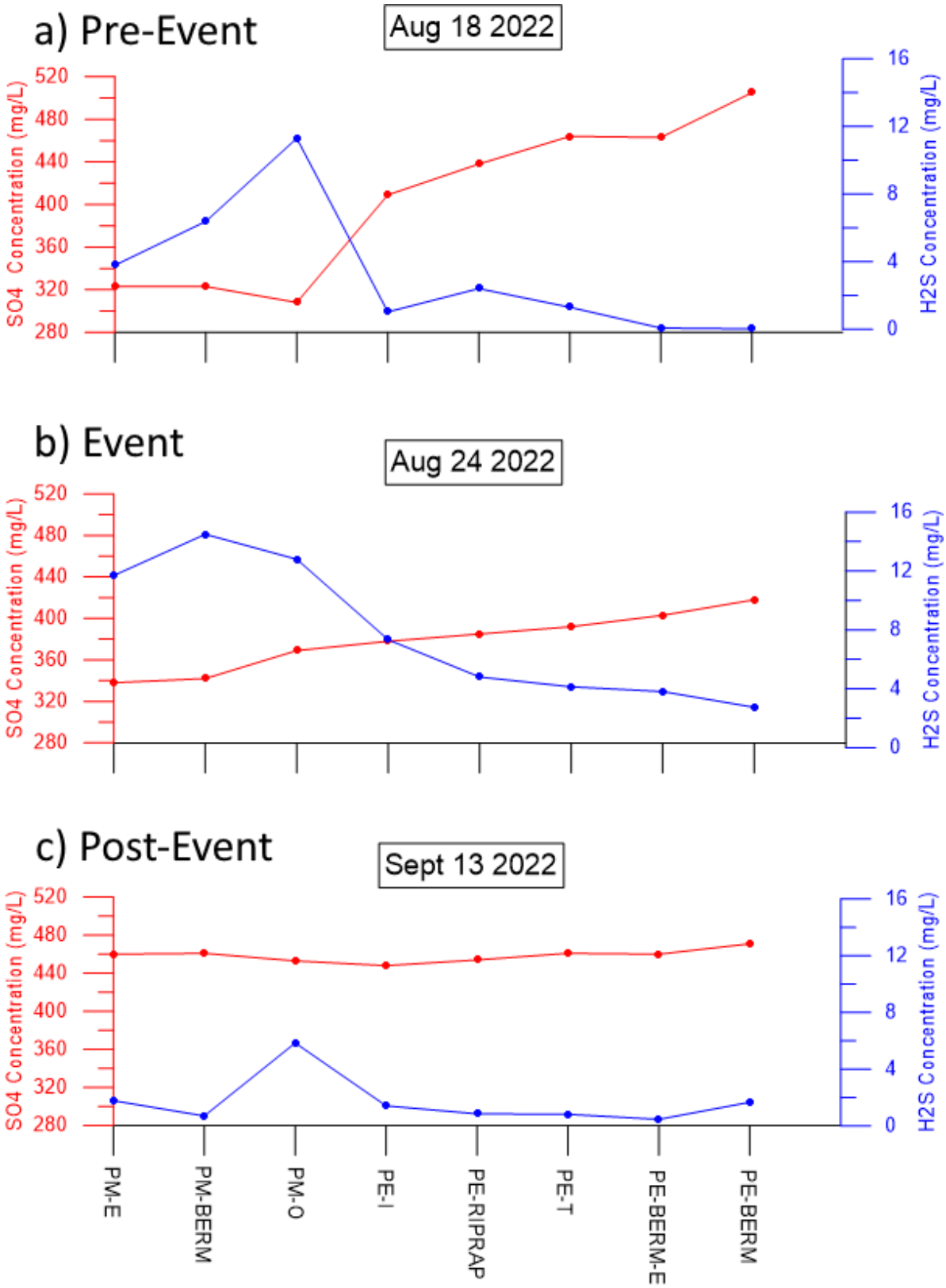

Figure 17 -Sulfate and hydrogen sulfide concentrations during the simulated storm event. Labels on the x-axis represent progressively downstream sampling locations in the storm drain network. A) Pre-Event concentrations. B) Event concentrations. C) Post-event concentrations.

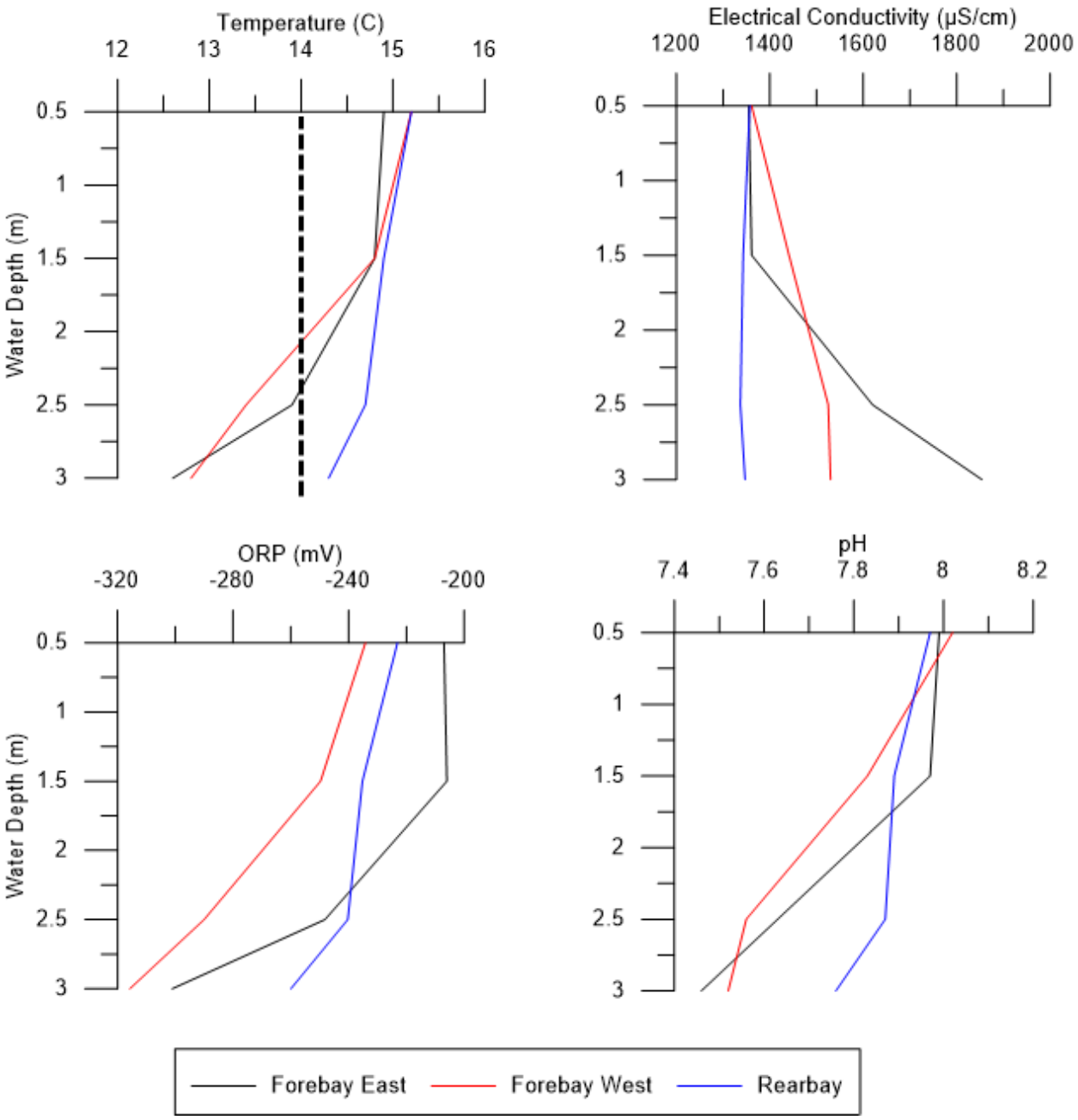

Figure 18 - Water column profiles for the forebay and rearbay of Pond M. Highlighted is the threshold for thermal stratification based on a water surface temperature of 1 C.

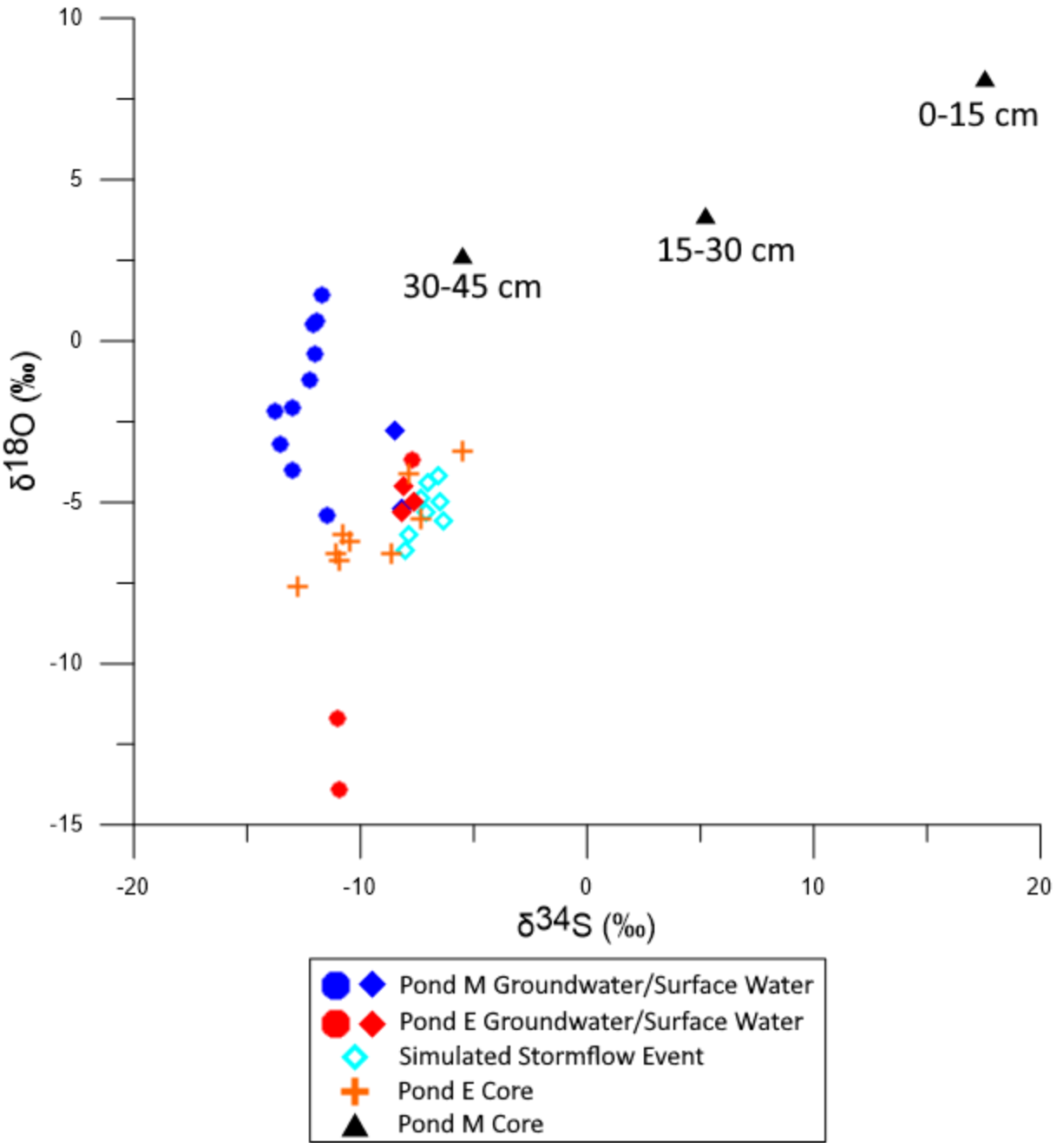

Figure 19 - Sulfate stable isotope results displaying distinct clustering between groundwater, surface water, and porewater from Pond M core sediments.

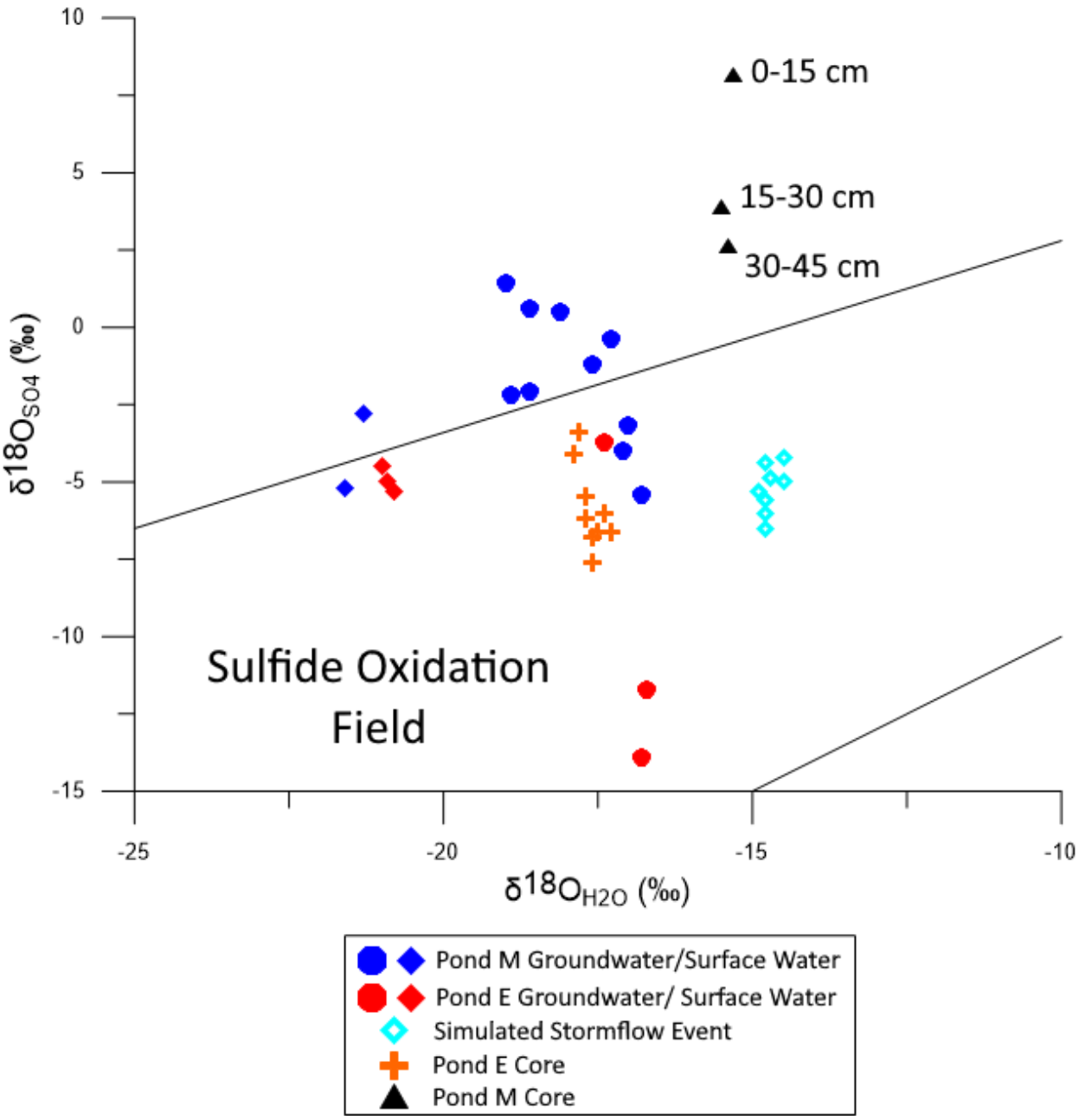

Figure 20 - Comparison of oxygen isotopes between sulfate and water. Clustering by water δ18O values is likely an artifact of temporal difference between samples. Black lines on the plot indicate upper and lower boundaries for sulfide oxidation field given in Van Stempvoort & Krouse (1993).

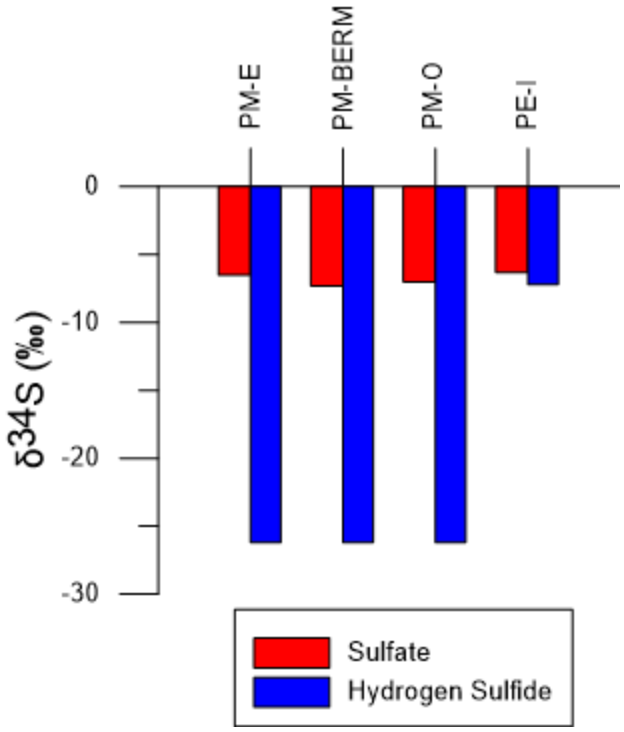

Figure 21 - Comparison of sulfur isotopes in sulfate and hydrogen sulfide during the simulated storm event. Hydrogen sulfide is heavily depleted in comparison to sulfate.

Chapter 3 – Implications, Future Research, and Recommendations

3.1 – Research Implications

By its design and nature, this study focused on investigating groundwater influences on a pair of stormwater ponds located at YYC. Because groundwater played a minor role in terms of water quantity that flowed into Pond M, it would be easy to dismiss it as an unimportant component in stormwater budgets. However, this study demonstrated that relatively small amounts of groundwater can significantly impact stormwater ponds if the groundwater has the right geochemical composition. Small quantities of high TDS groundwater can import appreciable volumes of solutes into stormwater infrastructure and can prove to be more complicated to mitigate than managing storm flows. This highlights the need to constrain groundwater quality in addition to groundwater elevations prior to siting and building stormwater ponds. Stormwater ponds can be lined with impermeable barriers to prevent exchange between stormwater and groundwater, but stormwater pipes cannot be similarly lined. Groundwater can still enter the stormwater pipes above the pond and influence pond chemistry, bypassing the liner system altogether. This may necessitate a re-evaluation on how stormwater infrastructure is operated or may require the installation of additional infrastructure, such as aeration systems, to mitigate the effects of groundwater on stormwater quality.

There is applicability of this study's work in the broader context, especially where large concentrations of sulfate exist such as seawater. Factors such as sea level rise and saltwater intrusion can similarly influence coastal stormwater ponds much like how evaporative concentration influenced Pond M geochemistry. Saltwater intrusions, whether through sea level rise or storm surge events, advances high TDS, sulfate rich saltwater into coastal aquifers where it can begin to interact with coastal stormwater ponds. The high TDS load into coastal stormwater ponds can lead to pond stratification, creating potentially anoxic and reducing conditions and possibly generate hydrogen sulfide. High sulfate content in seawater is documented to contribute to hydrogen sulfide generation in coastal sediments under reducing conditions (Pimenov et al. 2012, Briones-Gallardo et al. 2022). Seawater contaminated groundwater seeping into storm

ponds, whether by direct seepage or by leakage into stormwater pipes, could similarly generate hydrogen sulfide along reducing treatment efficacy due to chemical stratification.

Sulfate is not the only groundwater constituent that could influence storm pond chemistry. While sulfate was primarily examined in this study, other dissolved species such as sodium are abundant in the groundwater around Pond M. High sulfate loads into Pond M under reducing conditions contributes to hydrogen sulfide generation, but elevated sodium can outcompete for sorption sites on pond sediments and eject contaminants that were previously stored such as heavy metals (Bäckström et al. 2004, Tromp et al. 2012, Kaushal et al. 2022). These ejected contaminants would only be discharged under high flow conditions that can overcome the stratification present at Pond M. Low or moderate flow periods would display short-circuiting of the pond with flows bypassing the forebay bottom waters and allow metals to accumulate in the bottom water as sodium seeps into the pond.

Another implication of this study is that it adds to the growing body of evidence that shallow stormwater ponds can indeed stratify, leading to reducing conditions and potential water quality issues. Research does exist on stratification of shallow ponds (Koretsky et al. 2012, Holgerson et al. 2022), of which stormwater ponds are a subset. This research adds to the existing literature potentially showing that stormwater pond design influences water column structure. In the case of Pond M, the forebay showed stratification and not the rearbay. The submerged berm contained the stratification to the forebay and restricted outflow water to the less dense water that flowed on top of the denser bottom water in the forebay. Solely monitoring the outflow of Pond M would not be sufficient to identify the stratification taking place in the forebay and the corresponding impacts to water quality. Similarly, wet storage ponds that utilize a forebay, or multiple forebays can encounter the same problem if they receive high chloride inputs from road deicing applications. Less dense precipitation and melt water may bypass the forebay altogether and give a false impression of pond performance. If stratification leads to reducing conditions in the forebay, the forebay can be a source of

legacy contaminants that are slowly exported during low flow periods with larger concentrations being mobilized during high flow periods.

3.2 – Future Research

While this study was able to identify groundwater interacting with a stormwater pond, it was not able to identify all possible sources of groundwater. As noted previously, there is the potential for groundwater to enter the stormwater system above Pond M through the “urban karst” effect (Shepley et al. 2020), and based on the data collected during this study, the magnitude of groundwater potentially leaking into the stormwater system could not be constrained. To that end, additional flow monitoring should be installed to measure not just the flow rates, but other parameters such as EC. It has been shown that groundwater in the area is elevated in dissolved solids, particularly sulfate and sodium. Since rainwater will likely have lower TDS content than the site groundwater, identifying groundwater contributions to storm flows and during low flow periods could be accomplished by monitoring EC as a proxy for TDS. Such instruments should be deployed at all inlets at Pond M as well as the outlet to Pond K.

Another area in need of further study is the water levels on the benches of Pond M and the hydraulic conductivity of the till on the benches. By monitoring the water levels in the shallow wells adjacent to Pond M with pressure transducers, the groundwater response to storm events and snow melt events could be constrained to enhance understanding of potential lateral flows into the pond. This would be facilitated by simultaneously monitoring pond water levels during the same monitoring period. Lateral flows could be important due to the previously discussed secondary porosity and preferential flow paths that fractured till presents and could better constrain groundwater contributions to the overall stormwater budget rather than relying solely on diffusion estimates from the bottom of the forebay. This lateral groundwater contribution would require establishing the hydraulic conductivity of the Pond M bench material using single well tests on shallow wells installed there or using ring infiltrometers to estimate near surface hydraulic conductivity estimates.

To further constrain interactions between groundwater and Pond M, mini-piezometers should be installed within the south bank of the pond and, if possible, within the bottom of the Pond M forebay. When used in tandem with flow directions, the mini-piezometers in the pond banks would help enhance understanding the potential role of density driven exchange between pond water and groundwater adjacent to Pond M. Since groundwater on the south bench has the highest dissolved solid content encountered anywhere in the study area, this would be the ideal location to instrument. Ideally two such mini-piezometers would be installed as a shallow/deep pair to help constrain the mixing zone between high TDS groundwater and more fresh stormwater. Such work would likely benefit from existing literature examining density driven flows in coastal settings. Installing mini-piezometers in the forebay would assist in constraining water quality and hydraulic head directly below Pond M and clarify whether the assumption that the vertical gradient between PM-NE3S and PM-NE3D is valid.

There is opportunity to better constrain groundwater and surface water interactions across the entire YYC site using additional stable isotope analysis. Regular sampling for water stable isotopes would assist in determining the lag time between a precipitation event and when that precipitation enters the stormwater system as groundwater. Such data would shed light on whether there are seasonal contributions to groundwater seeping into the stormwater system. Additionally, this study focused on a small portion of the entire YYC site for stable sulfate isotope analysis. Obtaining sulfate stable isotope samples across the site would help characterize where groundwater may be leaking into the stormwater system and identify sulfur cycling within the groundwater at YYC.

Another crucial line of research in better understanding hydrogen sulfide generation at Pond M would be examining stratification mechanics. It has been shown that after a simulated precipitation event that the forebay was stratified. It is unclear to what degree stratification resists mixing during high flow events or what flow rate threshold needs to be crossed for stratification to be disrupted. Such stratification contributes to reducing conditions and can negatively impact water quality downstream. To better understand stratification in Pond M, regular water column surveys should be conducted during open

water periods. Ideally measurements would be taken weekly with measurement procedures being more robust and repeatable than what was presented in this study (e.g. repeated or automated measurements at specific locations). One would only need to measure EC and temperature, but other parameters such as oxidation-reduction potential (ORP) would help complete the picture. Such regular measurements would also help to understand how much water is displaced during high flow events and identify the depths at which stratification persist after such events. Regular water column monitoring will also help identify the factors that lead to the onset of stratification and in turn reducing conditions.

Using the increased water column dataset alongside flow rates and inflow EC measurements, one could then develop a simple 2D model of flow within Pond M. Such a model would help determine the efficacy of Pond M and whether it is functioning as designed. It would also help quantify possible short-circuiting effects of storm flows that bypass the forebay altogether with little interaction. A short-circuited stormwater pond is less effective at treating stormwater than one that is consistently fully mixed (Semadeni-Davies 2006).

This work and the proposed avenues of future research at the YYC site highlight the need to increase investigations on how groundwater can impact stormwater infrastructure operations. Part of the motivation of this study is the lack of research on groundwater and stormwater interactions where groundwater could potentially influence stormwater chemistry. Further research is required on regions where high TDS groundwater could influence stormwater chemistry. This is especially true for regions susceptible to saltwater intrusion, but even contaminant spills or road salts can create plumes of high TDS water that can easily be intercepted by stormwater infrastructure. With cities contemplating on using stormwater as a water resource, understanding these groundwater and stormwater interactions would help guide stormwater infrastructure design to ensure adequately treated stormwater.

3.3 – Recommendations

Partial solutions to water quality concerns at Pond M do exist. To eliminate diffusion of sulfate into the forebay, Pond M could be redesigned to have an impermeable barrier rather than relying on clay material. An impermeable barrier would prevent direct diffusion into Pond M as well as potential lateral flow through the fractured till on the benches, but it would not address potential groundwater leaks in the stormwater network above the pond which could still contribute to stratification in the forebay. However, the installation of permanent aerators could disrupt stratification and help mitigate the formation of hydrogen sulfide in the forebay by providing oxygen at depth and oxidizing the hydrogen sulfide. This would not be able to address sulfate reduction that occurs within the pond sediments though and would likely increase turbidity through the formation of elemental sulfur. By changing Pond E to be more of a treatment wetland, elemental sulfur could be allowed to settle out of suspension during low flow periods and effectively filter it out to improve the quality of water being discharged into Nose Creek.

3.4 – Personal Reflections

This entire research project was a learning experience for me, and I did learn a lot of things along the way. I would say that the project, as a whole, went surprisingly well. While work on the project started out slow, by the time that data collection started in earnest, enough monitoring was in place to build a picture of groundwater conditions in the study area and obtain a good idea as to what was contributing to hydrogen sulfide generation in the first place. Throughout it all, I had tremendous support from my research supervisor along with colleagues in our research group and the environment team at YYC. It was great that we were able to get pressure transducers not only for long term groundwater monitoring, but also for performing single well tests. Not to mention having flow monitoring installed during the course of the project so that pond water budgets could be performed.

Of course, now that I have some more experience in doing groundwater and surface water monitoring, there are some things that I would have done differently if I was to do

this research project again. One would be to run the EM31 survey prior to siting the shallow wells on the Pond M benches. As it was, it was fortunate that PM-S1 and PM-S2 were installed in the high EC area on the south bench since they were originally planned to be installed closer to the middle of the pond across from PM-N1 and PM-N2. Another thing I would do differently is being more consistent with analytes of interest during initial groundwater sample collection. Sample collection started in September 2021 after the installation of monitoring wells, but not all locations had sufficient water for all the analytes of interest. There was not a priority list of analytes constructed before sampling began which would have been helpful in determining what analytes should be sampled for.

Bibliography

AECOM. 2010. Parallel runway project volume V – Item 5 groundwater baseline report. Calgary (AB).

Afonso M, Stumm W. 1992. Reductive dissolution of iron(III) (hydr)oxides by hydrogen sulfide. Langmuir. 8:1671-1675.

Ahmed S, Loewn M, Zhang W, Ghobrial T, Zhu D, Mahmood K, van Duin B. 2022. Field observations of stratification in stormwater wet ponds. Journal of Environmental Management. 322:115988 doi: 10.1016/j.jenvman.2022.115988

[APHA] American Public Health Association. 2012. Standard methods for the examination of water and wastewater 22nd edition Port City Press, Baltimore, Maryland USA

Avetisyan K, Eckert W, Findlay A, Kamyshny Jr A. 2019. Diurnal variations in sulfur transformations at the chemocline of a stratified freshwater lake. Biogeochemistry. 146:83-100. doi: 10.1007/s10533-019-00601-5

Bäckström M, Karlsson S, Bäck,am L, Folkeson L, Lind B. 2004. Mobilization of heavy metals by deicing salts in a roadside environment. Water Research. 38:720-732. doi: 10.1016/j.watres.2003.11.006

Baldwin D, Mitchell a. 2012. Impact of sulfate pollution on anaerobic biogeochemical cycles in a wetland sediment. Water Research. 46:965-974. doi: 10.1016/j.watres.2011.11.065

Berthold S, Bentley L, Hayashi M. 2004. Integrated hydrogeological and geophysical study of depression-focused recharge in the Canadian prairies. Water Resources Research. 40. W0605. doi: 10.1029/2003WR002982

Boehrer B, Schultze M. 2008. Stratification of Lakes. Reviews of Geophysics. 46. RG2005. doi: 10.1029/2006RG000210

Bonneau J, Fletcher T, Costelloe J, Burns M. 2017. Stormwater infiltration and the ‘urban karst’ – a review. Journal of Hydrology. 552:141-150. doi: 10.1016/j.jhydrol.2017.06.043

Bonneau J, Fletcher T, Costelloe J, Poelsma P, James R, Burns M. 2018. Where does infiltrated stormwater go? Interactions with vegetation and subsurface

anthropogenic features. Journal of Hydrology. 567:121-132. doi: 10.1016/j.jhydrol.2018.10.006

Briones-Gallardo R, González-Muñoz M, García-Bautista I, Valdés-Lozano D, Toledano-Thompson T, Polanco-Lugo E, Rivera-Madrid R, Valdez-Ojeda R. 2022. Hydrogen sulfide production with a microbial consortium isolated from marine sediments offshore. Journal of Marine Science and Engineering. 10:436. doi: 10.3390/jmse10030436

van Buren M, Watt W, Marsalek J. 1997. Removal of selected urban stormwater constituents by an on-stream pond. Journal of Environmental Planning and Management. 40(1):5-18. doi: 10.1080/09640569712254

Camponelli K, Lev S, Snodgrass J, Landa E, Casey R. 2010. Chemical fractionation of Cu and Zn in stormwater, roadway dust and stormwater pond sediments. Environmental Pollution. 158:2143-2149. doi: 10.1016/j.envpol.2010.02.024

Canfield D. 2001a. Biogeochemistry of Sulfur Isotopes. Reviews in Mineralogy and Geochemistry. 43(1):607-636. doi: 10.2138/gsrmg.43.1.607

Canfield D. 2001b. Isotope fractionation by natural populations of sulfate-reducing bacteria. Geochemica et Cosmochemica Acta. 65(7):1117-1124.

Canfield D, Olesen C, Cox R. 2006. Temperature and its control of isotope fractionation by a sulfate-reducing bacterium. Geochemica et Cosmochemica Acta. 70:548-561. doi: 10.1016/j.gca.2005.10.028

Chen K, Morris J. 1972. Kinetics of oxidation of aqueous sulfide by O_2. Environmental Science and Technology. 6(6):529-537. doi: 10.1021/es60065a008

Chen L, Delatolla R, D'Aoust P, Wang R, Pick F, Poulain A, Rennie C. 2019. Hypoxic conditions in stormwater retention ponds: potential for hydrogen sulfide emission. Environmental Technology. 40(5):642-653. doi: 10.1080/09593330.2017.1400112

City of Calgary. 2011. Stormwater management & design manual. Calgary (AB).

Clark I, Fritz P. 1997. Environmental isotopes in hydrogeology. 2nd ed. New York: CRC Press.

Corely S. 2015. Quantifying water budgest to evaluate the hydrologic performans of two stormwater detention ponds in coastal South Carolina [master's thesis]. Coastal Carolina University.

Cullis C, Hirschler M. 1980. Atmospheric sulphur: natural and man-made sources. Atmospheric Environment. 14:1263-1278.

D'Aoust P, Delatolla R, Poulain A, Guo G, Wang R, Rennie C, Chen Liyu, Pick F. 2017. Emerging investigators series: hydrogen sulfide production in municipal stormwater retention ponds under ice covered conditions: a study of water quality and SRB populations. Environmental Science: Water Research Technology. 3:686-698. doi: 10.1039/c7ew00117g

D'Aoust P, Pick F, Wang R, Poulain A, Rennie C, Chen L, Kinsley C, Delatolla R. 2018. Sulfide production kinetics and model of stormwater retention ponds. Water Science and Technology. 77(10):2377-2387. doi: 10.2166/wst.2018.150

[ECCC] Environment and Climate Change Canada. 2010. Ottawa (ON): Government of Canada; [Acccessed Jan 30 2023]. https://climate.weather.gc.ca/climate_normals/results_1981_2010_e.html?searchType=stnProv&lstProvince=AB&txtCentralLatMin=0&txtCentralLatSec=0&txtCentralLongMin=0&txtCentralLongSec=0&stnID=2205&dispBack=0

[ECCC] Environment and Climate Change Canada. 2022. Ottawa (ON): Government of Canada; [Acccessed Nov 7 2022]. https://climate.weather.gc.ca/climate_data/hourly_data_e.html

Egemose S, Sønderup M, Grudinina A, Hansen A, Flindt M. 2015. Heavy metal composition in stormwater and retention in ponds dependent on pond age, design, and catchment type. Environmental Technology. 36(8):959-969. doi: 10.1080/09593330.2014.970584

[EPA] Environmental Protection Agency. 2003. Toxicological review of hydrogen sulfide. Washington (DC): Environmental Protection Agency. Report No.: EPA 635-R-03-005

[ESRD] Alberta Environment and Sustainable resource Development. 2013. Evaporation and Evapotranspiration in Alberta. Edmonton (AB).

Fee E, Hecky R, Kasian S, Cruikshank D. 1996. Effects of lake size, water clarity, and climatic variability on mixing depths in Canadian Shield lakes. Limnology Oceanography. 41(5):912-920. doi: 10.4319/lo.1996.41.5.0912

Fennell J, Bentley L. 1998. Distribution of sulfate and organic carbon in a prairie till setting: natural vs industrial sources. Water Resources Research. 34(7):1781-1794. doi: 10.1029/98WR00827

Ferris D, Potter G, Ferguson G. 2020. Characterization of the hydraulic conductivity of glacial till aquitards. Hydrogeology Journal. 28:1827-1839. doi: 10.1007/s10040-020-02161-7

Fetter C. 2001. Applied Hydrogeology. 4th ed. Long Grove (IL): Waveland Press.

Frost P, Prater C, Scott A, Song K, Xenopoulos M. 2019. Mobility and Bioavailability of sediment phosphorus in urban stormwater ponds. Water Resources Research. 55(5):3680-3688. doi: 10.1029/2018WR023419

Grasby S, Osborn J, Chen Z, Wozniak P. 2010. Influence of till provenance on regional groundwater geochemistry. Chemical Geology. 273:225-237. doi: 10.1016/j.chemgeo.2010.02.024

Hamblin A. 2004. Paskapoo-Porcupine Hills formations in western Alberta: synthesis of regional geology and resource potential. Geological Survey of Canada. Open File: 4679

Hao A, Kobayashi S, Xia D, Mi Q, Yan N, Su M, Lin A, Zhao M, Iseri Y. 2021. Controlling eutrophication via surface aerators in irregular-shaped urban ponds. Water. 13:3360. doi: 10.3390/w13233360

He J, Valeo C, Chu A. 2015. Variation in water quality of a stormwater pond from diurnal thermal stratification. Journal of Water Resource and Hydraulic Engineering. 4(1-2):189-198.

Heagle D, Hayashi M, van der Kamp G. 2013. Surface-subsurface salinity distribution and exchange in a closed-basin prairie wetland. Journal of Hydrology. 478:1-14. doi: 10.1016/j.jhydrol.2012.05.054

Hendry M, Cherry J, Wallick E. 1986. Origin and distribution of sulfate in a fractured till in southern Alberta, Canada. Water Resources Research. 22(1):45-61.

Hendry M, Wassenaar L. 2000. Controls on the distribution of major ions in pore waters of a think surficial aquitard. Water Resources Research. 36(2):503-513.

Holgerson M, Richardson D, Roith J, Bortolotti L, Finlay K, Hornbach D, Gurung K, Ness A, Andersen N, Bansal S, et al. 2022. Classifying mixing regimes in ponds

and shallow lakes. Water Resources Research. 58:eWR03522. doi: 10.1029/2022WR032522

Houhou J, Lartiges B, France-Lanord C, Guilmette C, Poix S, Mustin C. 2010. Isotopic tracing of clear water sources in an urban sewer: a combined water and dissolved sulfate stable isotope approach. Water Research. 44:256-266. doi: 10.1016/j.watres.2009.09.024

[ISL – Sulfate] University of Calgary Isotope Science Lab. Calgary (AB). https://www.ucalgary.ca/labs/isotope-science-lab/sample-preparation/precipitation-baso4 Accessed Feb 2 2023

[ISL – Sulfide] University of Calgary Isotope Science Lab. Calgary (AB). https://www.ucalgary.ca/labs/isotope-science-lab/sample-preparation/aqueous-h2s-sampling Accessed Feb 2 2023

Ivanovsky A, Belles A, Criquet J, Dumoulin D, Noble P, Alary C, Billon. 2018. Assessment of the treatment efficiency of an urban stormwater pond and its impact on the natural downstream watercourse. Journal of Environmental Management. 226:120-130. doi: 10.1016/j.jenvman.2018.08.015

Janke B, Finlay J, Taguchi V, Gulliver J. 2022. Hydrologic processes regulate nutrient retention in stormwater detention ponds. Science of the Total Environment. 823:153722. doi: 10.1016/j.scitotenv.2022.153722

Johnson N, Pastor J, Swain E. 2018l. Cumulative sulfate loads shift porewater to sulfidic conditions in freshwater wetland sediment. Environmental Toxicology. 38(6):1231-1244. doi: 10.1002/etc.4410

Johnston S, Nurton E, Aaso T, Tuckerman G. 2014. Sulfur, iron and carbon cycling following hydrological restoration of acidic freshwater wetlands. Chemical Geology. 371:9-26. doi: 10.1016/j.chemgeo.2014.02.001

van der Kamp G, Hayashi M. 2009. Groundwater-wetland ecosystem interaction in the semiarid glaciated plains of North America. Hydrogeology Journal. 17:203-214. doi: 10.1007/s10040-008-0367-1

Karlsson K, German J, Viklander M. 2010. Stormwater pond sediments: temporal trends in heavy metal concentrations and sediment removal. Soil and Sediment Contamination. 19(2):217-230. doi: 10.1080/15320380903548490

Karpf C, Krebs P. 2013. Modelling of groundwater infiltration into sewer systems. Urban Water Journal. 10(4):221-229. doi: 10.1080/1573062X.2012.724077

Kaushal S, Reimer J, Mayer P, Shatkay R, Maas C, Nguyen W, Boger W, Yaculak A, Doody T, et al. 2021. Freshwater salinization syndrome alters retention and release of chemical cocktails along flowpaths: from stormwater management to urban streams. Freshwater Science. 41(3):420-441. doi: 10.1086/721469

Kidmose J, Nilsson B, Engesgaard P, Frandsen M, Karan S, Landkildehus F, Søndergaard M, Jeppesen E. 2013. Focused groundwater discharge of phosphorus to a eutrophic seepage lake (Lake Væng, Denmark): implications for lake ecological state and restoration. Hydrogeology Journal. 21:1787-1802. doi: 10.1007/s10040-013-1043-7

Kidmose J, Troldborg L, Refsgaard J, Bischoff N. 2015. Coupling of a distributed hydrological model with an urban stormwater model for impact analysis of forced infiltration. Journal of Hydrology. 525:506-520. doi: 10.1016/j.jhydrol.2015.04.007

Koretsky C, MacLeod A, Sibert R, Snyder C. 2012. Redox stratification and salinization of three kettle lakes in southwest Michigan, USA. Water, Air, & Soil Pollution. 223:1415-1427. doi: 10.1007/s11270-011-0954-y

Ku J, Liang J, Ulrich A, Liu Y. 2016. Sulfide production and management in municipal stormwater retention ponds. Journal of Environmental Engineering. 142(2):04015071.

Kusin F, Jarvis A, Gandy C. 2010. Hydraulic residence time and iron removal in a wetland receiving ferruginous mine water over a 4 year period from commissioning. Water Science and Technology. 62(8):1937-1946.

Lissner H, Wehrer M, Jartun M, Totsche K. 2014. Degradation of deicing chemicals affects the natural redox system in airfield soils. Environmental Science and Pollution Research. 21: 9036-9053. doi: 10.1007/s11356-013-2096-9

Lyn T, Taylor J. 1992. Assessing sulfur turbidity formation following chlorination of hydrogen sulfide in groundwater. Journal (American Water Works Association). 84(9):103-112.

Marsalek P, Watt W, Marsalek J, Anderson B. 2000. Winter flow dynamics of an on-stream stormwater management pond. Water Quality Research Journal. 35(3):505-523.

Marsalek J. 2003. Road salts in urban stormwater: an emerging issue in stormwater management in cold climates. Water Science and Technology. 48(9):61-70.

Martinsen K, Andersen M, Sand-Jensen K. 2019. Water temperature dynamics and the prevalence of daytime stratification in small temperate shallow lakes. Hydrobiologia. 826:247-262. doi: 10.1007/s10750-018-3737-2

Mazumder A, Taylor W. 1994. Thermal structure of lakes varying in size and water clarity. Limnology and Oceanography. 30(4):968-976.

McEnroe N, Buttle J, Marsalek J, Pick F, Xenopoulos M, Frost P. 2013. Thermal and chemical stratification of urban ponds: are the ‘completely mixed reactors’?. Urban Ecosystems. 16:327-339. doi: 10.1007/s11252-012-0258-z

McQuiggan R, Andres A, Roros A, Sturchio N. 2022. Stormwater drives seasonal geochemical processes beneath an infiltration basin. Journal of Environmental Quality. 58:1198-1210. doi: 10.1002/jeq2.20416

Merrett, S. 2022. Characterization of baseline geology and hydrogeologic conditions at the Calgary International Airport (YYC). Technical Report. Calgary (AB).

Monteith, J. 1965. Evaporation and environment. Symposia of the Society for Experimental Biology. 19:205-234.

Moran S. 1986. Surficial geology of the Calgary urban area. Edmonton (AB): Alberta Reseearch Council. Bulletin No.: 53.

Nachson U, Ireson A, van der Kamp G, Wheater H. 2013. Sulfate salt dynamics in the glaciated plains of North America. Journal of Hydrology. 499:188-199. doi: 10.1016/j.jhydrol.2013.07.001

Noël V, Kumar N, Boye K, Barragan L, Lezama-Pacheco J, Chu R, Tolic N, Brown Jr G, Bargar J. 2020. FeS Colloids – formation and mobilization pathways in natural waters. Environmental Science Nano. 7:2102-2116. doi: 10.1039/c9en01427f

Ogata A. 1970. Theory of dispersion in a granular medium. Washington (DC): U.S. Geologic Survey. Professional Paper: 411-1

Pallud C, Van Cappellen P. 2006. Kinetics of microbial sulfate reduction in estuarine sediments. Geochimica et Cosmochimica Acta. 70:1148-1162. doi: 10.1016/j.gca.2005.11.002

Pester M, Knorr K, Friedrich M, Wagner M, Loy A. 2012. Sulfate-reducing microorganisms in wetlands – fameless actors in carbon cycling and climate change. Frontiers in Microbiology. 3:72. doi: 10.3389/fmicb.2012.00072

Pimenov N, Kanapatskii T, Sigalevich P, Rusanov I, Veslopolova E, Grigor A, Zhamoida V. 2012. Sulfate reduction, methanogenesis, and methane oxidation in the Holocene sediments of the Vyborg Bay, Baltic Sea. Microbiology. 81(1):79-89. doi: 10.1134/S0026261712010122

Popa R, Kinkle B, Badescu A. 2004. Pyrite framboids as biomarkers for iron-sulfur systems. Geomicrobiology Journal. 21(3):193-206. doi: 10.1080/01490450490275497

Pophillat W, Sage J, Rodriguez F, Braud I. 2022. Consequences of interactions between stormwater infiltration systems, shallow groundwater and underground structures at the neighborhood scale. Urban Water Journal. 19(8):812-823. doi: 10.1080/1573062X.2022.2090382

Persson J, Whittgren H. 2003. How hydrological and hydraulic conditions affect performance of ponds. Ecological Engineering. 21:259-269. doi: 10.1016/j.ecoleng.2003.12.004

Puls R, Barcelona M. 1996. Low-flow (Minimal drawdown) ground-water sampling procedures. Washington (DC): Environmental Protection Agency. Report No.: EPA 540-S-95-504.

Semadeni-Davies A. 2006. Winter performance of an urban stormwater pond in southern Sweden. Hydrological Processes. 20:165-182. doi: 10.1002/hyp.5909

Rasmussen T, Crawford L. 1997. Identifying and removing barometric pressure effects in confined and unconfined aquifers. Groundwater. 35(3):502-511

Reddy K, Dastgheibi S, Cameselle C. 2021. Mixed versus layered multi-media filter for simultaneous removal of nutrients and heavy metals from urban stormwater runoff. Environmnetal Science and Pollution Research. 28:7574-7585. doi: 10.1007/s11356-020-11120-4

Revitt D, Worrall P. 2003. Low temperature biodegradation of airport de-icing fluids. Water Science and Technology. 48(9):103-111.

Rickard D, Luther III G. 2007. Chemistry of iron sulfides. Chemical reviews. 107:514-562. doi: 10.1021/cr0503658

Shammaa Y, Zhu D, Gyürék, Labatiuk C. 2002. Effectiveness of dry ponds for stormwater total suspended solids removal. Canadian Journal of Civil Engineering. 29:316-324. doi: 10.1139/L02-008

Shepley M, Schmidt N, Senior M, Worthington S, Scheckenberger R. 2020. Assessing 'Urban Karst' effects from groundwater-storm sewer interaction in a till aquitard. Groundwater. 58(2):26269-277. doi: 10.1111/gwat.12908

Smith B, Smith J, Baeck M, Villarini G, Wright D. 2013. Spectrum of storm event hydrologic response in urban watersheds. Water Resources Research. 49:2649-2663. doi: 10.1002/wrcr.20223

Solinst. 2022. User guide levelogger series. Solinst Canada.

Song K, Xenopoulos M, Buttle J, Marsalek J, Wagner N, Pick F, Frost P. 2013. Thermal stratification patterns in urban ponds and their relationships with vertical nutrient gradients. Journal of Environmental Management. 127:317-323. doi: 10.1016/j.jenvman.2013.05.052

Sønderup M, Egemose S, Hansen A, Grudinina A, Madsen M, Flindt M. 2016. Factors affecting retention of nutrients and organic matter in stormwater ponds. Ecohydrology. 9:796-806. soi: 10.1002/eco.1683

Stein R, Schwartz F. 1990. On the origin of saline soils at Blackspring Ridge, Alberta Canada. Journal of Hydrology. 117:99-131.

Stutter M, Lumsdon D. 2008. Interactions of land use and dynamic river conditions on sorption equilibria between benthic sediments and river soluble reactive phosphorus concentrations. Water Research. 42:4249-4260. doi: 10.1016/j.watres.2008.06.017

Taguchi V, Olsen T, Natarajan P, Janke B, Gulliver J, Finlay J, Stefan H. 2020. Internal loading in stormwater ponds as a phosphorus source to downstream waters. Limnology and Oceanography Letters. 5:322-330. doi: 10.1002/lol2.10155

Thomas S, Lucius M. 2016. Groundwater seepage nutrient loading in a recently dug wet detention stormwater pond. Florida Scientist. 79(2-3):132-146.

Thompson J, Hathaway J, Perfect E, Schwartz J. 2021. The effect of stormwater infiltration and surrounding built infrastructure on local groundwater dynamics: a case study for regenerative stormwater conveyances. Sustainable and Resilient Infrastructure. 6(3-4):181-191. doi: 10.1080/23789689.2020.1772636

Torgeson J, Rosenfeld C, Dunshee A, Duhn K, Schmitter R, O'Hara P, Ng G, Santelli C. 2022. Hydrobiogeochemical interactions in the hyporheic zone of a sulfate-impacted, freshwater stream and riparian wetland ecosystem. Environmental Science Processes and Impacts. 24:1360-1382. doi: 10.1039/d2em00024e

Tromp K, Lima A, Barendregt A, Verhoeven J. 2012. Retention of heavy metals and poly-aromatic hydrocarbons from road water in a constructed wetland and the effect of de-icing. Journal of Hazardous Materials. 203-204:290-298. doi: 10.1016/j.jhazmat.2011.12.024

Utting D, Atkinson N. Proglacial lakes and the retreat pattern of the southwest Laurentide Ice Sheet across Alberta, Canada. Quaternary Science Reviews. 255:106034. doi: 10.1016/j.quascirev.2019.106034

[UN FAO] Allen R, Pereira L, Raes D, Smith M. 1998. Crop evapotranspiration – guidelines for computing crop water requirements. Food and Agriculture Organization of the United Nations. Paper 56. https://www.fao.org/3/X0490E/x0490e00.htm Accessed Feb 9 2023

Van Stempvoort D, Krouse H. 1993. Controls of d18O in sulfate review of experimental data and application to specific environments. In: Alpers C, Blowes D, editors. Environmental geochemistry of sulfide oxidation. Washington (DC): American Chemcial Society. p. 446-480. doi: 10.1021/bk-1994-0550.ch029

Van Stempvoort D, Hendry M, Schoenau J, Krouse H. 1994. Sources and dynamics of sulfur in weathered till, Western Glaciated Plains of North America. Chemical Geology. 111:35-56.

Vollersten J, Nilesen A. Jensen H, Wium-Andersen T, Hvitved-Jacobsen. 2008. Corrosion of concrete sewers – The kinetics of hydrogen sulfide oxidation. Science of the Total Environment. 394:162-170. doi: 10.1016/j.scitotenv.2008.01.028

Walsh C, Roy A, Feminella J, Cottingham P, Groffman P, Morgan II R. 2005. The urban stream syndrome: current knowledge and the search of a cure. Journal of the North American Benthological Society. 24(3):706-723.

Walsh C, Fletcher T, Burns M. 2012. Urban stormwater runoff: a new class of environmental flow problem. PLoS One. 7(9):E45814. doi: 10.1371/journal.pone.0045814

Wiessner A, Kappelmeyer U, Kuschk P, Kästner. 2005. Sulphate reduction and the removal of carbon and ammonia in a laboratory-scale constructed wetland. Water Research. 39:4643-4650. doi: 10.1016/j.watres.2005.09.017

Woiciechowska E, Waara S. 2011. 2011. Distribution and removal efficiency of heavy metals in two constructed wetlands treating landfill leachate. Water Science and Technology. 64(8):1597-1606.

Wright D, Smith J, Willarini G, Baeck M. 2012. Hydroclimatology of flash flooding in Atlanta. Water Resources Research. 48:W04524. doi: 10.1029/2011WR011371

Yazdi M, Scott D, Sample D, Wang X. 2021. Efficacy of a retention pond in treating stormwater nutrients and sediment. Journal of Cleaner Production. 290:125787. doi: 10.1016/j.jclepro.2021.125787

Yeskis D, Zavala B. 2002. Ground-water sampling guidelines for superfund and RCRA project managers. Washington (DC): Environmental Protection Agency. Report No.: EPA 542-S-02-001

Appendix A – Borehole Logs and Well Completion Details

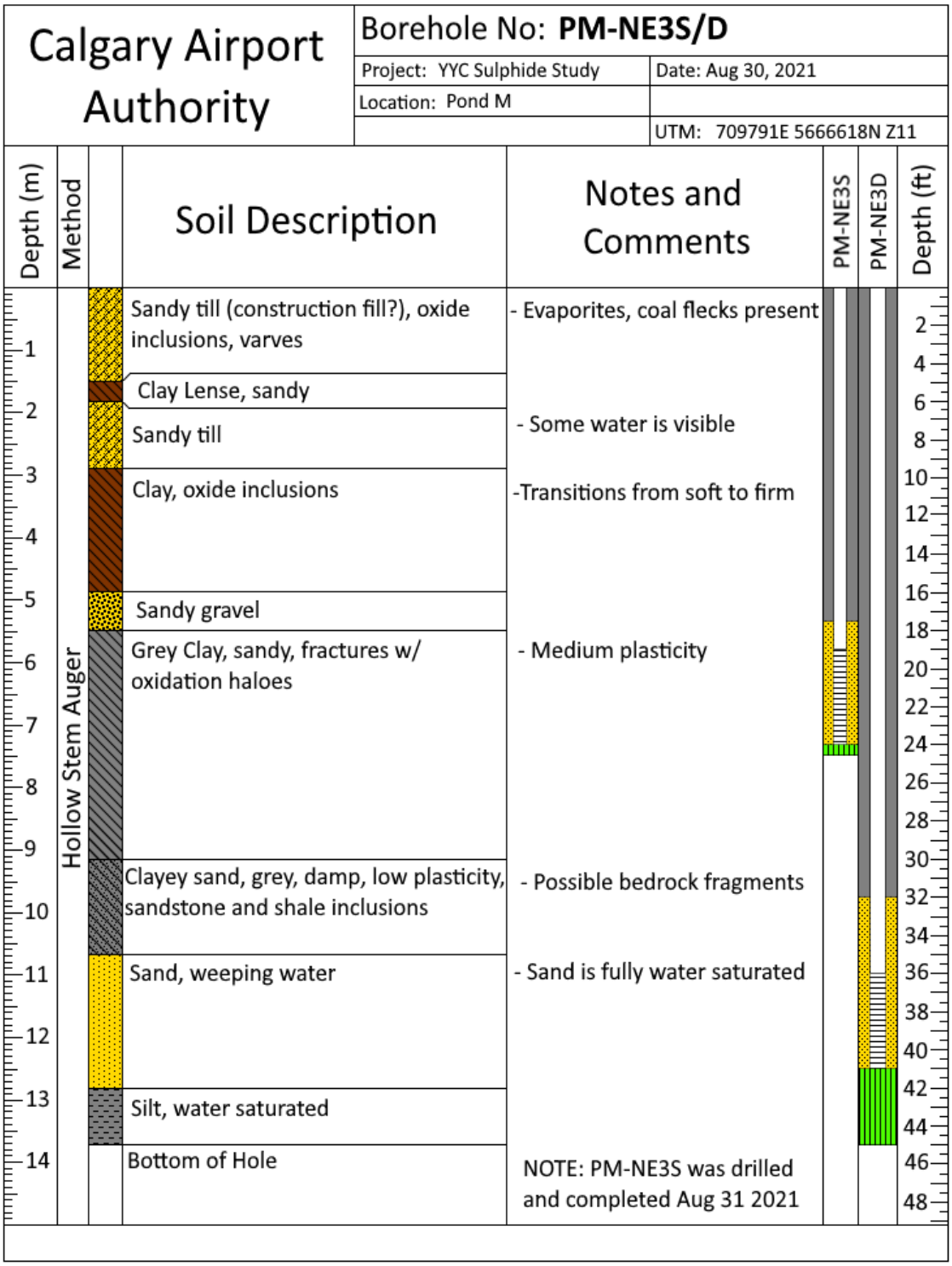

Calgary Airport Authority	Borehole No: **PM-N1**	
	Project: YYC Sulphide Study	Date: Aug 30, 2021
	Location: Pond M	
		UTM: 709620E 5666557N Z11

Depth (m)	Method	Soil Description	Notes and Comments	PM-N1	Depth (ft)
0–1	Solid Stem Auger	Clay till, stiff			2
1–2		Clay till, firm	- Increasing water content - Grey mottling		4, 6, 8
2–3		Grey Clay, stiff			10
3		Bottom of Hole			12
4					14
5					16
6					18, 20
7					22
8					24, 26
9					28
10					30, 32
11					34, 36
12					38, 40
13					42
14					44, 46, 48

Calgary Airport Authority	Borehole No: **PM-N2**	
	Project: YYC Sulphide Study	Date: Aug 30, 2021
	Location: Pond M	
		UTM: 709622E 5666572N Z11

Depth (m)	Method	Soil Description	Notes and Comments	PM-N2	Depth (ft)
0–3	Solid Stem Auger	Gravelly clay	- Sand lens present		0–10
		Clay till			
		Gravelly clay	- Silt content increases		
		Bottom of Hole			
3–14					10–48

Calgary Airport Authority

Borehole No: **PM-NE1**

Project: YYC Sulphide Study | Date: Aug 30, 2021

Location: Pond M

UTM: 709752E 5666565N Z11

Depth (m)	Method	Soil Description	Notes and Comments	PM-NE2	Depth (ft)
0–2	Solid Stem Auger	Gravelly clay	- Firmness increases with depth		0–8
2–3		Grey clay	- Grey mottling		8–10
3		Bottom of Hole			10
3–14					10–48

Calgary Airport Authority

Borehole No: **PM-NE2**

Project: YYC Culphide Study | Date: Aug 30, 2021

Location: Pond M

UTM: 709757E 5666578N Z11

Depth (m)	Method	Soil Description	Notes and Comments	PM-NE2	Depth (ft)
0–2	Solid Stem Auger	Gravelly clay	- Evaporites in fractures - Some silt - Iron oxide staining - Stiff, grey mottling		
2–3		Grey clay			
3		Bottom of Hole			

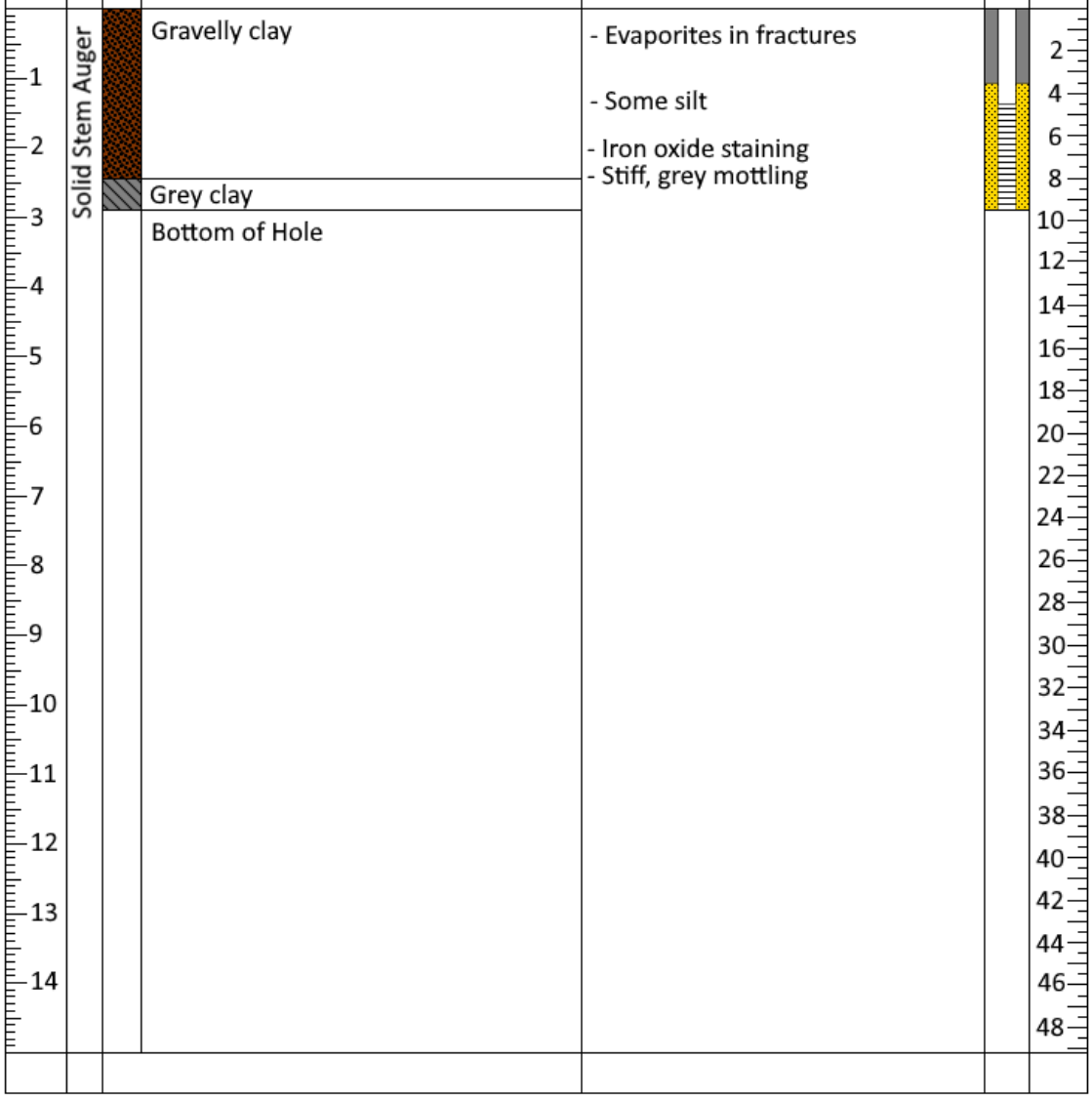

Calgary Airport Authority	Borehole No: **PM-S1**	
	Project: YYC Sulphide Study	Date: Aug 30, 2021
	Location: Pond M	
		UTM: 709713E 5666483N Z11

Depth (m)	Method	Soil Description	Notes and Comments	PM-S1	Depth (ft)
0–1	Solid Stem Auger	Gravelly Clay	- Moist, firm		0–2
1–2		Brown clay			2–6
2–3		Grey clay	- Grey mottling		6–10
		Bottom of Hole			

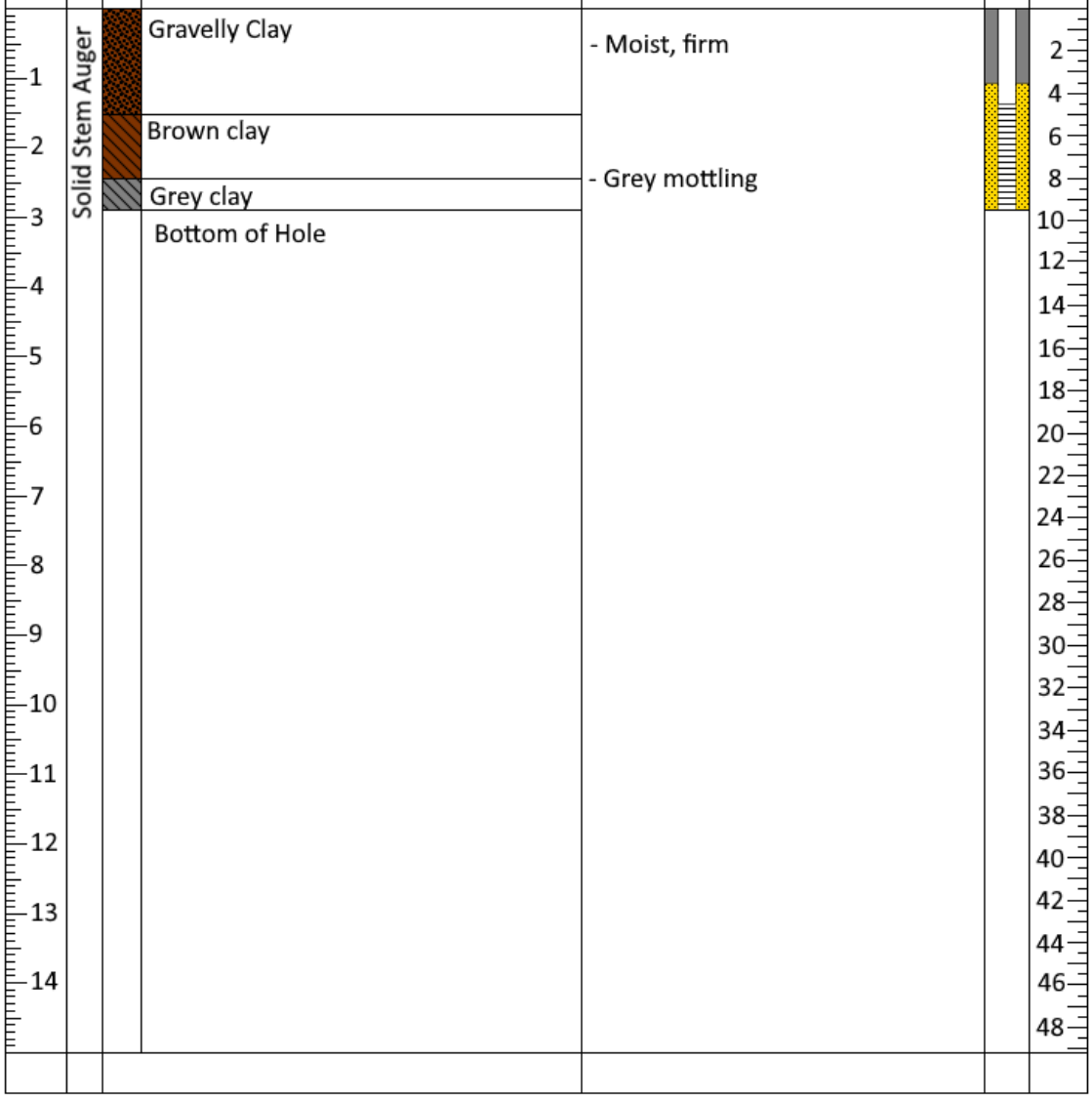

Calgary Airport Authority

Borehole No: **PM-S2**

Project: YYC Sulphide Study | Date: Aug 30, 2021

Location: Pond M

UTM: 709715E 5666466N Z11

Depth (m)	Method	Soil Description	Notes and Comments	PM-S2	Depth (ft)
0	Solid Stem Auger	Brown Clay	- Sand/silt lens (approx 6" thick)		0
1		Gravelly clay	- Iron oxide stains		2
2		Grey clay	- Grey mottling		4
3		Bottom of Hole			6
4					8
5					10
6					12
7					14
8					16
9					18
10					20
11					22
12					24
13					26
14					28
					30
					32
					34
					36
					38
					40
					42
					44
					46
					48

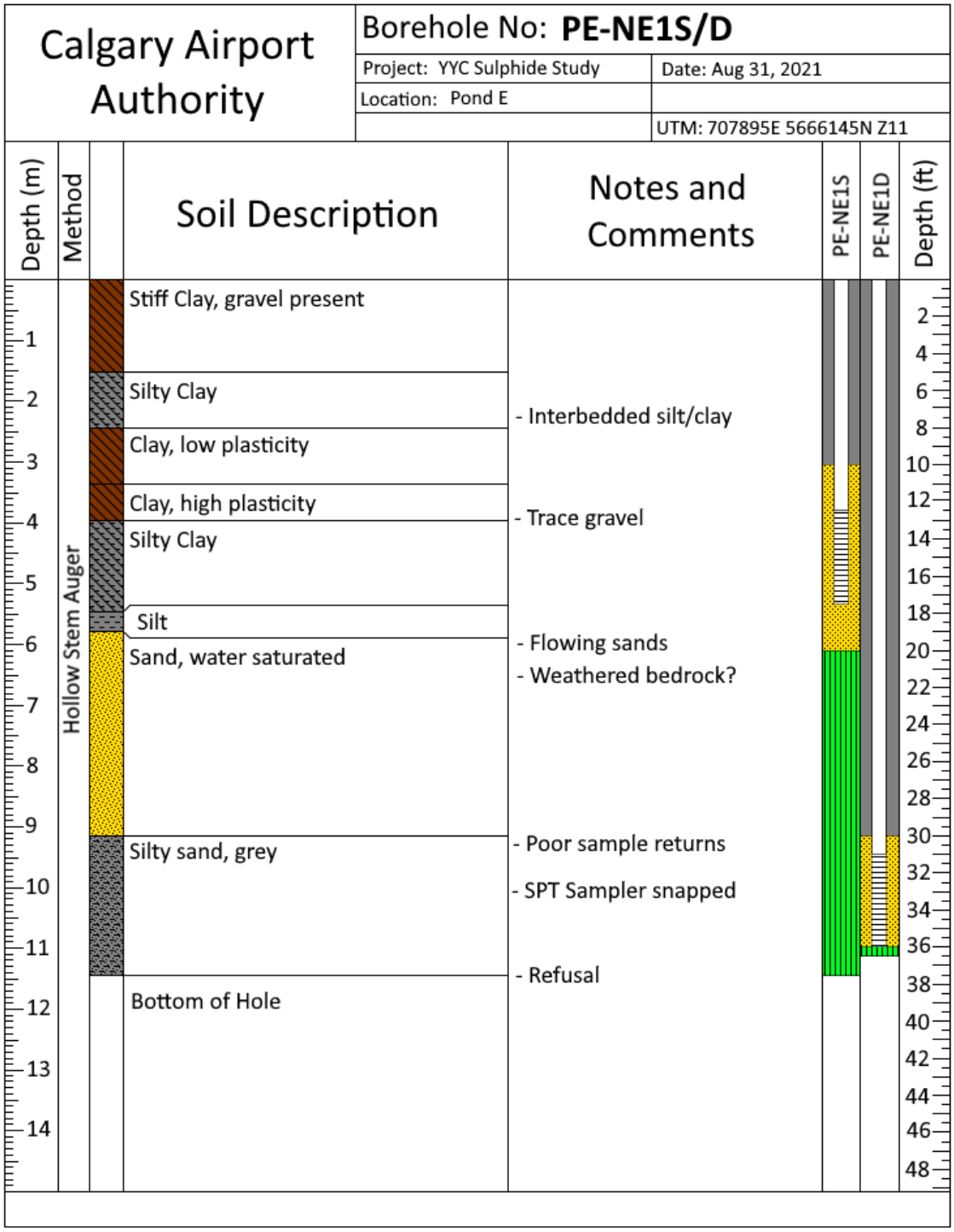
Calgary Airport Authority
Borehole No: PE-NE1S/D
Project: YYC Sulphide Study
Date: Aug 31, 2021
Location: Pond E
UTM: 707895E 5666145N Z11
Depth (m)
Method
Soil Description
Notes and Comments
PE-NE1S
PE-NE1D
Depth (ft)
Hollow Stem Auger
Stiff Clay, gravel present
Silty Clay
- Interbedded silt/clay
Clay, low plasticity
Clay, high plasticity
- Trace gravel
Silty Clay
Silt
- Flowing sands
Sand, water saturated
- Weathered bedrock?
Silty sand, grey
- Poor sample returns
- SPT Sampler snapped
- Refusal
Bottom of Hole
1
2
3
4
5
6
7
8
9
10
11
12
13
14
2
4
6
8
10
12
14
16
18
20
22
24
26
28
30
32
34
36
38
40
42
44
46
48

Table A1 – List of wells used as part of the broader hydrogeological investigation at YYC. Wells in this list include ones used in this study as well as wells used in Merrett (2022). Hydraulic conductivity estimates come from Merrett (2022). All well were constructed with 50 mm (2") PVC.

Well ID	Northing (m)	Easting (m)	TOC elevation (masl)	Well Depth (mBTOC)	Screen Length (m)	Hydraulic Conductivity (m/s)
1C-MW1	5661960	-1287	1082.48	6.87	1.5	-
1C-MW4	5662281	-1790	1078.73	11.60	1.5	2E-7
1C-MW5	5662282	-1791	1078.66	4.50	1.5	-
3B-MW2	5663329	-2098	1076.28	8.89	3.0	3E-6
3B-MW9	5663493	-2334	1056.22	6.37	1.5	4E-5
3D-MW14	5663773	-692	1080.72	12.76	1.5	6E-8
3D-MW15	5663774	-691	1080.99	5.04	3.0	3E-7
5B-MW37	5665070	-2037	1078.30	5.94	1.5	4E-7
5B-MW38	5665070	-2036	1078.39	14.04	1.5	1E-7
5G-MW1	5664668	1233	1089.81	9.47	1.5	4E-7
5G-MW2	5664670	1233	1083.74	5.65	1.5	2E-7
8C-MW9	-	-	-	5.96	1.5	-
8C-MW10	5666925	-1579	1081.32	12.04	1.5	-
PE-NE1S	5663647	-2099	1061.13	8.17	1.5	-
PE-NE1D	5663649	-2100	1061.36	12.19	1.5	-
PM-N1	5663991	-360	1076.75	3.85	1.5	-
PM-N2	5664006	-358	1076.67	3.65	1.5	-
PM-NE1	5663994	-360	1076.42	3.69	1.5	-
PM-NE2	5664007	-223	1076.48	3.73	1.5	-
PM-NE3S	5664045	-186	1080.22	8.60	1.5	4E-8
PM-NE3D	5664044	-187	1080.16	13.19	1.5	3E-7
PM-S1	5663913	-271	1076.58	3.74	1.5	-
PM-S2	5663896	-269	1076.83	3.85	1.5	-

Appendix B – Correlation Between EC and TDS and Water Density

EC was correlated with TDS by plotting measured EC against laboratory calculated TDS and obtaining a line of best fit using spreadsheet software. EC and TDS both came from all the water quality samples collected over the course of the monitoring period. Plotting EC against TDS produced Fig B1.

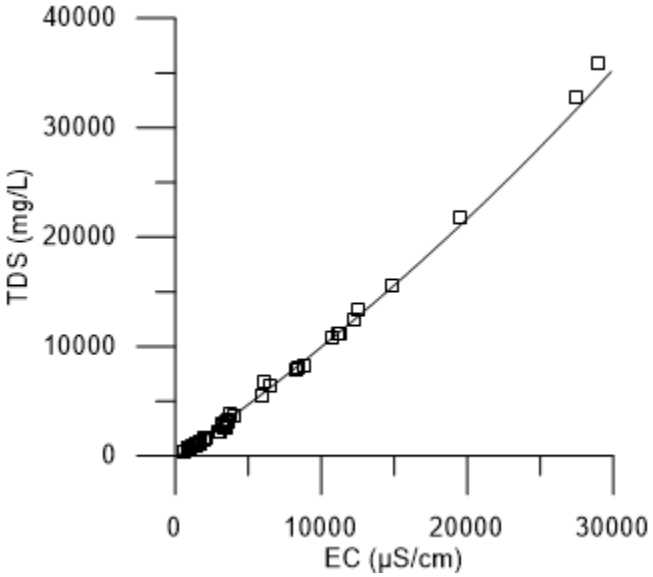

Figure B1 – Correlation curve between TDS and EC

The trendline (R^2=0.9985) gives the following relationship between EC and TDS:

$$TDS = 0.215 * EC^{1.17} \quad (1)$$

which calculates TDS in units of mg/L using EC (µS/cm). This relationship was used to estimate TDS at the top and bottom of Pond M. Salinity was approximated by dividing TDS by 1000 to convert it to g/L. This is an approximation in lieu of analytical methods to estimate salinity since water samples were not taken when the Pond M water column was profiled. Water density was calculated using the approximated salinity and measured water temperature.

Pure water density (ρ_0 kg/m^3) was calculated using the following:

$$\rho_0 = 999.842594 + 6.793952 \times 10^{-2}T - 9.095290 \times 10^{-3}T^2 + 1001685 \times 10^{-4}T^3 - 1.120083 \times 10^{-4}T^3 - 1.120083 \times 10^{-6}T^4 + 6.536332 \times 10^{-9}T^5 \quad (2)$$

where T is the measured temperature in °C.

Water density (ρ kg/m^3) where salinity is also accounted for was calculated using the following:

$$\rho = \rho_0 + AS + BS^{3/2} + CS^2 \quad (3)$$

where S is the estimated salinity in g/L. A and B are terms that incorporate t and C is a constant with a value of 4.8314×10^{-4}. A is calculated using the following:

$$A = 8.24493 \times 10^{-1} - 4.0899 \times 10^{-3}T + 7.6438 \times 10^{-5}T^2 - 8.2467 \times 10^{-7}T^3 + 5.3875 \times 10^{-9}T^4 \quad (4)$$

and B is calculated using the following:

$$B = -5.72466 \times 10^{-3} + 1.0227 \times 10^{-4}T - 1.6546 \times 10^{-6}T \quad (5)$$

where T is the measured temperature in °C.

Differences in density were calculated by taking the difference between the density of the bottom of the water column with the density of the top of the water column.

Appendix C – Estimated Evapotranspiration Calculations

The modified Penman-Monteith equation, along with the other calculations presented here, was sourced from the UN FAO (1998). ET was calculated with:

$$ET_0 = \frac{0.408*\Delta R_n + \gamma \frac{37}{T_{hr}+273} u_2 \delta e}{\Delta + \gamma(1+0.34u_2)} \quad (1)$$

where parameters are defined in table C1.

Table C1 – Parameter definitions for equation (1).

Parameter	Definition
ET_0	Water volume evaporated (m/hr)
Δ	Slope of the vapor pressure curve (kPa/°C)
R_n	Net irradiance (MJ/m^{2}hr)
T_{hr}	Hourly Temperature (°C)
δ_e	Vapor pressure deficit (kPa)
γ	Psychrometric constant (kPa/°C)
u_2	Windspeed at 2 m height (m/s)

Net irradiance was obtained by taking the difference between absorbed incoming shortwave radiation and the estimated outgoing longwave radiation. For net irradiance calculations, only incoming shortwave radiation was measured, requiring the calculation of the net shortwave radiation and the net longwave radiation.

Absorbed incoming shortwave radiation (R_{ns} in MJ/m^{2}hr) was calculated using:

$$R_{ns} = (1-\alpha)R_s \quad (2)$$

where R_s is the measured incoming shortwave radiation (R_{ns} in MJ/m^{2}hr), and α is the surface albedo (unitless). Because ET was being estimated for a pond water body, albedo was set to be 0.08. Outgoing longwave radiation (R_{nl} in MJ/m^{2}hr) was not measured and was estimated by using a modified version of the Stefan-Boltzman law to account for water vapor and cloud cover influences:

$$R_{nl} = \sigma T^4 \left(0.34 - 0.14\sqrt{e_a}\right)\left(1.35\frac{R_s}{R_{so}} - 0.35\right) \quad (3)$$

where σ is the Stefan-Boltzman constant (2.04 E^{-10} MJ/m^2hr/K^4), T is the average temperature during the measured time interval (K), e_a is the actual vapor pressure (kPa), R_s is the measured solar radiation (MJ/m^2hr), and R_{so} is the clear-sky radiation (MJ/m^2hr). One drawback with this equation is that numerical instabilities can arise while performing net longwave radiation calculations close to sunrise or sunset, causing erroneous ET estimates when the ratio R_s/R_{so} exceeds 1.

Clear-sky radiation (R_{so}) Is calculated using the following:

$$R_{so} = (0.75 + 2 * 10^{-5} z) R_a \quad (5)$$

where z is the station elevation above mean sea level and R_a is extraterrestrial radiation (MJ/m^2hr) which accounts for the influence of latitude on incoming solar radiation. R_a is calculated using the following:

$$R_a = \frac{12(60)}{\pi} G_{sc} d_r [(\omega_2 - \omega_1) \sin\varphi \sin\delta + \cos\varphi \cos\delta (\sin\omega_2 - \sin\omega_1)] \quad (6)$$

where G_{sc} is the solar constant (0.082 MJ/m^2min), d_r is the inverse relative distance between the sun and the earth (rad), δ is the solar declination (rad), φ is the station latitude (rad), and ω_1 and ω_2 are solar time angles at the start and end of the time period respectively (rad). The solar time angle at the start of the time period is calculated using:

$$\omega_1 = \omega - \frac{\pi}{24} \quad (7)$$

and the solar time angle at the end of the time period is calculated using:

$$\omega_2 = \omega + \frac{\pi}{24} \quad (8)$$

where ω is the solar time angle in the middle of the time period (rad). This solar time angle is calculated using:

$$\omega = \frac{\pi}{12} [(t + 0.06667(L_z - L_m) + S_c) - 12] \quad (9)$$

where t is the standard clock time at the middle of the time period (hr), L_z is the longitude at the center of the local time zone (105° for MST), L_m is the station longitude (114.05°), and S_c is the seasonal correction term. The seasonal correction term is calculated using:

$$S_c = 0.1645 \sin 2b - 0.1255 \cos b - 0.025 \sin b \quad (10)$$

with b being calculated with:

$$b = \frac{2\pi(J-81)}{364} \quad (11)$$

where J is the day number in the year between January 1 and December 31. The inverse relative distance between the sun and the earth (d_r) is calculated using:

$$d_r = 1 + 0.033\cos\left(\frac{2\pi}{365}J\right) \quad (12)$$

and the solar declination (δ) is calculated using:

$$\delta = 0.409\sin\left(\frac{2\pi}{365}J - 1.39\right) \quad (13)$$

where J is the day number in the year between January 1 and December 31.

Δ (kPa/°C) was calculated using the following:

$$\Delta = \frac{4098\left[0.6108e^{\frac{17.27T}{T+237.3}}\right]}{(T+237.3)^2} \quad (14)$$

where T is the average hourly temperature (°C).

The psychrometric constant (γ kPa/°C) was calculated using the following:

$$\gamma = \frac{c_p P}{\varepsilon\lambda} \quad (15)$$

where c_p is the specific heat for air at a constant pressure ($1.013E^{-3}$ MJ/kg°C), P is the average air pressure during the time period (kPa), λ is the latent heat of vaporization for water (2.45 MJ.kg), and ε is the molar ratio of water vapor to dry air (0.622).

Wind speed had to be corrected since the monitoring station measured wind speed at 10 m above ground level whereas the method used here required wind speed to be measured at 2 m above ground level (u_2). To correct for the discrepancy, the following equation was used:

$$u_2 = u_z\frac{4.87}{\ln(67.8z-5.42)} \quad (16)$$

where z is the wind speed measuring instrument above ground level (10 m), and u_z is the measured windspeed at the instrument height (m/s).

The vapor pressure deficit (δe) was taken to be the difference between the saturated vapor pressure and the measured vapor pressure. Saturated vapor pressure (e_s) was calculated using:

$$e_s = 0.6108e^{\frac{17.27T}{T+237.3}} \quad (17)$$

where T is the air temperature (°C). The actual vapor pressure (e_a) was calculated using the following:

$$e_a = e_s\left(\frac{RH}{100}\right) \quad (18)$$

where e_s is the saturated vapor pressure and RH (%) is the measured relative humidity.

Appendix D – Diffusion Model Calculations

The 1D Ogata-Banks solution (Ogata 1970) was used to model sulfate concentrations with respect to depth in the Pond M sediment core. The Ogata-Banks solution is given as:

$$C = \frac{C_0}{2}\left[erfc\left(\frac{L-v_x t}{2\sqrt{D_L t}}\right) + e^{\left(\frac{v_x L}{D_L}\right)} erfc\left(\frac{L+v_x t}{2\sqrt{D_L t}}\right)\right] \quad (1)$$

where parameters are defined in table D1.

Table D1 – Parameter definitions for equation (1).

Parameter	Definition
C	Solute concentration (mg/L)
C_0	Initial solute concentration (mg/L)
L	Flow path length (m)
v_x	Average linear groundwater flow velocity (m/s)
t	Time since the release of the solute (s)
D_L	Longitudinal dispersion coefficient (m^2/s)

The longitudinal dispersion coefficient (D_L) was calculated using the following:

$$D_L = \alpha_L v_x + D^* \quad (2)$$

where α_L is longitudinal dispersivity (m), v_x is the average linear groundwater flow velocity(m/s), and D* is the effective molecular diffusion coefficient (m^2/s). D* is calculated using the following:

$$D^* = \omega D \quad (3)$$

where D is the diffusion coefficient for the species of interest (m^2/s) and ω is an empirical tortuosity term used to account for diffusion in porous media (unitless).

The average linear groundwater flow velocity (v_x) was calculated using Darcy's Law:

$$v_x = -\frac{K_{sat}}{n_e}\frac{dh}{dl} \quad (4)$$

where K is the hydraulic conductivity (m/s), n_e is effective porosity (unitless), and dh/dl is the hydraulic gradient (unitless).

Not all parameters were previously measured. To fit the modeled curve to the estimated sulfate concentrations, effective porosity (n_e), longitudinal dispersivity (α_L), and the diffusion coefficient (D) were used as fitting parameters with fitness being determined visibly. K_{sat} was obtained by taking the harmonic mean of K_{sat} values for PM-NE3S and PM-NE3D. The change in hydraulic head (dh) was assumed to be constant. The flow path (L) was taken to be the length of the sediment core and was used in 0.01 m intervals. The time (t) was taken to be the estimated time since Pond M was constructed. Initial concentration (C_0) was calculated by correlating calculated TDS with measured sulfate and establishing a line of best fit (Fig D1).

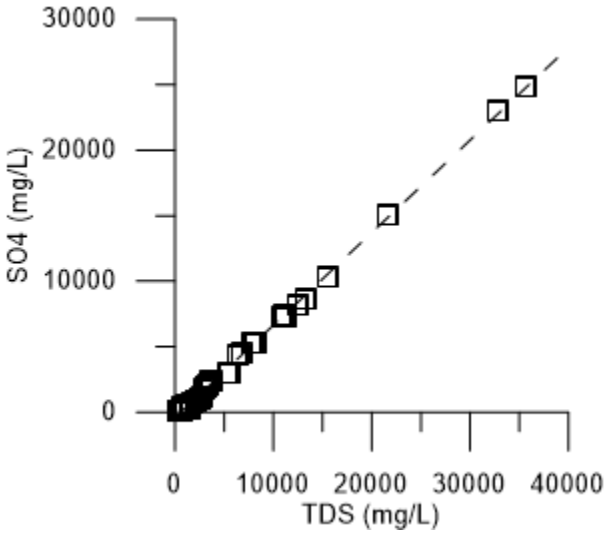

Figure D1 – Correlation curve between TDS and sulfate (SO4) concentrations.

The function of the line of best fit (R^2=0.9986) is:

$$C_0 = 0.7062 * TDS - 409.29 \quad (5)$$

which has an underlying assumption that the proportion sulfate to TDS is constant across the entire site. While sulfate concentrations vary significantly at Pond M, the assumption is that such variance would be limited at the sediment-water interface. Parameters used, including fitted parameters, are given in the following table:

Table D2 – Parameter values used in the diffusion model calculations.

Parameter	Value	Units
C_0	579	mg/L
n_e	0.32	-
ω	0.5	-
K_{sat}	$7E^{-8}$	m/s
dh	0.1	m
dz	-4.65	m
α_L	0.001	m
D	$8.5E^{-10}$	m^2/s
t	441806400	s

Appendix E – Spring Snowmelt and Precipitation Responses

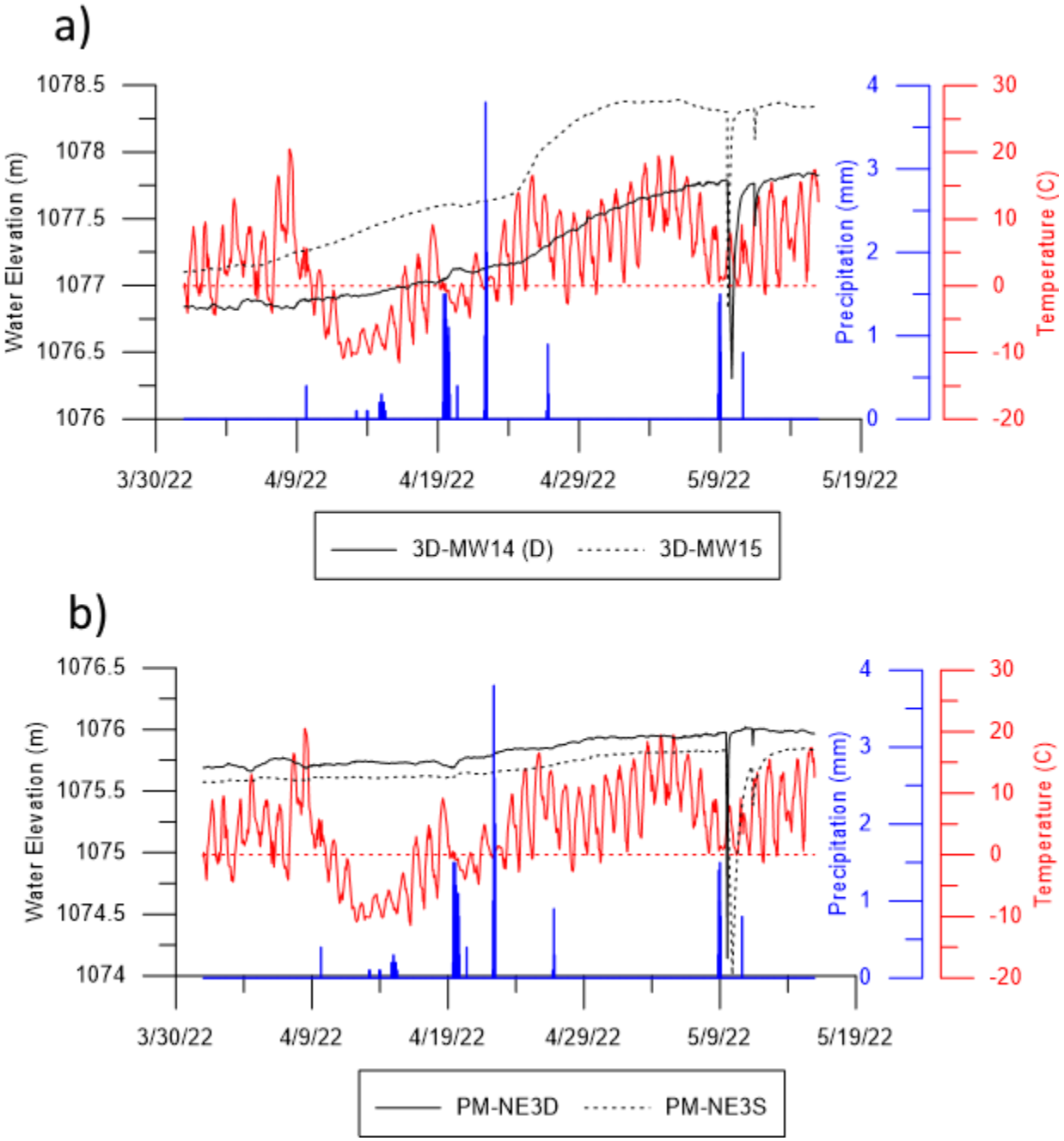

Figure E1 – Groundwater responses near Pond M to a spring snowmelt event. Groundwater elevations were already increasing prior to event. Wells in the recharge region (a) are more responsive to the event than wells closer to Pond M (b).

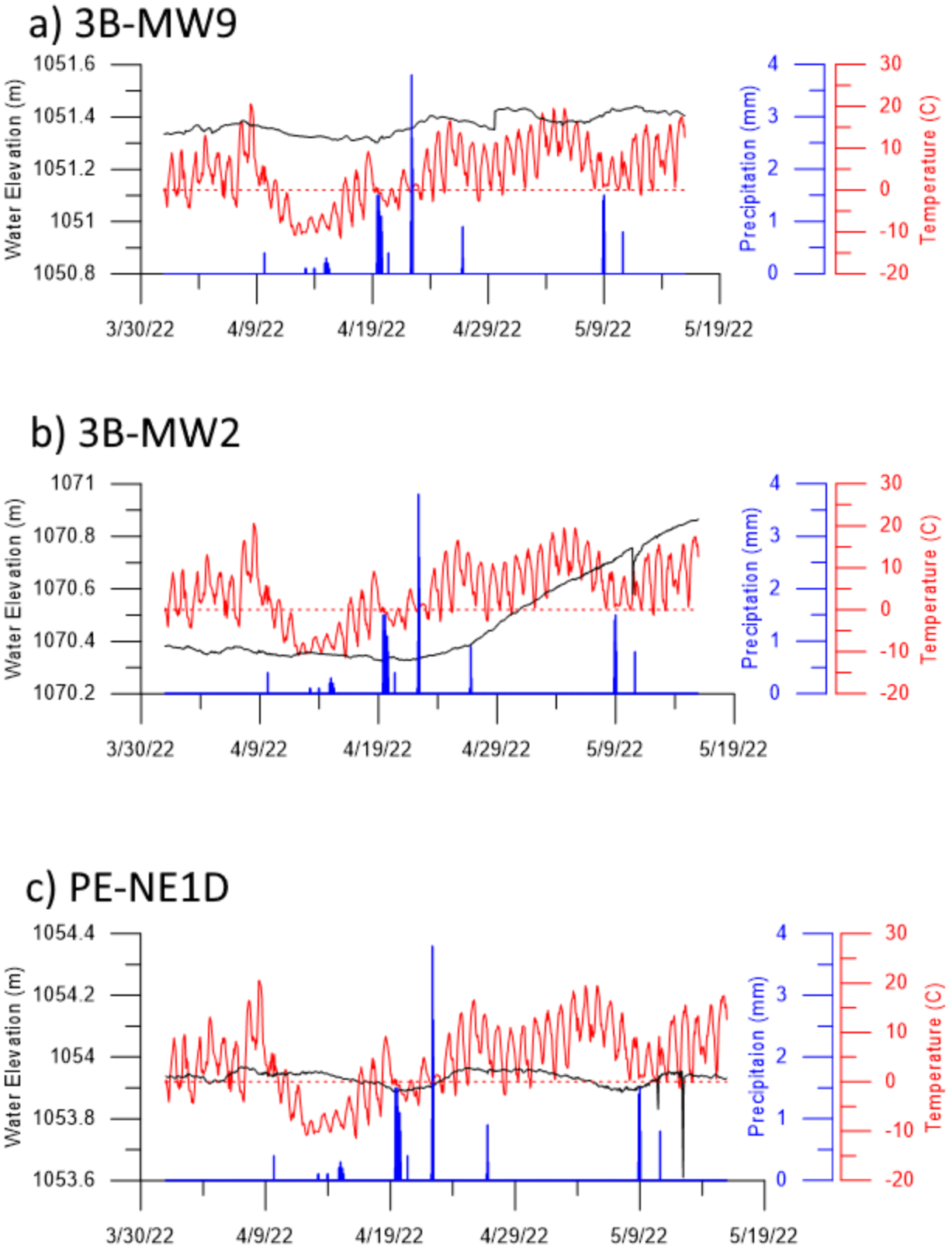

Figure E2 – Groundwater responses near Pond E to a spring snow melt event. Upland groundwater elevations (b) show the most response to the melt pulse whereas wells closer to Pond E show no noticeable response (a,c).

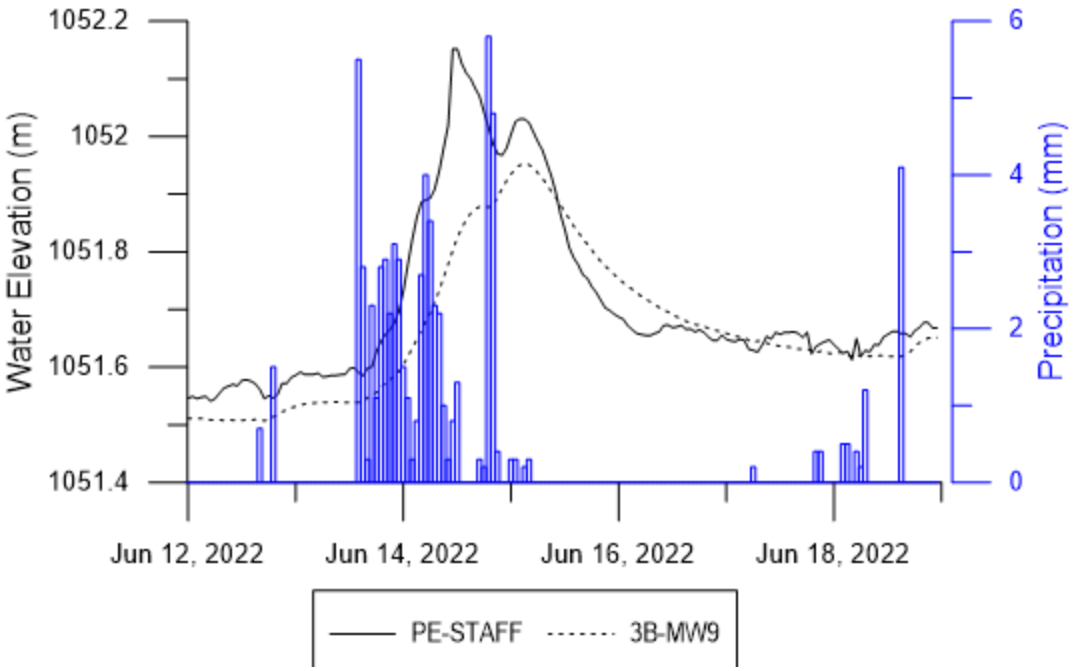

Figure E3 – Pond (PE-STAFF) and groundwater (3B-MW9) elevation response to precipitation event in mid June 2022. Pond water levels increase in response to precipitation and groundwater elevations also increase with some lag time.

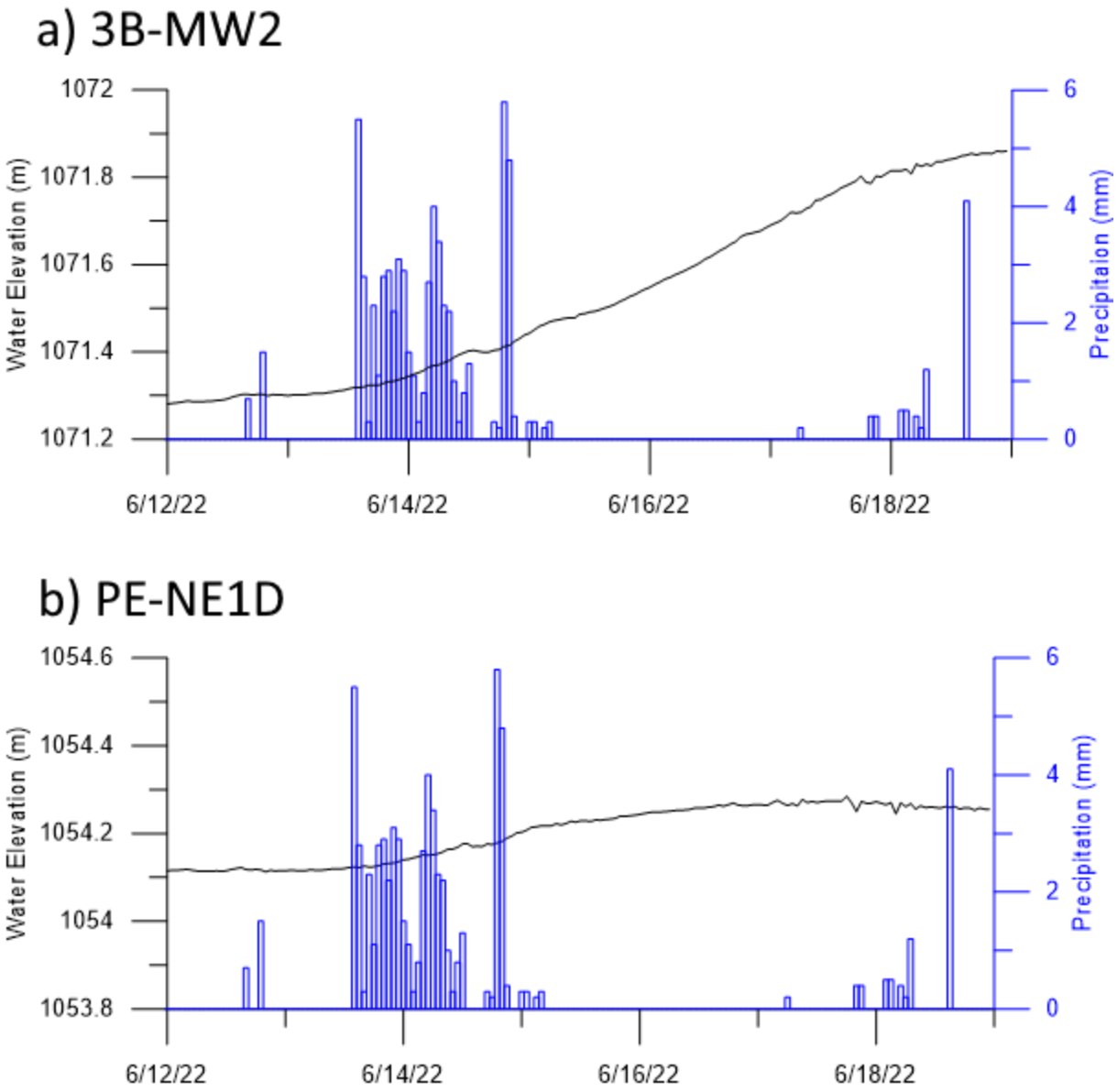

Figure E4 – Groundwater responses near Pond E to a precipitation event in mid June 2022. Response is more significant in the uplands above Pond E (a) with a more muted response closer to the pond (c).

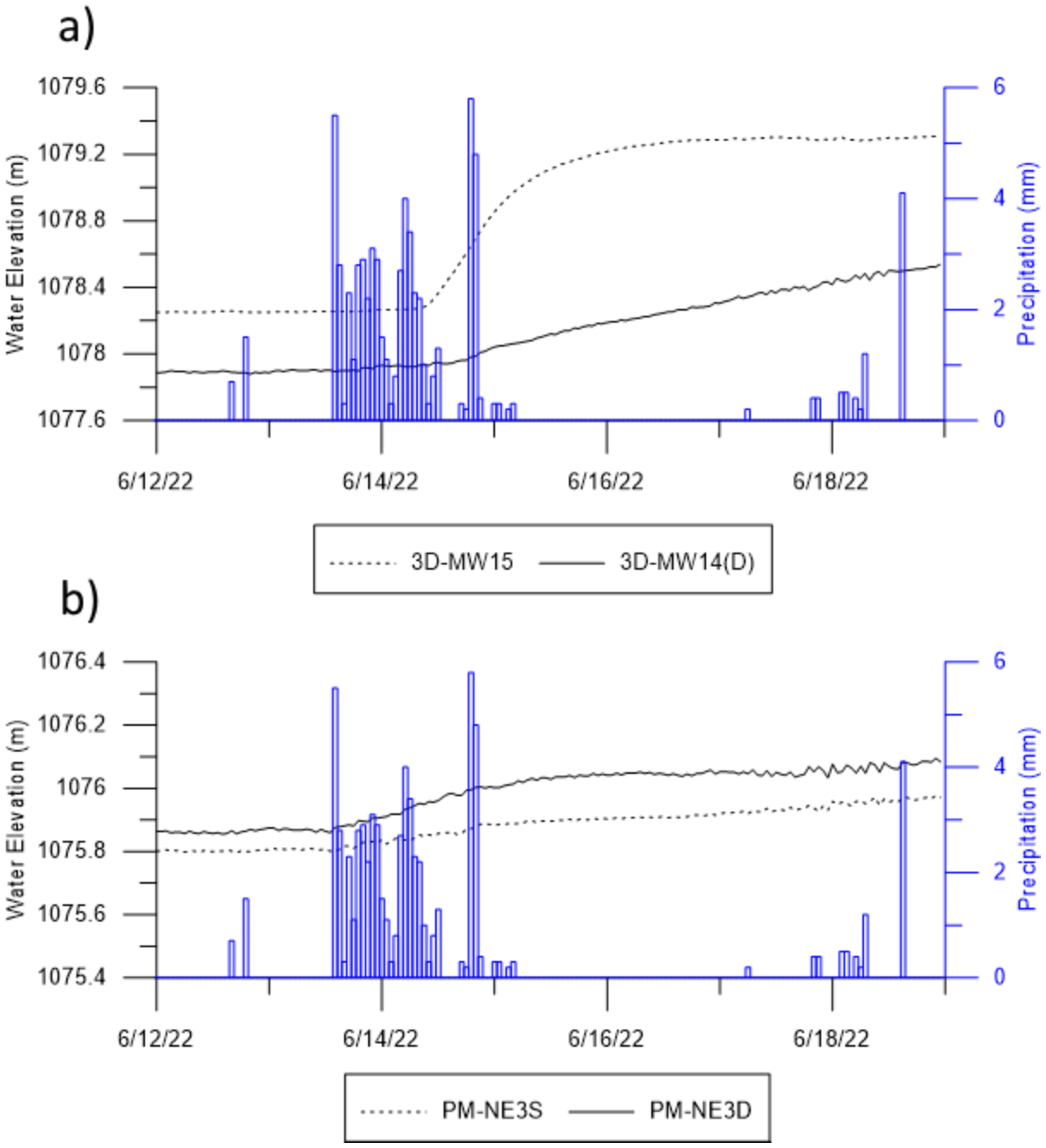

Figure E5 – Groundwater responses near Pond M to a precipitation event in mid June 2022. Response is more significant in the recharge area (a) compared to closer to the pond (b). The shallower well near Pond M (PM-NE3S) responds more slowly than the deeper well (PM-NE3D).

Appendix F – Geochemistry

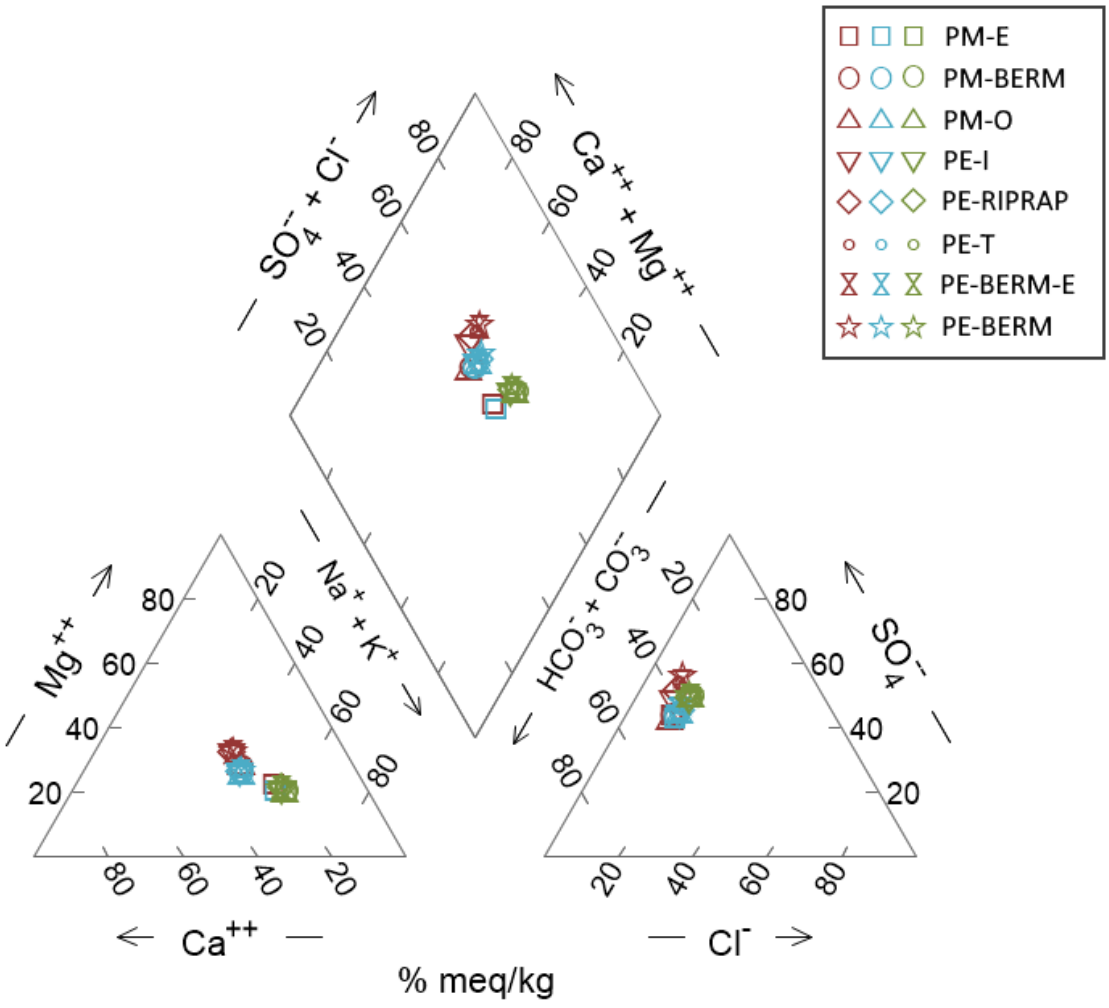

Figure F1 – Evolution of water composition during the simulated storm flow event. Brown indicates pre-event, blue is during the event, and green is post-event. There is a noticeable shift in composition towards more uniformity after the event is completed.

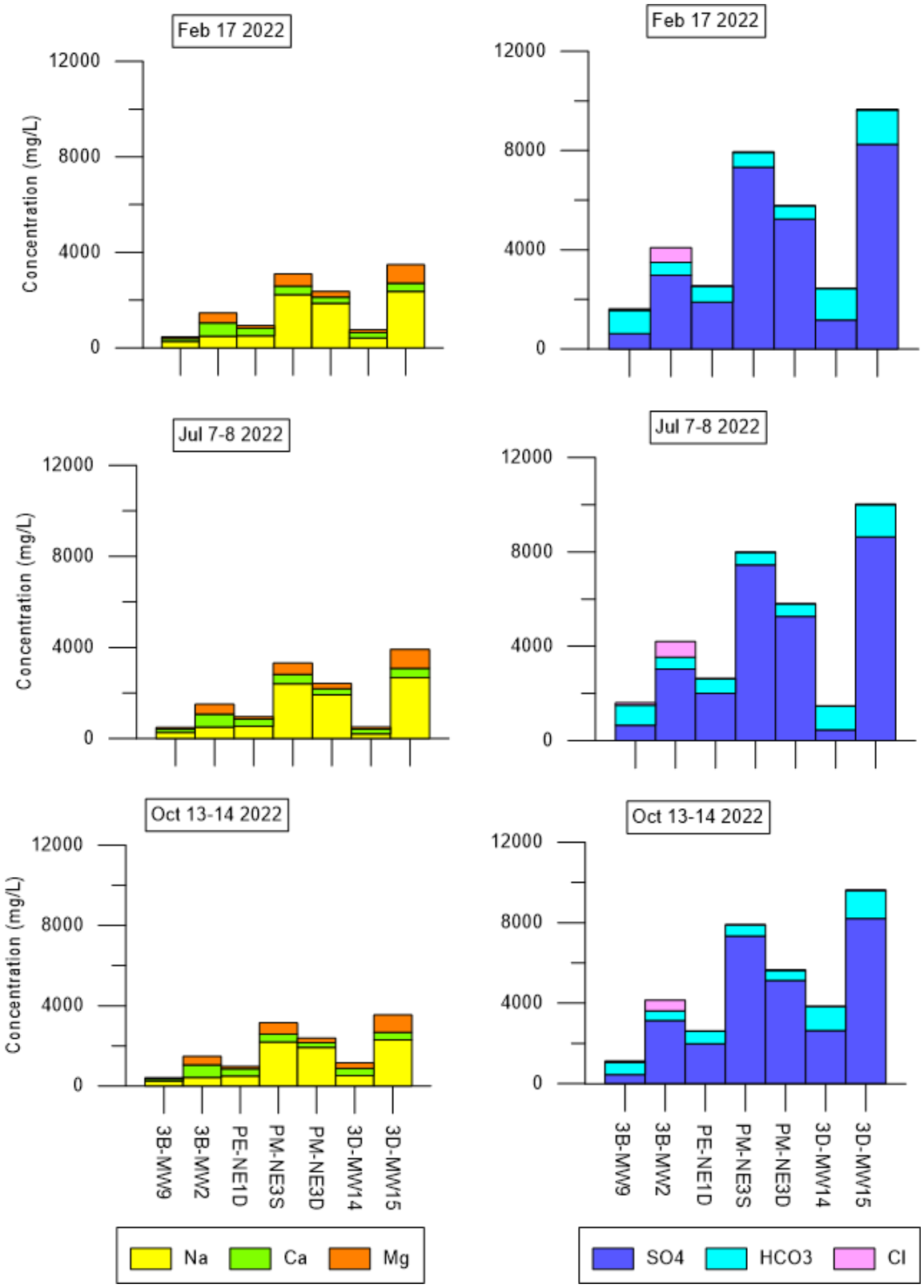

Figure F2 – Groundwater major ion concentrations during each of the sampling periods. Sodium and sulfate dominate water chemistry at most locations. Potassium is not shown due to consistently low concentrations relative to the other ions present.

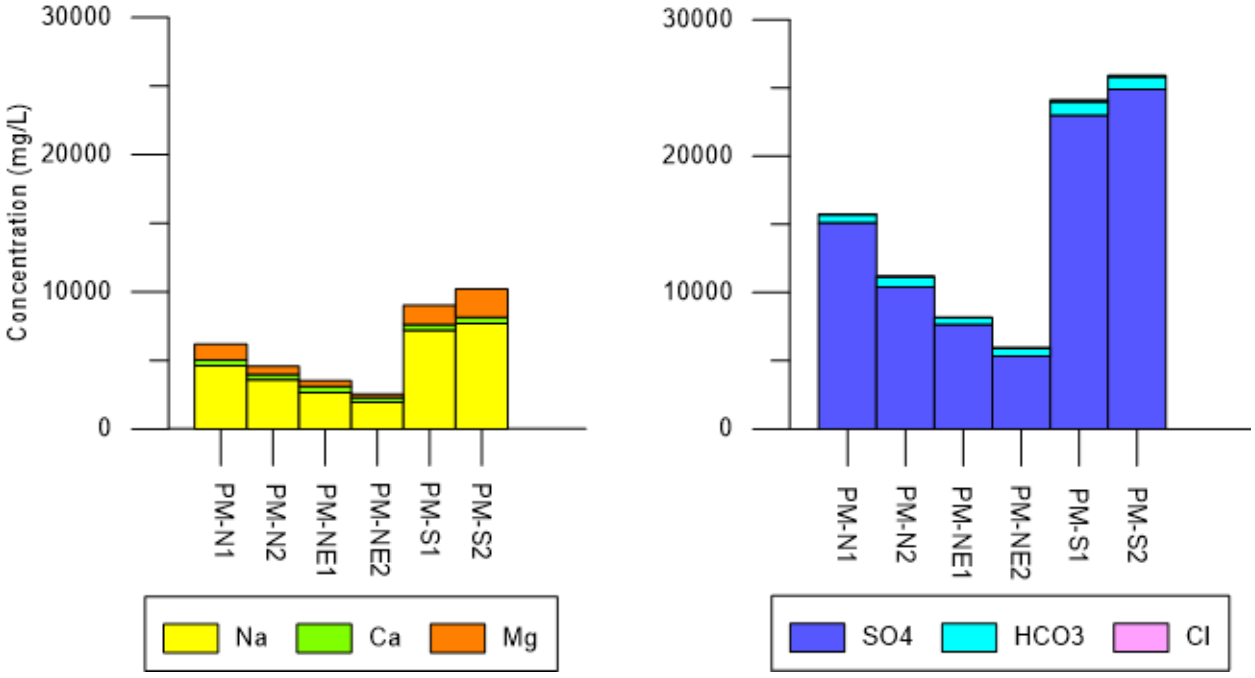

Figure F3 - Shallow well major ion concentrations around Pond M during the July 7-8 2022 sampling period. Potassium was negligible relative to the other ions present.

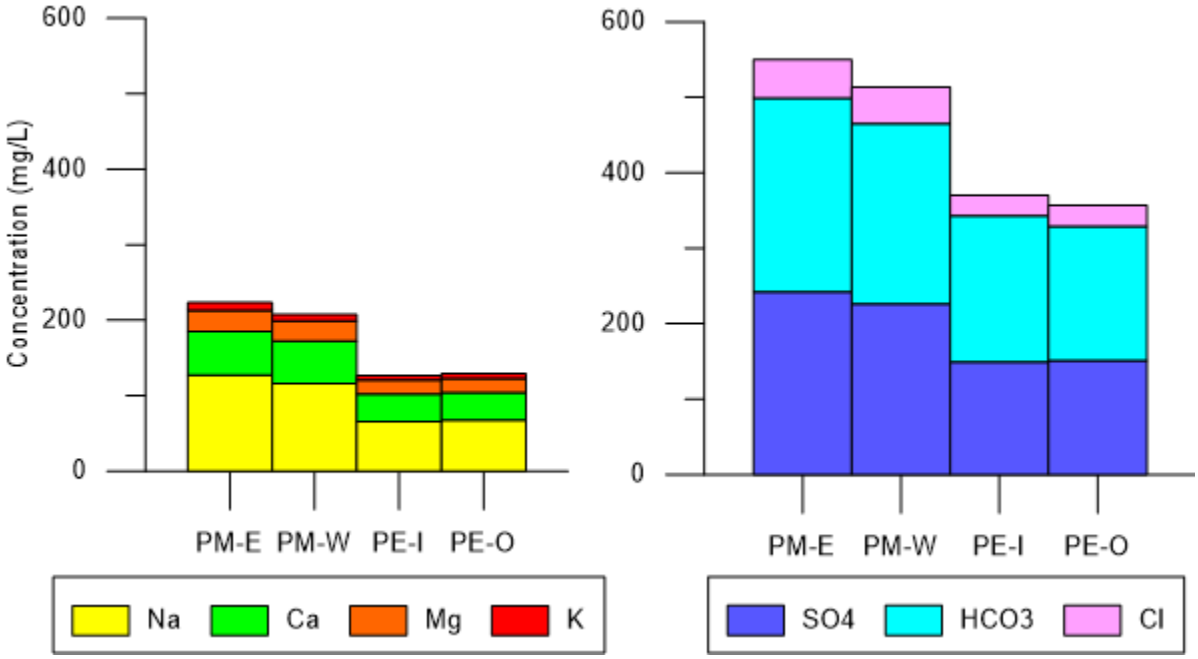

Figure F4 - Surface water major ion concentrations during the July 7-8 2022 sampling period. Concentrations of all species are much lower compared to groundwater at all locations.

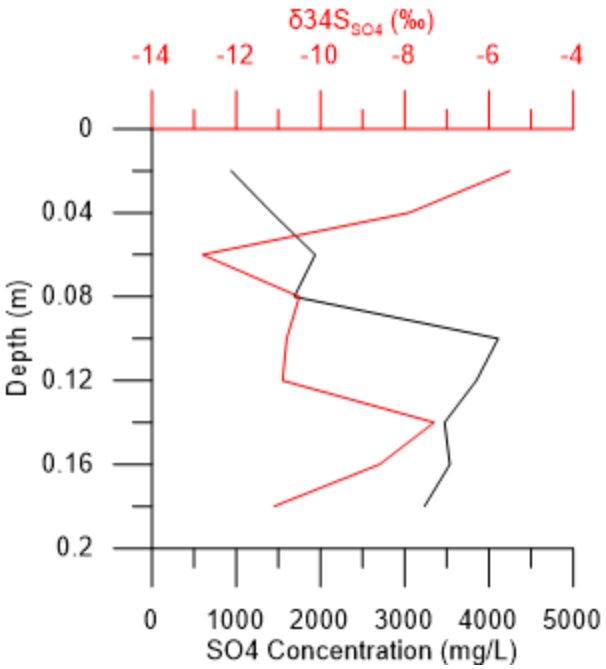

Figure F5 – Estimated sulfate content in the Pond E sediment cores along with δ34S values for the same intervals.

Table F1 – Analytical uncertainty in water quality samples collected during February-March 2022 sampling period.

Location	Na (mg/L)	K (mg/L)	Ca (mg/L)	Mg (mg/L)	SO_4 (mg/L)	Cl (mg/L)	HCO_3 (mg/L)
3B-MW9	± 28.3	± 0.941	± 12.3	± 9.37	± 30.5	± 3.55	± 40.4
3B-MW2	± 51.7	± 1.30	± 55.7	± 53.5	± 148	± 33.6	± 22.0
PE-NE1D	± 53.7	± 0.928	± 31.1	± 14.3	± 94.6	± 1.13	± 27.2
PM-NE3S	± 237	± 2.58	± 35.9	± 63.8	± 367	± 1.72	± 25.1
PM-NE3D	± 199	± 1.40	± 25.2	± 30.9	± 262	± 0.74	± 22.6
3D-MW14	± 251	± 2.61	± 34.8	± 97.2	± 412	± 1.89	± 59.1
3D-MW15	± 52.5	± 1.37	± 26.4	± 26.2	± 58.5	± 0.86	± 54.0

Table F2 – Analytical uncertainty in water quality samples collected during June-July 2022 sampling period.

Location	Na (mg/L)	K (mg/L)	Ca (mg/L)	Mg (mg/L)	SO_4 (mg/L)	Cl (mg/L)	HCO_3 (mg/L)
3B-MW9	± 28.9	± 1.02	± 13.5	± 9.73	± 32.8	± 6.01	± 56.8
3B-MW2	± 53.7	± 1.44	± 56.7	± 54.4	± 152	± 37.3	± 34.4
PE-NE1D	± 55.8	± 0.946	± 32.4	± 14.1	± 100	± 1.22	± 41.1
PM-NE3S	± 256	± 2.74	± 40.8	± 62.5	± 372	± 1.42	± 35.5
PM-NE3D	± 204	± 1.36	± 27.5	± 27.8	± 263	± 0.72	± 36.2
3D-MW14	± 284	± 2.96	± 42.0	± 103	± 432	± 1.93	± 92.5
3D-MW15	± 20.9	± 1.15	± 21.9	± 11.6	± 22.8	± 0.82	± 67.3
PM-N1	± 490	± 3.81	± 40.8	± 145	± 757	± 2.01	± 41.3
PM-N2	± 382	± 2.75	± 38.9	± 73.5	± 521	± 2.79	± 50.7
PM-NE1	± 280	± 2.69	± 44.9	± 56.3	± 367	± 1.80	± 33.9
PM-NE2	± 208	± 1.86	± 32.6	± 31.4	± 266	± 2.75	± 39.3
PM-S1	± 765	± 4.16	± 42.4	± 175	± 1150	± 7.18	± 67.5
PM-S2	± 817	± 7.04	± 44.9	± 259	± 1240	± 5.15	± 61.7
PM-E	± 13.4	± 1.08	± 5.84	± 3.53	± 12.1	± 2.89	± 17.5
PM-W	± 12.4	± 0.932	± 5.70	± 3.29	± 48.8	± 2.75	± 16.3
PE-I	± 6.95	± 0.662	± 3.68	± 2.32	± 7.48	± 1.54	± 11.3
PE-BERM	± 7.16	± 0.676	± 3.70	± 2.35	± 7.55	± 1.60	± 12.2

Table F3 – Analytical uncertainty in water quality samples collected during October 2022 sampling period.

Location	Na (mg/L)	K (mg/L)	Ca (mg/L)	Mg (mg/L)	SO_4 (mg/L)	Cl (mg/L)	HCO_3 (mg/L)
3B-MW9	± 25.6	± 1.04	± 10.3	± 7.53	± 22.7	± 4.07	± 39.0
3B-MW2	± 45.8	± 1.45	± 62.5	± 53.8	± 157	± 30.0	± 31.6
PE-NE1D	± 52.0	± 0.929	± 37.0	± 15.3	± 99.0	± 1.11	± 40.6
PM-NE3S	± 232	± 2.89	± 39.1	± 71.8	± 367	± 1.42	± 35.3
PM-NE3D	± 172	± 1.28	± 24.1	± 29.1	± 256	± 1.49	± 33.4
3D-MW14	± 243	± 2.84	± 38.3	± 108	± 410	± 1.85	± 90.3
3D-MW15	± 54.8	± 1.80	± 36.2	± 33.9	± 132	± 1.10	± 77.1

Table F4 – Analytical uncertainty in water quality samples collected during simulated stormflow event.

Location	August 18		August 24		September 13-14	
	SO_4 (mg/L)	H_2S (mg/L)	SO_4 (mg/L)	H_2S (mg/L)	SO_4 (mg/L)	H_2S (mg/L)
PM-E	± 16.2	± 0.606	± 16.9	± 1.87	± 23.0	± 0.284
PM-BERM	± 16.2	± 1.02	± 17.1	± 2.32	± 23.1	± 0.113
PM-O	± 15.4	± 1.80	± 18.5	± 2.04	± 22.7	± 0.936
PE-I	± 20.5	± 0.165	± 19.6	± 0.660	± 22.4	± 0.228
PE-RIPRAP	± 21.9	± 0.387	± 19.3	± 0.768	± 22.7	± 0.137
PE-T	± 23.2	± 0.209	± 18.9	± 1.17	± 23.1	± 0.132
PE-BERM-E	± 25.8	± 0.0131	± 20.2	± 0.610	± 23.0	± 0.0747
PE-BERM	± 25.3	± 0.0046	± 20.9	± 0.438	± 23.6	± 0.267

Appendix G – Pond E Geophysical Survey

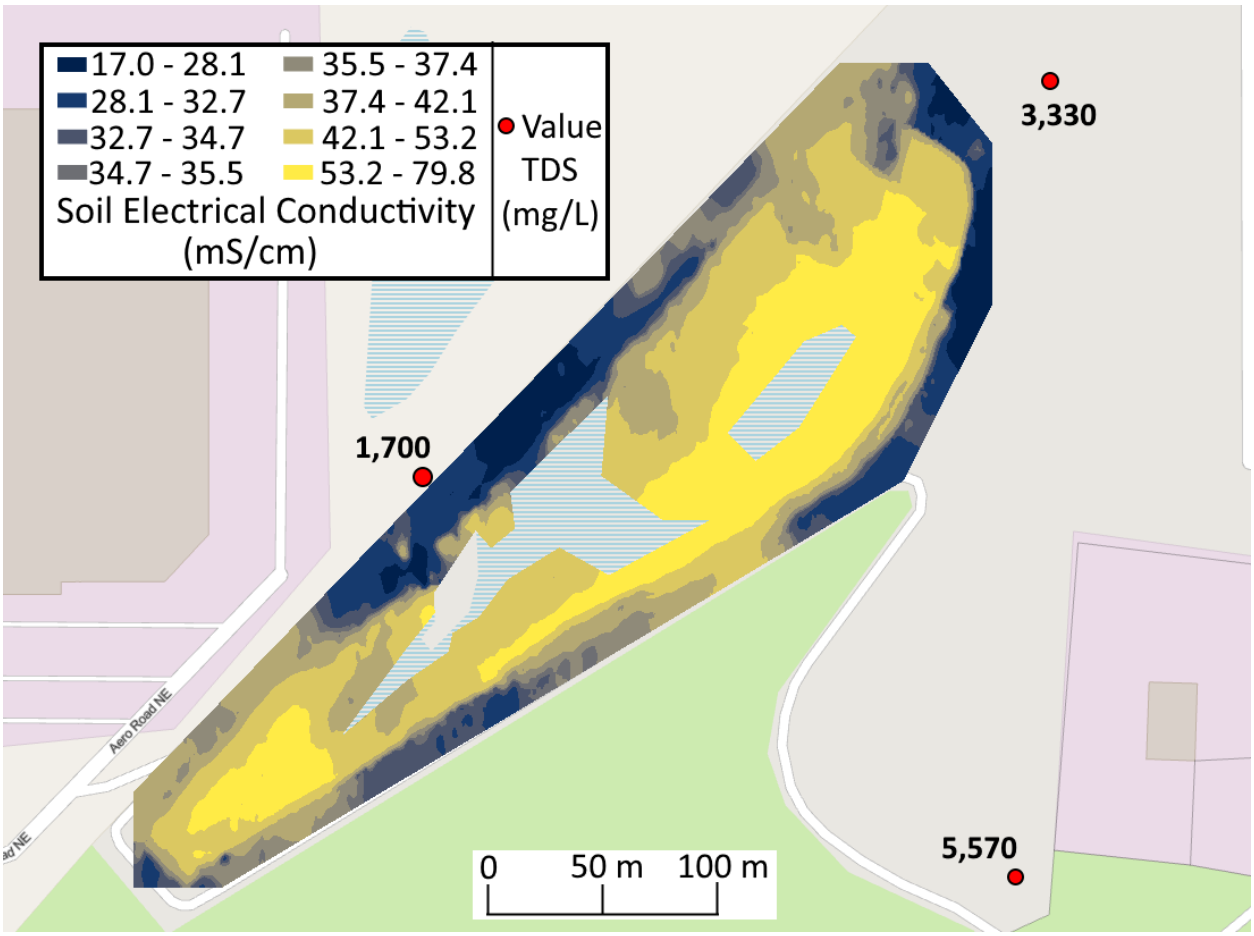

Figure G1 – Shallow electromagnetic survey results for Pond E. Also displayed are laboratory estimated TDS in groundwater samples.

Appendix H – Sediment Core and SEM

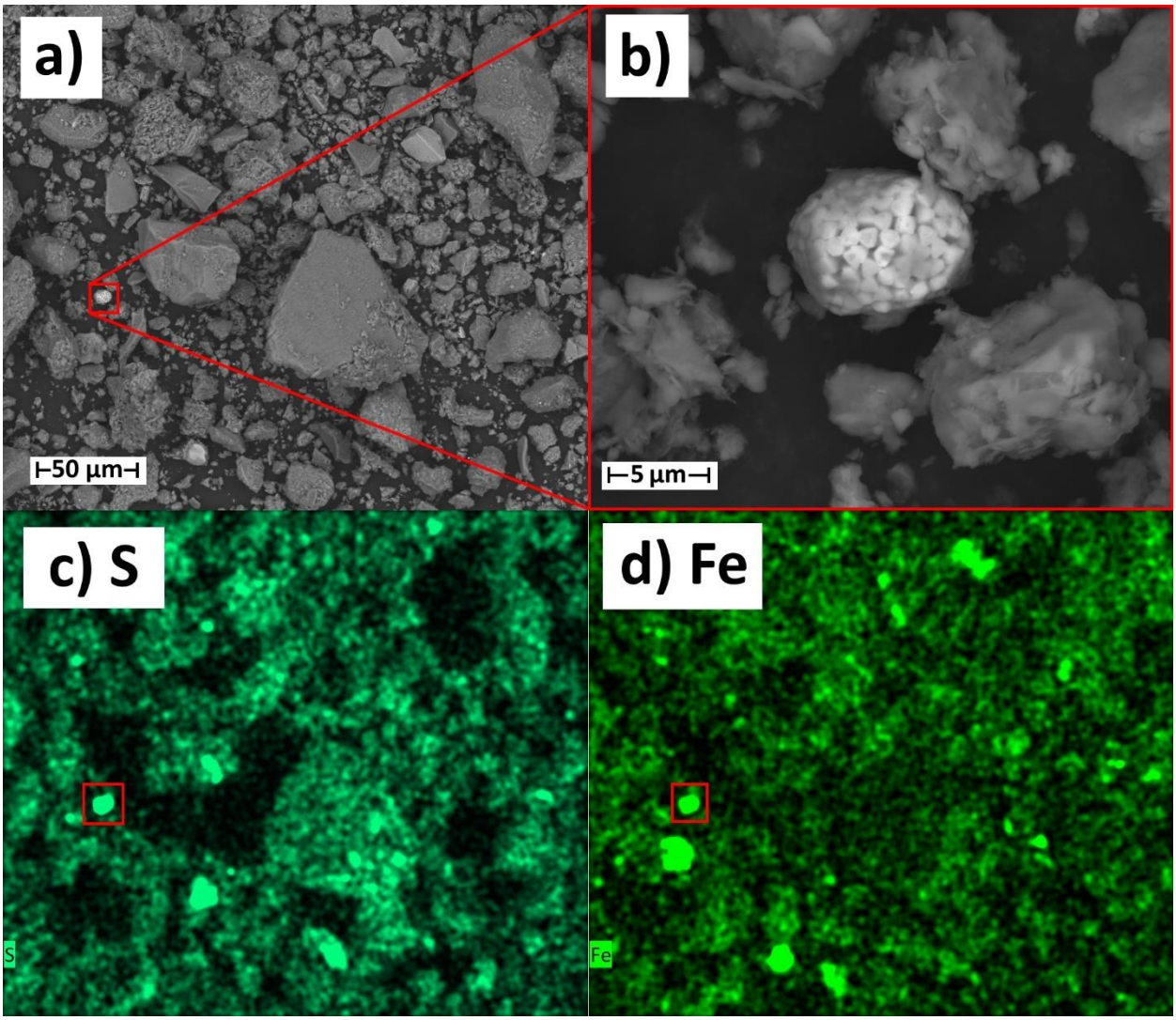

Figure H1 - Pond M sediment core SEM analysis results. Sample was from 10-15 cm in depth near the base of the stormwater deposits. A framboidal pyrite grain is visible.

Figure H2 - Photo of the Pond M core used for porewater extraction. Top of core is on the right-hand side of the image. Combined length of all segments is approximately 45 cm

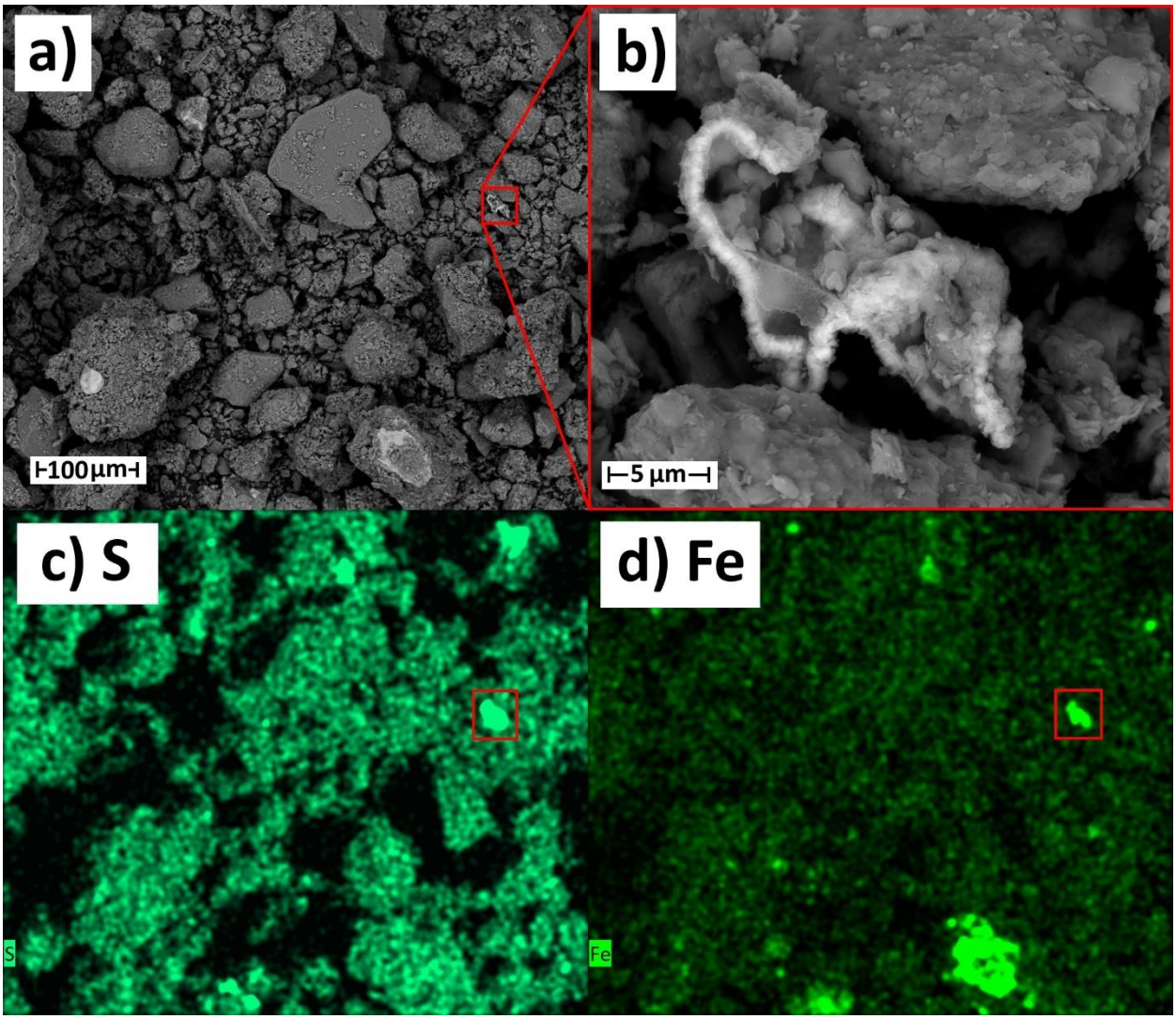

Figure H3 - Pond E sediment core SEM analysis results. Sample was from 8 – 12 cm depth.

Figure H4 - Pond E sediment core that has been split open to be used for porewater extraction. Top of core is to the right of the image. The total length of the core segments is approximately 20 cm.